Satellite remote sensing observations of snow cover extent during the melt-out season in the Thompson-Okanagan Region, British Columbia from 2003-2019

by

Julia Predusca

A thesis
presented to the University of Waterloo
in fulfillment of the
thesis requirement for the degree of
Master of Science
in
Geography

Waterloo, Ontario, Canada, 2021

Author's Declaration

I hereby declare that I am the sole author of this thesis. This is a true copy of the thesis, including any required final revisions, as accepted by my examiners.

I understand that my thesis may be made electronically available to the public.

Abstract

Snow is a critical component of the earth's overall energy budget and it contributes significantly to water resources especially in mountainous regions, coining the term the "water towers" for downstream communities (Viviroli et al., 2006). Studies have shown an increase in snow cover variability due in part by climate change. Most evident throughout the research is an earlier freshet period throughout the northern hemisphere, elevation-dependent warming in mountainous regions and regional climate models indicating transitions from snow to rain dominated basins (Pepin et al., 2015; Rangwala & Miller, 2012). Studies throughout British Columbia have shown evidence of earlier peak runoff from river gauges, a decrease in snow duration and increases in temperature by 1.4^{o} (Shrestha et al., 2012; Kang et al., 2014; Islam et al., 2017). The Thompson Okanagan region is a semi-arid snow dominated region located in the southern portion of British Columbia (Kang et al., 2014). The spring freshet in Thompson Okanagan is affected by large atmospheric systems as well, including the Pacific North American Pattern (PNA), the Pacific Decadal Oscillation (PDO) and the Oceanic Nino Index (ONI).

This research focuses on identifying variations in snow cover during the spring freshet (April 1st-June 30th) in Thompson Okanagan with remote sensing observations from 2003-2019. Snow cover mapping is achieved using visible-infrared observations of snow. High albedo is easily distinguishable in the visible spectrum; however, cloud contamination impedes analysis using visible infrared observations. Steps to mitigate the impact of cloud cover adopted a multi-step methodology. This improved the ability to characterize snow cover extent variability during the spring freshet. The methodology includes: i) a daily combination of Terra/Aqua (from 2003-2012) and VIIRS (from 2012-2019) observations; ii) an adjacent temporal deduction (ATD) technique which replaces cloud pixels with non-cloudy pixels from +/-2 adjacent days; iii) a spatial filter to interpolate snow in cloudy pixels; iv) and the identification of a regional snowline elevation above which cloud-labelled pixels are classified as snow, and cloud pixels below the elevation for no-snow are classified as no-snow. This methodology significantly reduced cloud cover from an average of 71.5% to 1.6% annually.

Using stratified random sampling approach, reference points were gathered for a range of elevation bands for four watersheds within the region to test the snow mapping accuracy. The last day of snow (LDS) was extracted for each point from 2003-2019. Large scale atmospheric patterns (Pacific Decadal Oscillation (PDO), Pacific-North American (PNA) teleconnection pattern and

Oceanic Nino Index (ONI)) were analyzed using simple and multiple linear regression to assess the variability within the LDS dataset that could be explained by these patterns. This analysis showed that the PNA did not significantly account the variability, but the PDO did with an R^2 value reaching 64%, with a significance level of >95%. The simple linear regression models showed that the ONI explained 78% of the LDS variation during the March-April-May (MAM) months, with p>95%; this was more than any other 3-month interval studied. Also, the ONI R^2 value decreased as elevation increased. Overall, El Nino years showed snow disappearance of ~23 days earlier than La Nina years at low elevation, ~18 days sooner at mid elevation and ~13 days sooner at high elevations. Earlier snow melt-out during El Nino phases have implications for water resources in the region, for residential and crop use as well as economic impacts for tourism (Westering, 2016; Winkler et al., 2017). This also contributes to area burned in forest fires and rapid melting snow can cause flooding in surrounding urban areas within Thompson Okanagan. Extending the study period into the future could allow further insights on potential effects of climate change within the region.

Acknowledgements

I would like to thank my supervisor, Dr. Richard Kelly, for guiding me and granting me creative freedom throughout my research. This would not have been possible without his direction and support as well as the funding support from the University of Waterloo. Also, I would like to show my gratitude to my committee, Dr. Fletcher, and Dr. Duguay. A special thank you to my colleagues in academia, especially my good friend Samantha Chu for being the most supportive friend anyone could ask for. Of course, my family and friends for constantly listening to my rambling about snow and programming. A big thank you to my cats, Stella, and Pinot, for the continuous companionship throughout my studies and quarantine. Lastly, my deepest appreciation to my wonderful partner, Jordan, who always believed in me and reassured me every step of the way.

Table of Contents

List of Figures

List of Tables

List of Abbreviations

NASA	National Aeronautics and Space Administration
NOAA	National Oceanic and Atmospheric Administration
VIIRS	Visible Infrared Imaging Radiometer Suite
MODIS	Moderate Resolution Imaging Spectroradiometer
FSC	Fractional Snow Cover
OLI	Operational Land Imager
ETM	Enhanced Thematic Mapper
NDSI	Normalized Difference Snow Index
NDVI	Normalized Difference Vegetation Index
NDFSI	Normalized Difference Forest Snow Index
ROI	Region of Interest
BC	British Columbia
SWIR	Shortwave Infrared
NIR	Near-Infrared
TAC	Terra Aqua Combination
LDS	Last Day of Snow
ATD	Adjacent Temporal Deduction
SF	Spatial Filter
SNOWL	Regional Snow-line method
PNA	Pacific-North American Teleconnection Pattern
PDO	Pacific Decadal Oscillation
ONI	Oceanic Nino Index
MLR	Multiple Linear Regression
OA	Overall Accuracy
DJF	December, January, February
JFM	January, February, March
FMA	February, March, April
MAM	March, April, May
AMJ	April, May, June
NA	Not Available, Not Applicable
DEM	Digital Elevation Model
IGBP	International Geosphere-Biosphere
LCCS	Land Cover Classification System
STRM	Shuttle Radar Topographic Mission
m.a.s.l.	Meters Above Sea Level

Chapter 1
Introduction

Snow is a crucial resource for sustaining human life; an estimated sixth of the world's population relies on snow melt for freshwater resources (Sturm & Goldstein, 2017). Snowmelt patterns affect ecology, hydrological patterns, and water availability during the spring and summer in mid-latitudes (Lehning et al., 2011; Smith et al., 2008). Snow cover influences the earths overall energy balance by reflecting solar radiation and keeping air temperatures cool and acting as an insulator (Metsamaki et al., 2018; Liston, 1999). Snow cover variability is especially crucial in mountain environments where variations in temperature can lead to natural hazards like avalanches and flash flooding (Brown & Mote, 2008, Marty & Blanchet, 2012). Climate change studies have shown decreases in snow extent throughout the northern hemisphere, specifically in the off season and duration of snow throughout the winter season (Derksen et al., 2014; Hori et al., 2017; Hernandez-henriquez et al., 2015). Mountain regions show patterns of elevation-dependent warming, as lower elevations are more affected by temperature variations (Pepin et al., 2015; Rangwala & Miller, 2012). Long term remote sensing observations have been instrumental in helping us to understand the impacts of climate change on snow cover.

Climate modeling in mountain regions have predicted a decrease in snow cover during the springtime, specifically below 2000 meters above sea level (m.a.s.l.) (Mote et al., 2005; Pepin et al., 2015; Marty & Blanchet, 2012). A potential shift from snow dominated to rain dominated regions has also been modelled, especially in semi-arid regions such as the western interior of Canada (Islam et al., 2019; Shrestha et al., 2015). These changes directly impact water resource management as seasonal reserves begin to diminish with earlier snowmelt (Dedieu et al., 2014). Impacts of increasing temperatures in western Canada influence the ongoing forest degradation via pine beetle infestation, as well as potentially increasing variability and spatial extent of forest fires (Shrestha et al., 2015; Shrestha et al., 2012; Winkler et al., 2015). However, human-induced climate change is not the only cause of snow cover variability in mountain regions, it also affects large atmospheric circulation patterns which in turn impacts these regions as well (Harder et al., 2015). El Nino and La

Nina events have been shown to dramatically affect wintertime temperature and precipitation patterns in western Canada, directly impacting snow cover (Bevington et al., 2019).

1.1 Motivation

Snow cover extent (hereafter termed "SCE") during the spring freshet is vital for a multitude of reasons. The spring freshet is defined as the period when snow begins to melt and contribute to the surrounding water systems, the timing of these events varies depending on latitude (Kienzle et al., 2011). Studies to analyze snow cover dynamics (extent, duration, seasonality) have included observations form visible infrared, radar remote sensing, in situ data collection and modeling including both hydrological, land surface and climate modeling (Wang et al., 2018; Dong, 2018, Dedieu et al., 2014). However, visible infrared satellite remote sensing observations have finer resolution than models and thus can produce more reliable results (Dong, 2018). Although they are often hindered by the presence of cloud cover, which is a major limitation to visible-infrared remote sensing. This study is focused on estimating snow cover dynamics during the spring freshet in the Thompson Okanagan region located in southern interior British Columbia (BC), Canada. The study adopts a multistep methodology to reduce the impact of cloud cover in the analysis. The developed snow cover dataset is then used to estimate the freshet period information that can be correlated with teleconnection indices to further our understanding of snow cover during the freshet period and the impacts of teleconnections on snow off-date variability. The Thompson and Okanagan watersheds are diverse in landcover types, topography, human activity and contribute significantly to the economy via natural resources such as fishing, logging, and tourism activities (Rayne & Forest., 2016). This region has been underrepresented in the literature with respect to spring freshet dates which govern the runoff and water levels in surrounding tributaries and ground water levels as well (Kang et al., 2013). Climate modeling studies show that this region is highly sensitive to climate change and could exhibit substantial changes from small variations in temperature (Islam et al., 2017). Slight increases in temperature have been shown to increase inter-seasonal melting periods, reducing peak flow during the spring freshet, and reducing flows during the summer (Islam et al., 2017). These changes create drier conditions during the spring and summer, leading to increased

risk of water scarcity, reduction in crop yield, and potential increases in forest fires (Winkler et al., 2015; Islam et al., 2017). Given the importance of the spring freshet in this region with respect to water availability for agriculture, human use, and aquatic ecology as well as its connection with forest fires, further investigation on snow cover during the freshet is required.

1.2 Aims & Objectives

The overall goal of this thesis is to examine snow cover variability during the spring freshet (April 1st-June 30th) in Thompson Okanagan watershed region and explore how much of the variability in snow off-dates can be explained via large-scale teleconnection patterns. In order to accomplish this, a multi-step cloud reduction methodology is developed using multiple daily satellite observations, an adjacent temporal deduction (ATD) of +/- 2 days followed by a spatial filter (SF) and lastly the implementation of the Regional Snowline method (SNOWL) to remove maximum cloud cover. The aims and objectives are summarized as follows:

Aims:

I. Measure and analyze snow cover changes during the spring freshet in Thompson Okanagan region from visible infrared remote sensing methods from 2003-2019 (April 1st-June 30th) to determine the nature of snow cover change (Winkler et al., 2017);
II. Identify whether teleconnections play a role in explaining variability identified, including the Pacific Decadal Oscillation (PDO), Pacific North America Pattern (PNA) and the Oceanic Nino Index (ONI) using linear regression models

Objectives:

I. Combining multiple satellite products, MODIS Terra/Aqua and VIIRS;
II. Mitigating maximum cloud cover from visible remote sensing imagery with multi-step methodology;
III. Evaluate uncertainties of cloud mitigated snow mapping in a mountain environment through agreement with high resolution data for each step in the methodology;

IV. Quantifying cloud cover mitigation strategies with each additional method as well as with the addition of VIIRS

1.3 Thesis Structure

The remainder of this thesis is organized into the following chapters. Chapter 2 provides a background on snow dynamics, mountain snow hydrology and applications of snow cover. It includes an overview of methods to measure snow cover with visible infrared remote sensing as well as the uncertainties with these methods and insights on snow climatology from remote sensing observations in general and specific to the study region. Cloud mitigation strategies are also presented in this chapter. Chapter 3 describes the study region. The methodology used in this research including methods to conduct analysis are presented in Chapter 4. Chapter 5 presents results of the proposed method. Chapter 6 analyzes and discusses the findings. Chapter 7 summarizes main findings, their importance, and conclusions, including potential future research.

Chapter 2
Snow Cover and Remote Sensing

This chapter is made up of seven sections, first going through snow dynamics and properties. Secondly, an overview of snow hydrology in mountainous regions. Third being the applications of snow cover, and then moving into MODIS approaches to snow cover mapping. The fifth section summarizes remote sensing of snow in a climatological sense. The sixth section provides an overview of potential limitations with remote sensing approaches and the last section is an overview on cloud mitigation methodology most used with visible-infrared remote sensing throughout the literature.

2.1 Snow Dynamics

Snow plays a role as a climatic control variable, with high reflectivity, low thermal conductivity, and thermal inertia (Xu et al., 2015, Barry & Carleton, 2001). Fresh snow has an albedo of 0.8-0.9, for ice it is 0.6, 0.3-0.4 for melting ice containing debris and ponds of melt water and 0.25-0.4 for snow covered forests (Table 2.1) (Barry & Carleton, 2001). Snow is a complex substance in terms of its physical properties and its relationship with the atmosphere and the hydrological cycle, which can be seen in table 2.1 with the discrepancy between albedo of fresh snow and melting/old snow from 0.87 to 0.77 respectively (Table 2.1). This divergence of albedo can reduce the reliability of snow detection algorithms depending on seasonality (Pomeroy & Brun, 1990). Snowfall typically occurs when temperatures in the atmosphere reach 0^{o} C, water droplets will reach a supercooled state and will begin to form snowflakes by attaching to particles in the atmosphere (Pomeroy & Brun, 1990). Contacting warm air around falling snow can cause evaporation of the snowflake and a direct cooling effect of the air around it (Carey & Pomeroy, 2009). For falling snow to survive to the ground, the air temperature and the ground temperature must be at or below 0^{o}C (Derksen et al., 2012). As snow accumulates on the earth's surface, it continuously changes its structure with changing weather patterns. Blowing snow causes sublimation and redistribution of snow, rain on snow events can also change the internal structure of a

snowpack through latent heat exchange (Liston & Elder, 2006). Surface sublimation occurs when air temperature warms enough to evaporate the surface of the snowpack, and liquid runoff from the ground-snow interface also change the structure (Niwano et al., 2012).

Table 2.1: Surface type albedo's in the winter and summer (Barry and Carleton, 2001)

Surface	*Winter (snow-covered surfaces)*	*Summer*
Open water	0.07–0.24[b]	0.05–0.10
Tropical rain forest	–	0.07–0.10
Farmland, stony deserts	0.50	0.15–0.17
Rice paddies	–	0.12
Light-colored sand deserts	–	0.35–0.42
Deciduous/coniferous forests	0.33–0.36	0.14
Tundra	0.82	0.17
New snow	0.87	–
Melting old snow	–	0.77
Young ice (no snow)	0.21	–
First-year ice (no snow)	0.50–0.60	–
Melting white ice	–	0.56–0.68
Old melt pond	–	0.15

Snow cover creates an albedo feedback mechanism; as snow cover decreases an increased amount of bare earth is exposed to direct solar radiation which will absorb solar heat energy (Hernandez-henriquez et al., 2015, Minder et al., 2016). This absorbed heat increases overlying air temperatures through turbulent heat transfer (Wang et al., 2017). Snow is also an efficient natural insulator with a low thermal conductivity that creates a barrier between the energy exchange from the ground surface and the atmosphere (Niwano et al., 2012). This barrier is critical for maintaining soil temperatures, permafrost and vegetation throughout the winter season depending on the region (Debeer et al., 2016). Snow cover is very sensitive to radiation; net radiation, latent heat and sensible heat are the most important variables in snowmelt energy balance (Kim et al., 2017). Even slight changes in incoming solar radiation change the internal structure of a snowpack, as well as the presence of vegetation which cause changes in spatial distribution of snowmelt on a small scale through plant-snow energy interactions (Kormos et al., 2014). These characteristics make snow cover extremely variable, even on an hourly scale, during snowmelt periods. The snowmelt energy balance equation is given in equation 1 and figure 2.1 shows a visual representation of the energy exchange and water balance of a snowpack (Zeinivand & Smedt, 2010). Internal snow energy and the surface layers of frozen soil is U, net shortwave radiation is $S_{n,}$ L_a is atmospheric longwave radiation and L_t is terrestrial longwave radiation, H is the sensible heat exchange, E_l is latent heat and sublimation or deposition energy flux at the surface, G is the

snowpack's ground heat conduction, Q_p is heat advection via precipitation and Q_m is the removed heat through snowmelt (Zeinivand & Smedt, 2010). Essentially, the internal structure and energy balance of snow is governed by a series of variables, this equation simplifies the variables affecting the energy balance of a snowpack and depicts how energy is controlled. These processes could either be directly from the atmosphere above with a change in temperature or precipitation or from the surrounding environment such as vegetation canopies increasing the temperature directly adjacent to them.

$$\frac{dU}{dt} = S_n + L_a - L_t + H + E_l + G + Q_p - Q_m \tag{1}$$

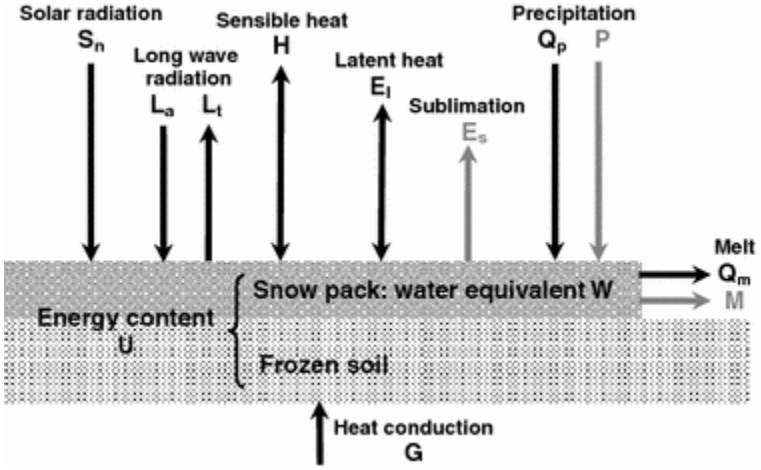

Figure 2.1 : Visual representation of energy fluxes and mass exchange within a snowpack for accumulation and melt (Zeinvand & Smedt, 2010)

In mountainous regions, snow dynamics are complicated by the variability in distribution of snow cover in these regions that are highly dependent on topography, wind speed and the presence and type of vegetation (Bhatti et al., 2016). Latent and sensible heat as well as net radiation are the most important for snowmelt energy and all these variables are unpredictable and varying with topography and presence of vegetation (Kim et al., 2017). For these reasons, quantifying changing snow cover patterns in mountainous regions can be complicated and difficult to predict or model.

2.2 Mountain Snow Climatology and Hydrology

Snow is a major part of the global hydrological system. Snow accumulation patterns vary in relation to latitude, altitude, and regional weather patterns (Mote et al., 2016). The northern hemisphere experiences seasonality of snow, as do some regions in the southern hemisphere (Robinson et al., 1993). While other areas experience perennial snow cover, such as high latitude and high-altitude regions like the Himalayas, the Cascade Mountains, and parts of the European Alps (Tong, 2009). Outside of seasonality, SCE can be influenced by large scale weather patterns, such as the North Atlantic Oscillation (NAO), Oceanic Nino Index (ONI), Pacific Decadal oscillation (PDO), Pacific North American pattern (PNA) etc. (Pollock & Bush, 2013 & Derksen et al., 2014). High altitude mountain regions can exhibit perennial snow cover due high elevation as temperatures remain cool enough to sustain snow cover throughout the seasons (Tang et al., 2017). In these regions, snow greatly contributes to the hydrological system through snowmelt that recharges groundwater, controls streamflow generation, provides nutrient recycling and controls soil moisture (Kormos et al., 2014). Thus, snow cover is a crucial component of the earth's water cycle providing significant renewable water to downstream communities, for this reason they are coined the water towers for these regions (Viviroli et al., 2007).

Under a changing climate, studies have shown variability in SCE patterns. Snow cover during the spring freshet has been the most effected. Studies have shown a varying range of snow extent changes in the past few decades. With over 50% of variations in snow cover extent explained by temperature increase through regression analysis, a decrease of snow extent by -17.8% per decade from 1979-2011 is shown among these studies (Derksen & Brown, 2012). Another study quantified the decline as -0.8 weeks/ decade from 1967-2008 (Gwangyong et al., 2010). As subsequent years' experience warmer air temperatures earlier in the season, snow cover will continue to recede earlier, and bare earth will be exposed to radiation which will absorb this heat and continue to accelerate snow cover decline with this positive feedback effect (Wang et al., 2017).

In mountainous regions, weather patterns are complex due to topographic and elevation effects. The surface heat flux effects in these areas are influenced by many

variables such as moisture advection, cloud formations, and stability of air masses as well as orthographic lift, heat inversion and variability in energy fluxes with hypsometry. These processes produce non-uniformity in the accumulation of snow through complex redistribution by wind and heterogenous radiation per unit depending on aspect, vegetation patterns and so on (Liston, 1999 & Hernandez-Henriquez et al., 2015). Studies have shown that these landscapes exhibit an elevation dependent warming effect which coincides with loss of snow cover at lower elevations (Bormann, 2018.; Elliot & Petruccelli, 2018; Huss et al., 2013). Also, because direct radiation to the surface in these areas is not homogenous, snow cover extent losses are controlled by aspect and slope as well as climatic variables such as precipitation, temperature, wind speed etc. (Brown & Mote., 2008). Snow cover losses in these areas are mostly concentrated at elevations at or below 2000 m.a.s.l. (Dedieu et al., 2016; Schnorbus et al., 2014). Land above this threshold typically remain cold enough to maintain snow cover throughout the year (Dedieu et al., 2016). While climate model predictions have shown potential increases in winter precipitation in mountainous areas, this precipitation may not necessarily fall as snow but as rain instead (Stewart, 2009). Rain-on-snow events can accelerate the loss of snow cover by snow melt through heat advection (Stewart, 2009 & Zheng et al., 2018). It is speculated that the increase of snowfall at high elevations may off-set the loss of snow extent, as some studies have verified using river gauge data (Stewart, 2009). However, this may not be the case in all mountainous regions. In Western Canada, measured air temperatures have increased on average by 4^{o}C since 1962 and there is evidence of the tree line shifting up slope with no evidence of increased snow accumulation at high elevations (Lapp et al., 2005; Li et al., 2018). Studies like this counter the argument of the potential for increased snow accumulation at higher elevations to offset the loss of snow extent at lower elevations. These patterns do not appear to be consistent for all mountainous regions, and further climatological research is needed to improve our understanding of the dynamics of mountain snow cover under a changing climate.

2.2.1 Teleconnections and Climate

The ONI has warm and cold phases termed the El Nino and La Nina. These phases are brought about by the anomalies in sea surface temperature (SST) over the eastern

equatorial Pacific Ocean by +/-0.5°C for a period exceeding 5-months consecutively (Shabbar, 2014; Bevington et al., 2019). El Nino events are caused by weakened trade winds that bring warmer ocean water the coast of North America, this shift is paired with above average winter temperatures and lower levels of precipitation (Fleming & Whitfield, 2010). La Nina events have an opposite effect on Western North America, characterized by strong trade winds, that push warm ocean water towards Asia allowing upwelling of cold water (Glantz et al., 2020). This causes wetter and cooler than normal winter temperatures in the north by the movement of the jet stream northward (Glantz et al., 2020). The PDO is a similar phenomenon in that it is associated with periods of warmer (cooler) SST spanning the Pacific Ocean up to the Gulf of Alaska (Newman et al., 2016). The cycle of phases in PDO span ~10-30 years, but the precise reason as to why they occur are still the subject of research (Newman et al., 2016). Potential reasons for the PDO are linked to ONI phases, atmospheric pressure, and natural variability (Newman et al., 2016). Positive (negative) phases in the PDO are associated with warmer (cooler) than average SST throughout the Pacific Coast and cooler (warmer) SST in the interior North Pacific (Newman et al., 2016). El Nino and positive phases in PDO have been associated with earlier snow melt out dates, drier conditions, and warmer air temperatures in the northwest, while La Nina and negative PDO have the opposite effect (Bevington et al., 2019). The PNA is associated with the ONI. A positive (negative) phase is defined by above (below) normal atmospheric pressure heights throughout the western United States and below (above) normal atmospheric pressure heights over eastern United States (Bevington et al., 2019). Positive PNA phases are associated with warmer (cooler) than normal temperatures in the west (east), while negative phases are associated with cooler (warmer) than normal temperatures in the west (east) (Bevington et al., 2019). These teleconnections play a role in mountain snow climatology affecting temperature and precipitation patterns on the west coast and interior B.C.

2.2.2 British Columbia Snow Climatology

Climate change can have major impacts on water resources because snowmelt is the primary driver of water supply due to the relative dryness in the interior BC and even slight changes could have large effects (Merritt et al., 2006). Studies have shown an increase in the

minimum temperature in the Okanagan basin and increased summer precipitation from gauging station data (Cohen et al., 2012). Water flowing through this region is governed by mountain snow which is projected to decrease in accumulation as temperatures increase (Kang et al., 2014). Decreasing total snow water equivalent accumulation throughout western Canada has been shown and linked to rising temperatures and decreased precipitation (Mote et al., 2005). There is also evidence that the interior of the Fraser River Basin, including the Northern Plateau and the Thompson-Okanagan region may transition from a hybrid of pluvial and nival river system to being rain dominated (Shrestha et al., 2012). An overall decrease in snow accumulation throughout the Fraser River Basin is correlated with an increase in temperature by 1.4^{o} Celsius (Kang et al., 2014). In the Fraser River basin, projections show increased runoff in winter and spring and a decrease in the summer and fall seasons because of changes in precipitation and snow storage (Shrestha et al., 2012). Mountain regions have been shown to exhibit elevation dependent warming, in this area the early onset of mountain snowmelt can lead to decreased streamflow in the interior of the Fraser River Basin throughout the summer and fall seasons (Islam et al., 2017). Smaller changes projected for higher elevations, however, indicate that the Thompson-Okanagan region is highly sensitive to changes in temperature and snow storage because of its semi-arid climate regime (Kang et al., 2014; Merritt et al., 2006). These changes are critical for water resource management and have ecological impacts (Kang et al., 2014).

Snow cover changes in this region are also highly affected by land cover change, notably forest cover loss. Clear cutting in southern interior BC has related to increases in snow accumulation caused by lack of snow loss to canopy interception (Winkler et al., 2017). Forest cover loss to the pine beetle infestation and forest fires are also influencing forest cover loss (Winkler et al., 2015). Though these landcover changes may increase snow accumulation during the cold season, the loss of forest cover also causes increased rapid melt responses (Schelker et al., 2013, Carey & Pomeroy, 2009). As these areas will be exposed to direct solar heating, snow will melt more rapidly and contributing rapid runoff to rivers and streams without vegetation interception (Schelker et al., 2013). One study showed that clear cut or burned regions had snow disappearance occur 10-days earlier than forest covered areas

in this region (Winkler et al., 2015). In the Okanagan Plateau, these land cover changes have cause significant shifts in the runoff regime (Winkler et al., 2017). This is problematic for water resources, as these changes cause increases in water yield early in the season (April) and decreases later (June and July) (Winkler et a., 2017).

The variations in snow season climatology in this region has been associated with several atmospheric circulation patterns, including the PDO, PNA and the most influential being the ONI. Correlation coefficients between BC snow cover and PDO or ONI in the onset of the snow season show the lowest correlations, whereas highest correlations occur in the winter and fall for snow duration and spring freshet (Bevington et al., 2019). The spring freshet is negatively correlated with both the PDO and the El Nino, meaning that increases in the severity of these indices tend to be associated with decreases in snow cover during the spring freshet, the same is found with snow cover duration (Bevington et al., 2019). Statistically, the significance of ONI and PDO on temperature and precipitation are confined to the cold months, one study showed that these teleconnections influence begins in February for the southern interior region of BC and in December for the Rocky Mountains to the east (Fleming et al., 2010). La Nina patterns in BC have also been linked to avalanche frequency as these years are characterized by colder temperatures, higher precipitation and therefore a greater amount of snow (McClung, 2013).

Studies have shown that a general trend exists in decreased mountain snow extent at lower elevations (Pederson et al., 2013). Areas at or below 2000 m.a.s.l. are particularly sensitive to warming (Dedieu et al., 2016). Elevation-dependent warming has been modeled and aided by data gathered through visible remote sensing (Pepin et al., 2015). With increased temperatures at lower elevations, snow extent is expected to decrease, allowing for continued warming through exposure of the bare ground through the albedo effect (Pepin et al., 2015). Overall variability of precipitation patterns with climate change indicate that dry (wet) regions will get drier (wetter) (Dore, 2005). Climate model predictions show projected increases in temperature across mountain regions which are expected to cause rain-on-snow events, thus reducing snow cover extent and overall snow depth (Stewart, 2009). Snow cover climatology is affected by more than temperature. Large scale atmospheric systems influence

the duration of snow cover, the rate of retreat and the accumulation (Bevington et al., 2019). High temporal and spatial resolution observations of snow cover provide insights into snow patterns and further guide our understanding of how they are changing.

2.3 Applications of Snow Cover

The changes observed with respect to snow cover extent have implications for various applications. Snow accumulation in mountain catchments is responsible for over 80% of human water resources in semi-arid tropical and subtropical regions (Saavedra et al., 2017). Snow water storage is crucial for economic, recreational demands and environmental requirements (Mote et al., 2005). Snow cover in mountainous regions affect seasonal recreational activities that generate revenue through tourism activities (Sturm & Goldstein, 2017). Throughout recent decades, the spring freshet has been occurring earlier in the season, thus snow related activities are at risk of being shortened, which subsequently has implications for these companies and the communities that depend on them (Shabarr, 2014). Changing snowmelt timing can affect types of vegetation that grows and the moisture of the soil in the following growing season (Kienzle et al., 2012). Anomalous warming temperatures can cause rapid snow melt in mountains which could lead to potential flooding (Harder et al., 2015). The timing and duration of snowmelt affects the ground water recharge and water tables for the entire year; regions that depend on snowmelt for irrigation could suffer from potential shifts in the snow off season (Winkler et al., 2017). The increase in climate warming potentially can induce increased instability of snowpack leading to increased avalanche occurrence in mountainous areas (Brown & Mote, 2008). However, a recent study in British Columbia has found this effect to be inconclusive (Belaire et al., 2016). Therefore, snow cover extent is vital from a macro to micro-scale mountain processes and continuing to model, predict and analyze these changes is important for various applications.

2.4 MODIS Approaches to Measuring Snow Cover Extent (SCE)

Traditional in situ data collection methods for climate-scale snow cover mapping are ineffective at capturing local to regional scale snow variability. The high spatial and temporal variability of snow cover requires frequent measurement schemes over large areas for effective mapping. In situ data from automated weather stations, snow courses and snow pillows are effective in aiding our understanding of snow variability at the very local scale, but their spatial domains are not easily scalable to snow mapping of large domains. Point data has limitations such as being time consuming to gather, requiring intensive labor and it is expensive, especially in remote areas (Bales et al., 2018). However, these datasets can assist in accuracy assessments of remote sensing methods or serve as input data for land surface modeling of snow cover extent and snow water equivalent (Dong, 2018). The MODIS algorithm is the focus here as it has been used extensively in mountain snow research and other regions with high accuracy. The moderate resolution enables a reliable depiction of snow cover and the daily imaging is a vital component necessary for snow mapping.

Remote sensing methods facilitate the acquisition of consistent daily observations of snow cover for snow cover extent mapping. Visible and infra-red remote sensing techniques for SCE and snow cover fraction (SCF) have been developed to assess variability. The most common method is the SNOWMAP algorithm developed for MODIS on both Terra/Aqua platforms with 500 m pixel resolution and daily acquisition (Hall et al., 2002). A nearly identical algorithm is available from VIIRS on the Suomi NPP satellite and is also used to produce a daily snow product at 375 m resolution (Hall et al., 2019). The SNOWMAP algorithm uses thresholding values of the Normalized Difference Vegetation Index (NDVI) (2) and the Normalized Difference Snow index (NDSI) (3) to identify pixels that are snow covered and their percentage based on the reflectance properties and the vegetation cover in the pixel (Riggs & Hall, 2015).

$$NDVI = \frac{NIR-Red}{NIR+Red} \quad (2)$$

$$NDSI = \frac{Visible-SWIR}{Visible+SWIR} \quad (3)$$

The basis of snow cover mapping with satellite observations is straightforward under cloud-free conditions; the albedo of snow is very high relative to other surfaces which makes it easily recognizable in an image (Riggs et al., 2017). However, cloud cover can complicate the process. Therefore, the NDSI is used more often because it takes information from the visible spectrum (0.545-0.565µm) as well as infrared channels (1.628-1.652 µm) which enables this distinction (Figure 2.2) (Riggs et al., 2017 & Hall et al., 2002). In non-forested regions, a pixel will be flagged as snow covered if it has an NDSI value equal to or greater than 0.4 and a reflectance greater than 11% in band 2 (0.841-0.876 µm) in areas non-densely forested (Hall et al., 2002). If these conditions are met, but the reflectance in band 4 is less than 10%, the pixel will not be mapped as snow to reduce the false detection of snow from dark forests (Hall et al., 2002). In forested regions, the reflectance of snow decreases in the visible and snow-covered forests have a lower NDVI (Hall et al., 2002). Pixels will be flagged as snow if they have an NDVI around 0.1, regardless of the NDSI being lower than 0.4 (Hall et al., 2002). This is then converted into fractional snow based on the percentage of the pixel that passes these thresholds using equation 4 for all regions (Riggs & Hall, 2015).

$$FSC = \left(-0.01 + (1.45 * NDSI)\right) * 100.00 \; for \; 0.0 \leq NDSI \geq 1.0 \qquad (4)$$

In earlier collections of the MODIS snow products there was a temperature screen that removed pixels classified as snow if the temperature was above 281k, however this caused snow commission errors regarding snow cover at high elevations (Hall et al., 2019). To remedy this, the screen was changed in collection 6 to include an estimated elevation threshold of 1300 m (Riggs & Hall, 2015). Therefore, if a pixel is snow below this threshold with a temperature above 281K it is not snow, and if it is above this elevation it is snow (Riggs & Hall, 2015). This screen is set to reduce false detection in tropical forests and warm coastal regions (Riggs & Hall, 2015). Non-snow surfaces may be flagged as snow if the SWIR is too high. A high SWIR screen is applied so that pixels with SWIR values from 0.25-0.45 are flagged as unusual snow as snow cover usually has a SWIR value <0.20 (Riggs & Hall, 2015). The last screen applied is a solar zenith mask of >70° so nothing with low illumination is mapped, and anything with a zenith angle of >85° is night (Riggs & Hall, 2015).

The MODIS snow product uses the MOD35_L2 cloud mask, a 1 km resolution mask which applies the mask to 4 corresponding pixels (Hall et al., 2002). This mask has been described as an aggressive and conservative approach, meaning that errors off commission may be a consequence of the mask (Morriss et al., 2016; Xue et al., 2014). The VIIRS product uses the cloud mask VNP35_L2 which is less conservative than the MODIS cloud mask, this is thought to be the biggest difference between these two snow cover products (Hall & Riggs 2019).

2.5 Remote Sensing and Snow Climatology

Reflected visible and infrared remote sensing plays a significant role in understanding snow cover climatology. An accurate depiction of snow cover at large spatial extents and high temporal resolution is required for change analysis of snow patterns with a changing climate. Onset and offset snow season dates are important variables when analyzing snow pattern changes as snow offset date is very sensitive to increases in temperature (Kang et al., 2014). Using multiple remote sensing platforms, studies have shown an overall decrease in spring snow cover extent in the Northern Hemisphere (Brown et al., 2007). An amplified decrease of snow extent is shown in the last 40 years using a combination of ten datasets pre-satellite era and with satellite data (Brown & Robinson, 2011). Correlation analysis found that over 50% of these variations can be explained by temperature increases (Brown & Robinson, 2011). The NOAA climate data record is the longest snow cover extent product, using a combination of in situ, visible and radar imaging to map snow since 1966-present (Brown et al., 2010). In the early years, the temporal resolution was monthly and then weekly, to daily starting in 1999 when MODIS Terra was launched (Hori et al., 2017). With these datasets, it is possible to quantify the decrease in snow extent throughout the Northern Hemisphere, as studies have done. For example, in a study done from 1967-2008 showed a spring snow cover decline of 0.8 weeks/decade (Gwangyong et al., 2010). From 1979-2011 there was a decrease of spring snow cover by -17.8%/decade (Derksen & Brown, 2012).

The NOAA CDR has coarse spatial resolution at 190.5 km, and coarse temporal resolution for part of the dataset (Hori et al., 2017). This dataset is also subject to human

error as the decisions for snow covered pixels are not made by an algorithm but rather were manually selected (Brown & Derksen, 2013). The temporal resolution is coarse, particularly for snow cover which can change hourly under certain conditions especially in mountain environments. The Interactive Multi-Sensor Snow and Ice Mapping System (IMS) is another SCE product available. This product is available from 1997-present at 24 km spatial resolution and daily temporal resolution (Roy et al., 2010). This product uses visible infrared as well as passive microwave data to mitigate cloud coverage (Romanov et al., 2000). Coarse spatial resolution is not suitable for mountainous basins, as topographic complexity complicates the process of identifying snow with coarse spatial resolutions and is further complicated with the use of radar imagery within their analysis (Wang et al., 2016). In fact, when studying snow extent with these products on a hemispheric extent, mountain regions are often masked to increase overall accuracy of the study (Bormann, 2018).

The NOAA CDR and Interactive Multi-sensor Snow and Ice mapping system (IMS) are used extensively when discussing the changes of snow cover extent climatologically and over large spatial extents (Hori et al., 2017; Mudryk, 2017; Hernandez-henriquez, 2015). Yet, there are uncertainties within these datasets that extend from uncertainties of visible remote sensing alone, especially in mountain domains where snow cover is heterogenous and subject to extensive cloud cover. The spatial resolution of MODIS is finer at 500 m, maintaining a daily temporal resolution. The exclusion of passive microwave sensors enables the finer spatial resolution in this dataset, with the tradeoff of cloud contamination. However, to maintain the moderate spatial resolution of the MODIS datasets without passive microwave data, steps to mitigate cloud cover must be performed. For these reasons, MODIS datasets are mainly used for studies done from 2000-present as the spatial and temporal resolution is much higher than the CDR and the IMS datasets.

2.6 Uncertainties

Visible-infrared remote sensing observations of snow cover are complicated by several issues. Satellites measuring within the visible spectrum are sun synchronous. However, during times of polar night, in the high Arctic especially, these methods are unusable (Wang et al., 2011). Forest cover causes uncertainties with snow cover methods as

well. The reflectance of underlying vegetation will affect the spectral signature of snow which causes misclassifications (Wang et al., 2015). Forest canopies obscure underlying snow leading to errors of omission (Berman et al., 2018; Tait & Hall, 2000). In mountainous regions, forest cover uncertainties add to uncertainties caused by the spatially variable distribution of snow cover in mountainous terrain that is complicated by slope, elevation, effects of shadows and varying solar illumination, aspect and patchy snow cover (Czyzowska et al., 2015). The MODIS fractional snow cover, MOD10_L2 product has shown to have similar accuracy as Landsat-7 30 m resolution snow maps in mountainous terrain with a least-squared regression analysis between these two datasets showing an R^2 value ranging from 0.86-0.98, although some places had lower agreement at 0.47 and 0.58 (Crawford, 2015). These low accuracy dates are attributed to transient snow patterns, cirrus cloud contamination as well as changes in viewing angle throughout the day when these images are collected and local solar illumination (Crawford, 2015). These studies allow for a better understanding of how well the MODIS snow algorithm performs in comparison to high resolution imagery, they give insights on areas of improvements as well as uncertainties.

Snowpack metamorphosis can change its reflectance properties (Solberg et al., 2006). This will lead to misclassifications as reflectance values may shift depending on the size of the snow crystals (Figure 2.2) (Dietz et al., 2012). NDSI uses the red and SWIR band which make this less of a concern for visible-infrared remote sensing, however when including passive microwave data, it can become a limitation (Dietz et al., 2012). Also, during periods of snow melt, snow changes and becomes contaminated consequently changing the albedo and the reflectance properties (Eckerstorfer et al., 2016). Depending on weather factors the off-season can also bring transient snow, which can bring about errors of over/underestimation depending on the timing of overpass of the satellite (Wagnon et al., 2009). Given the overpass of MODIS at 10:00 am over the equator, if a snow event occurs later in the day, the image for that day will be underestimating snow cover because it occurred after the overpass of the satellite. Transient snow is common during the spring freshet (Kim et al., 2015).

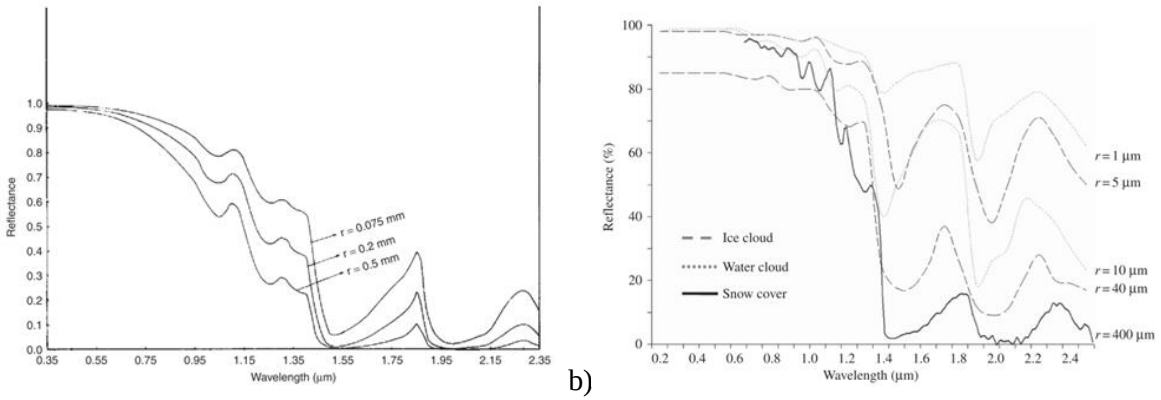

a) b)

Figure 2.2: a) Spectral signiture of snow depending on difference in snow crystals (Dietz, 2012), b) Difference in spectral signatures between ice clouds (cirrus), water clouds and snow cover (Dietz, 2012).

The most challenging aspect is snow-cloud separability uncertainty which hinders visibility of the underlying ground cover. Clouds are highly reflective in infrared channels and snow is not, this difference allows for distinguishing between the two objects in the image (Riggs et al., 2017). However, cirrus clouds, formed of ice crystals, remain difficult to separate from snow using the SNOWMAP algorithm because the spectral signatures are very similar (Hall et al., 2001). The visible closeness of spectral signatures between types of clouds and snow can be visualized in figure 2.2 (Dietz et al., 2012). Studies that use machine learning algorithms to further separate various cloud types from snow cover that have been relatively successful, such as convolution neural networks and support vector machines (Zhang et al., 2013 & Varshney et al., 2018). Improving models to further separate cloud and snow in classification algorithms does not assist in our understanding of what lies beneath the surface of cloud contamination. It can improve accuracy by reducing errors of omission and commission but methods to mitigate this contamination are necessary to map snow cover variability with temporal and spatial accuracy.

2.7 Cloud Mitigation Methods

There have been several methods introduced with the purpose of mitigating cloud cover from visible remote sensing, as this is persistently reducing accuracy and introducing

uncertainties. Categories of these methods include spatial methods, temporal methods, multi-sensor, and multi-step combinations.

2.7.1 Spatial Methods

This category of cloud removal or reconstruction is done by taking surrounding information and essentially interpolating the cloud cover pixels (Chen et al., 2017). Many methods exist to mitigate cloud cover in this category, however some of these are unusable for a temporally variable and heterogenous variable like snow cover (Liao, 2017). Spatial methods that are used for snow cover mapping that retain most of the accuracy include spatial filters (SF), snow line mapping approach (SNOWL) and locally weighted logistical regression (LWLR) (Parajka et al., 2010 & Li et al., 2019). Spatial filtering uses a given window, usually four or eight nearest neighbors, of adjacent pixels and uses this information to replace cloud contaminated pixels (Figure 2.3) (Hou et al., 2019). In the Austrian Alps this method retained an accuracy of 92% while mitigating 6-13% of cloud pixels (Hou et al., 2019).

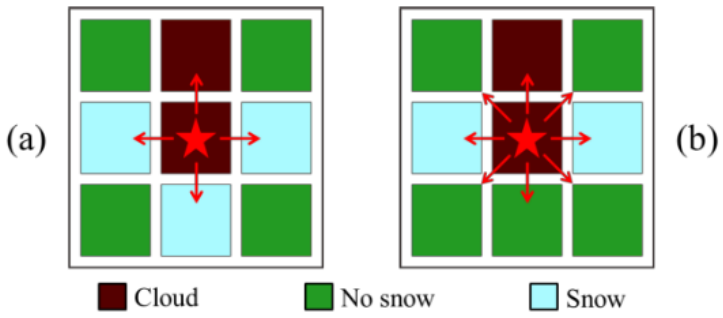

Figure 2.3: Spatial filtering reconstruction using a) Four pixel nearest neighbor, b) Either-pixel nearest neighbor (3x3 kernel) (Li et al., 2019).

Mountain snow is more prevalent and permanent at high elevations, this is the premise of the regional snow-line elevation method (SNOWL). This methodology uses the mean elevation of snow cover and no-snow covered pixels to interpolate cloud covered pixels based on their elevation (Parajka et al., 2010). If a cloud pixel is above the mean snow elevation it will be designated as snow, and if it is below the mean land elevation it will be

reclassified as land and those in-between will be partially snow covered (Figure 2.4) (Paraijka et al., 2010). The SNOWL method has been shown to reduce cloud cover percentage from 60% to 10% retaining an accuracy of 91.5% from 95.1% in the Austrian Alps (Parajka et al., 2010). However, elevation dependent interpolation shows higher accuracy when the image is already 70% cloud free (Gafurov & Bardossy, 2009). Therefore, there are steps that must be taken before implementing SNOWL.

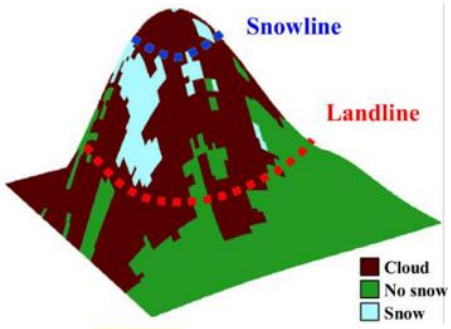

Figure 2.4: Snow line and land line designations for SNOWL method (Li et al., 2019)

Weighted logistic regression methods have also been effective in mountainous regions with respect to snow cover. Spatial and topographic characteristics of cloudy pixel are used to estimate probability of snow occurrence under that cloud cover (Lopez-Burgos et al., 2012). Depending on the study region there are a few combinations that can be used as explanatory variables, such as elevation, aspect, slope, etc. Overall, this regression method will assign a logistical curve with the inverse distance of neighboring pixels based on the characteristics of that pixel (Lopez-Burgos et al., 2013). In the Salt River basin in Arizona, this method reduced cloud cover by 93.8% while maintaining similar accuracy to the original image (Li et al., 2019). However, this is a complex method and requires high computation power compared to other spatial methods (Li et al., 2019).

2.7.2 Temporal Methods

Temporal methods utilize the movement of clouds to combine images that are temporally correlated. The most popular temporal method is the Terra and Aqua combination (TAC). Since these satellites are of similar design and the snow product uses the same

algorithm, it is possible to combine them to reduce cloud coverage without reducing the accuracy of the product significantly (Li et al. 2019). This method assumes that there is no significant snowmelt between the overpass times of these two satellites (Li et al., 2019). Although Aqua MODIS band 6 failed early on its life, the substituted band 7 has proven a useful replacement to facilitate the snow cover product continuance (Gladkova et al., 2012). While there are slight differences between Terra MODIS and Aqua MODIS snow products, the TAC has comparable errors as the two products separately (Li et al., 2019). This method was used in western USA and found that 5-14% of cloud cover was removed with an overall accuracy of 89.7% which is 1.4% higher than Aqua and 0.7% lower than Terra (Gao et al., 2010).

Temporal filtering uses the same type of logic as TAC but is not same day combinations. Adjacent temporal deductions (ATD) use the day before and after an image to replace cloud cover pixels (Parajka et al., 2012). These methods do not reduce temporal resolution and retain accuracy. In one study, the accuracy of ATD was 96.3% whilst reducing cloud fraction by 25% (Gafurov & Bardossy, 2009). However, these methods assume that snow cover is unchanged between the interval of time used, which may be untrue during transitional periods. Thus, transitional periods, the accuracy of this method can be reduced (Gao et al., 2010). Multi-day combinations are also popular for snow cover mapping, an 8-day MODIS product is available for this (Hall et al., 2002). Multi-day combinations will reduce accuracies but will reduce cloud percentage more than ATD with the sacrifice of temporal resolution (Dong & Menzel., 2016). In transitional periods, multi-day combinations tend to overestimate snow cover, or hold onto snow longer than it is present (Li et al., 2017). Flexible multi-day combinations are not operational but do show decreases in cloud percentage with overall accuracies decreasing by 2.2% and 2.6% for 6 day and 8 day, respectively (Gao et al., 2010). However, with slight decreases in accuracy there is a reduction of cloud cover by 45.7% and 48.4% (Table 2.2) (Gao et al., 2010).

Table 2.2: Accuracy metrics for Terra and Aqua snow products with combined, ATD, and fixed day combination in clear (Oc), all sky conditions (Oa), cloud percentage (Pc), and snow accuracy for both clear sky (Sc) conditions and all sky conditions (Sa) (Gao et al. 2010)

		O_c (%)	P_c (%)	O_a (%)	Total images	S_c (%)	S_a (%)
Terra	MOD10A1	90.4	52.2	40.0	363 (151)	79.5	25.4
Aqua	MYD10A1	88.3	56.2	34.3	365 (152)	76.7	20.0
Daily combined	MODISDC	89.7	44.5	45.6	365 (152)	82.2	31.1
Adjacent temporal deduction	MODISATD	90.0	37.1	51.5	365 (152)	83.0	36.0
Fixed-day combination	2 days	89.5	27.0	60.8	183 (76)	85.5	47.7
	4 days	89.0	12.5	73.9	91 (39)	89.1	66.4
	6 days	88.2	6.5	79.9	61 (27)	90.9	77.8
	8 days	87.8	3.8	82.6	46 (21)	92.6	83.9
Multi-day combined	MODISMC4	89.2	14.3	72.0	160 (68)	87.6	64.3
	MODISMC8	89.3	7.2	79.4	141 (61)	89.2	76.5

2.7.3 Multi-Step Methods

Multi-step methods provide a combination of previously mentioned strategies for cloud removal. To maximize the amount of information available, these usually begin with a Terra and Aqua combination, followed by a spatial filter of sorts and an ATD or multi-day combination to reduce as much cloud as possible or remove clouds entirely (Li et al., 2019). There are various combinations of multi-step methods. Those mentioned have been developed in a variety of landscapes, SNOWL is focused in mountainous regions, TAC is universally used regardless of the landscape as are multi-day combinations.

The strategy for cloud mitigation in this research uses a multi-step methodology in a mountain dominated landscape. While adopting approaches from the literature, an addition of the VIIRS snow product (VNP10A1) to the TAC for a same-day combination with three observations instead of two. However, instead of prioritizing cloud pixel reclassification based on pixel value, it will be done based on the reported overall accuracy of each of the products themselves. This will be followed by an ATD of +/- 2 days to reduce as much cloud as possible whilst retaining maximum accuracy in the off season, followed by a spatial filter and finally the implementation of SNOWL. These methods will be applied to the Thompson-Okanagan region, from valleys to the Rocky Mountains this method will be tested on a variety of landcover. Overall objectives of this research are to identify the benefits of adding VIIRS snow product to reducing cloud contamination, as well as comparing the accuracies

between all methods, and quantifying how much cloud is removed throughout the entire process. Finally, we aim to identify and understand variability of snow cover patterns in this diverse region through this methodology.

Chapter 3
Study Area

This chapter provides an overview of the study area. It is divided into subsections that explain the geographic, economic, and climatological aspects of the region.

3.1 Thompson Okanagan Region

This study will focus on the Thompson Okanagan region of British Columbia (Figure 3.1). This portion of central BC is classified as an economic region which consists of several watersheds, most of which are partially covered. These watersheds include South Thompson, Thompson, Okanagan, and Columbia, which form the largest tributary to the Fraser River, the Thompson River (Figure 3.2) (Beacham & Withler, 2017). This region occupies 94,197.76 km^2 of central BC (Statistics Canada, 2017).

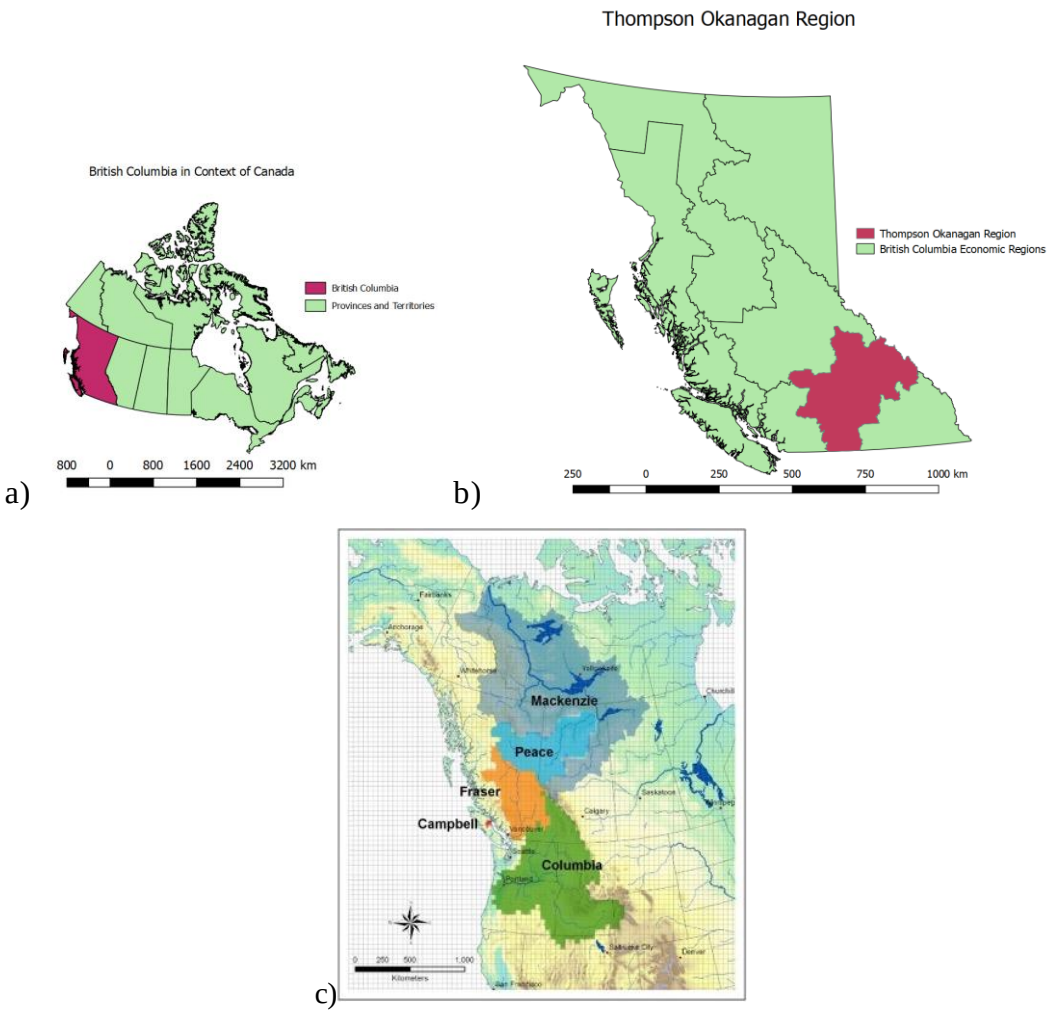

Figure 3.1: a) British Columbia in the context of Canada, b) BC economic regions including Thompson Okanagan and c) major water basins in BC

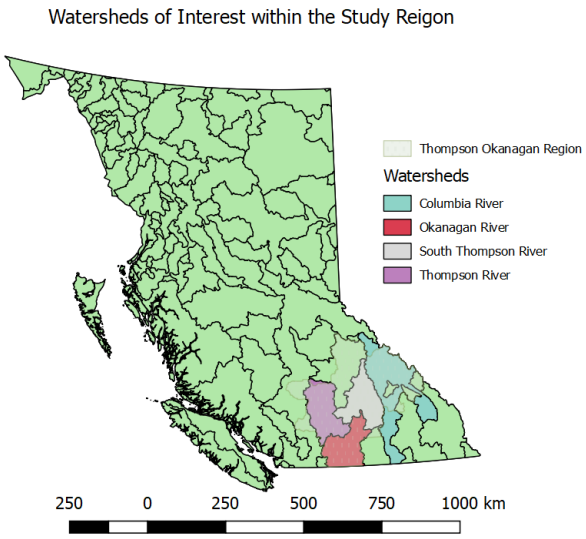

Figure 3.2: Watersheds in southern British Columbia with Thompson-Okanagan region overlapping

This study focuses on the economic south-central region of BC because of the influence snow has on the economic activity of this region (Picketts et al., 2012). The highest ranked climate impacts on this region are forest fires and disease, water quality degradation and water shortages (Picketts et al., 2012). Each of these impacts are directly connected to snow patterns in the region. The cloud index in this region is also lower than other mountainous regions because of its unique geographic position (Wilson & Jetz, 2016). The SCE data are analyzed throughout the watersheds within the Thompson Okanagan region (figure 3.2). The area in general was chosen for several reasons;

1) The climate in this region is characterized as semi-arid and therefore is less affected by continuous cloud coverage compared to other mountainous areas which makes it an excellent candidate for the proposed method (Caprio & Quamme, 2002),
2) It contains various landscapes including mountain ranges, valleys, forested land and developed areas, which allows for the proposed method to be investigated under a variety of conditions,
3) Snow cover in this area is crucial to economic success (see section 3.1.2).

3.1.1 Geographic Characteristics

The Thompson region is in the southern central interior of British Columbia. BC has a very diverse landscape, from the Coast Mountains on the west to the Rocky Mountains and Cariboo Mountains on the eastern extent to the central plateau and Thompson Plateau in the interior (Church & Ryder, 2018). This diverse landscape was formed through tectonic regimes throughout the Tertiary times, extreme erosion, glacier movement and volcanic activity (Church & Ryder, 2018). The Thompson-Okanagan region itself varies in elevation, from low valleys at 150 m.a.s.l. to about 3500 m.a.s.l. (Shrestha et al., 2012). This region is incased with mountain ranges, Coastal on the west and Cariboo, Selkirk, and Monashee to the east (Tribe, 2005). These mountains are massive sources of drainage into the Fraser River from this region, these drainage patterns are mostly characterized by a south and southwest movement (Tribe, 2005). There are some exceptions to this, for example the Shuswap River flows northwest to the South Thompson River (Tribe, 2005). Main river systems in this region are the Thompson River, North and South Thompson Rivers which meet in Kamloops and flow into the Fraser River at Lytton (Merritt et al., 2006). The Nicola River and Clearwater Rivers are also notably large tributaries from this area into the Fraser (Merritt et al., 2006). Overall, the area is mostly covered by vegetation, alpine or coniferous forests (Shrestha et al., 2012).

3.1.2 Human & Economic Activity

There are a few major cities in the region including Kamloops, Kelowna, Osoyoos and Princeton (Destination BC Corp, 2019). Thompson-Okanagan is home to an estimated 15% of the population of British Columbia (Statistics Canada, 2017). Most of the economic activity here is natural resources, forest industry, mining, agriculture, manufacturing, and tourism (Fraser Basin Council, 2013). The wine industry is especially important in this region because of the favorable climate for growing grapes, Okanagan is known for wine production (Rayne & Forest, 2016). However, this is an extremely sensitive process and fluctuations and increased variability in weather patterns have destroyed harvests in the past and can continue to do so with increasing variability (Caprio & Quamme, 2002). Studies

show that elevated temperatures throughout April-July are favorable for grape production, however, increasing temperatures passed a certain threshold during these periods cause a dramatic decrease production (Caprio & Quamme, 2002).

Tourism activities here are very heavily dependent on snow. This area is home to several ski resorts that attract people from all over the world. There are 3 major ski resorts (Big White, Silver Star and Sun Peaks) within this region, as well as the Okanagan Valley wine country which heavily depends on temperature stability for the growth of healthy wine grapes, and the salmon fishing industry is largely impacted by changes in water levels and storage in mountains- directly impacted by snow cover variations (Rayne & Forest, 2016 & Islam, 2017). However, with increasing temperatures projected by many studies, the snow season could potentially shorten, and parts of this region could transition into rain dominated areas (Islam et al., 2017). Understanding the patterns of snow in this region also affect potential hazards of flooding in cities surrounding the Fraser River because its flow is dominated by snowmelt during the spring freshet (Kang et al., 2014). The Fraser River is also home to one of the largest salmon populations in the world, changes in spring freshet may risk these salmon populations by increasing winter flows and decreasing spring and summer flows (Kang et al., 2014). Snow storage is also an important source for water resources for irrigation and domestic use in this region (Merritt et al., 2006).

Temperature warming has proven to directly impact the economy in Canada as economic losses due to the El Nino event in 1997-98, for example, brought by drought were $2 billion to crop damage alone (Shabbar, 2014). Irrigation of crop lands in interior BC depend on mountain snow melt in the Rockies (Winkler et al., 2017). Economic loss this year spanned a loss in $1.5 billion to the heating industry, $300 million in recreation industry and $500 million in Canadian fisheries (Shabbar, 2014).

3.1.3 Weather and Climate

The semi-arid climate in Thompson-Okanagan contrasts with that of other areas in BC. The Coast Mountains control the climate in this region acting as a barrier and setting up the distinct climate on the leeward side of these mountains (Smith et al., 2008). This causes

the semi-arid climate in this area, the reduction of precipitation caused by air subsidence due to its proximity and alignment with the mountains (Smith et al., 2008). During the winter, temperatures are around -5.7 degrees Celsius (Merritt et al., 2006). The Fraser River Basin is classified as containing snow dominated basins, but this south interior region is a hybrid of rain and snow (Shrestha et al., 2012). The weather systems in this region are affected by upper troughs which cause vertical lift leading to clouds and ultimately precipitation, and by orthographic lift on the coast (Klock & Mullock, 2001).

The Thompson Okanagan region, partly located within the Fraser River Basin, is ecologically, economically, geographically, and climatologically diverse. This area is extremely sensitive to warming and there are vast implications climate change will have on the economy, through natural resources and tourism, wine production and salmon populations as well as water resources (Islam et al., 2017). For these reasons, the regions springtime snow cover should be monitored and analyzed to contribute to recent findings and trends in snow cover variability and potential impacts on water storage.

Chapter 4
Cloud Mitigation Methodology

This chapter is split into four sections. This includes the satellite and other data used in the methodology followed by the pre-processing steps taken. The multi-step cloud mitigation methodology is then presented followed by the evaluation of the technique. This also includes methods taken to analyze the snow cover data extracted.

4.1 Satellite Instruments and Data

This study uses the Moderate Imagine Spectroradiometer (MODIS) daily snow product data from both Terra and Aqua satellites (MOD10A1 and MYD10A1), as well as the Visible Infrared Imaging Radiometer Suite (VIIRS) snow product (VNP10A1). Terra was released in December of 1999 and Aqua in May of 2002 (Hall et al., 2002). This instrument collects data in 36 bands, with wavelengths from 0.4-14.4 micrometers, it has a revisit period of 1-2 days and the repeat period is 16 days (Hall et al., 2002). Its large swath of 2330 km allows for daily imaging of the Earth (Hall et al., 2002). The imaging spatial resolution varies from 250 m in two bands, 500 m in 5 bands and the remaining 29 bands are in 1 km resolution, Aqua specifications are identical (Hall et al., 2002). The high temporal resolution and moderate spatial resolution of MODIS observations, and the accessibility of MODIS products make them a critical tool for earth observation science. MODIS products include soil moisture, fire indices, evapotranspiration, surface temperature, chlorophyll etc. which can be accessed through the EarthData database created by NASA. For this study, the snow product will be used (MOD10A1, MYD10A1). These products use the SNOWMAP algorithm developed by Dorothy Hall to calculate snow cover percentage in each pixel based on radiances and indices calculated through thresholds of NDVI and NDSI (Hall et al., 2001).

VIIRS was launched in October of 2011 on the NOAA's Suomi National Polar-orbiting Partnership (Suomi NPP) carried out by NOAA. It carries 9 visible and near-infrared bands (NIR), 8 mid-infrared bands, and 4 longwave infrared bands (Riggs et al., 2017). It has

a spectral sampling of 0.412-12.01 micrometers (Riggs et al., 2017). VIIRS has a 16-day repeat cycle and a daily revisit made possible by its large swath of 3060 km (Riggs et al., 2017). The spatial resolution is variable, 16 of the bands are at 750 m and 6 of the bands are at 375m (Riggs et al., 2017). The VIIRS snow product follows Riggs et al., (2017) and includes a fractional snow product. VIIRS observations are also incorporated into the IMS and Globsnow products since 2013 (Riggs et al., 2017). These products are available in an EASE-Grid format. Both MODIS and VIIRS products incorporate cloud masks (Hall & Riggs, 2015 & Riggs et al., 2017). Overall, the algorithms of MODIS and VIIRS snow products are essentially the same, with differing resolutions and slight differences in spectral sampling. The biggest difference with the snow products is the differences in the cloud masks. Some bands used in the MOD35_L2 mask are not available for the VNP35_L2 which cause inherent differences in classification between the two products (Hall et al., 2019).

Landsat-8 OLI is the most recent satellite in the Landsat series, launched in February of 2013 and is continuing to orbit (Barsi et al., 2014). Landsat-8 OLI overpass time is 10:00 am over the equator +/- 15 minutes (Li & Roy, 2017). The USGS provides various levels of Landsat-8 data, for the purposes of this study collection 2 level 2 data will be used. Level-2 process is done only on level-1 data that meets the requirement of a solar zenith angle less than 76^{o} (Engebretson, 2020). Level-1 data is radiometrically calibrated using ground control points and digital elevation models (DEM) in this instance, as the products used in this research are L1TP (Engebretson, 2020). These datasets are also geometrically corrected using cubic convolution resampling method (Engebretson, 2020). Level-2 data processed after these corrections and are radiometrically, atmospherically corrected and delivered as surface reflectance (Engebretson, 2020). Table 4.1 shows the band specifications of the collection 2 level 2 Landsat OLI data products.

Table 4.1: Landsat-8 OLI band designations (Adeyeri et al., 2017)

Band name	Band Width (μm)	Resolution (m)
Band 1 Coastal	0.43–0.45	30
Band 2 Blue	0.45–0.51	30
Band 3 Green	0.53–0.59	30
Band 4 Red	0.64–0.67	30
Band 5 Near Infrared (NIR)	0.85–0.88	30
Band 6 Short Wave Infrared (SWIR) 1	1.57–1.65	30
Band 7 SWIR2	2.11–2.29	30

For evaluation based on landcover type, a MODIS landcover product (MCD12Q1) was used. This is an annual product with a resolution of 500 m that contains a variety of classification methods, for the purposes of this study the International Geosphere-Biosphere (IGBP) land classification scheme was used. This classification scheme uses a year of 8-day MODIS adjusted reflectance data (Sulla-Menashe & Friedl, 2018). Collection 6 was classified using the Land Cover Classification System (LCCS) developed by the Food and Agriculture Organization, using a nested classification system (Sulla-Menashe & Friedl, 2018). There are some uncertainties within this product including underrepresentation of wetlands, misclassification of grasslands and glacial regions that are covered by topographic shadows being mapped as water (Sulla-Menashe & Friedl, 2018). This product was gathered for each year that is included in the validation portion, where data is available (2018, 2019). The NASA Shuttle Radar Topographic Mission (SRTM) digital elevation model (DEM) was used as ancillary data. The 30 m resolution data was gathered from the USGS EROS archive. Table 4.2 provides a summary of the snow datasets used in this research.

Table 4.2: Data details for satellite imagery used in this study (Riggs et al., 2017 & Hall, 2002)

	Launch date	***Spectral Sampling***	***Repeat/Revisit/Swath***	***Spatial Resolution***	***Product***	***Bands Used for Snow Product***
MODIS	Terra: 12/1999 Aqua: 5/ 2002	36 bands 0.4-14.4 micrometers	Repeat: 16 days Revisit: 1-2 days Swath: 2330 km	2 bands: 250m 5 bands: 500m 29 bands: 1km	M*D10A2 MCD12Q1	4,6/7, 13, 16, 20, 26, 31 & 32
VIIRS	Launch:10/ 2011	9 visible/NIR infrared bands, 8 mid-IR, 4 LW-IR bands 0.412-12.01 micrometers	Repeat: 16 days Revisit: Daily Swath: 3060km	16 bands: 750m 6 bands: 375m	VNP10A1	I1, I3, M10
Landsat -8 OLI	02/2013	11 bands, Visible, NIR, SWIR, TIR	Repeat: 16 days Revisit: 8 days Swath: 185km	Band 1:15 m Vis and SWIR: 30 m	Level-2 Data	3,4,5,6

Analysis was focused on the three months from the year 2003 to 2019 during the spring freshet from April-June. However, the data was gathered from March 30th to July 2nd from 2003-2019 to ensure that the periods were covered. Landsat-8 OLI data is present from 2013-2019, these images are gathered within the study area for all these years where there is <20% cloud cover present.

4.2 Data Pre-processing

MODIS Terra/Aqua products were acquired through NASA's Earth Data platform in two tiles (h10v03, h10v04). These products were downloaded in a geographic coordinate system and are georeferenced and corrected for slope and aspect through the Global 30 Arcsecond digital elevation model (GTOPO30 DEM) (Hall & Riggs, 2015). For each year

the files were separated by tile identification and date and mosaicked as such. Then they were cropped and masked to a Thompson Okanagan shapefile acquired from the GIS database from the University of British Columbia. VIIRS data was gathered from the same source from 2012-2019. However, VIIRS is only available in sinusoidal EASE-grid format, so these files were re-projected to the WGS84 geographic coordinate system using a nearest neighbor method. VIIRS images were resampled to the same resolution as MODIS from 375 m to 500 m using nearest neighbor interpolation once more. These VIIRS images were also collected in 2 tiles (h10v03, h10v04). The projected, re-sampled VIIRS images are then separated by tile and date and mosaicked and cropped and masked to the same Thompson Okanagan shapefile. The DEM was resampled to 500 m and cropped to the study region. Landcover classification MODIS images were cropped to the study region.

4.3 Multi-Step Cloud Mitigation

Terra and Aqua acquisition times are 3 hours apart, as Terra crosses the equator at 10:30 am and Aqua at 1:30 pm, VIIRS crosses at 1:00 pm (Miller et al., 2013). To mitigate cloud contamination, a simple workflow was adopted. First, all pixels that are classified as "cloud", "missing data", "no decision" and "detector saturated" are all removed and replaced with NA values for Terra, Aqua and VIIRS. This is a conservative approach to mapping; however, this is done to ensure that all the valid pixels from all sources are utilized. The Terra images are prioritized as they have the highest reported cloud accuracy throughout compared with Aqua and VIIRS (Key et al., 2013; Wang et al., 2009; Chelamallu et al., 2014). The pixels labelled NA for Terra are replaced with cloud-free pixels from VIIRS or Aqua if VIIRS data are cloud contaminated. No class is prioritized in this method, it is based on the raw classification of each dataset and their position in the algorithm. The workflow for this combination is summarized below (figure 4.1).

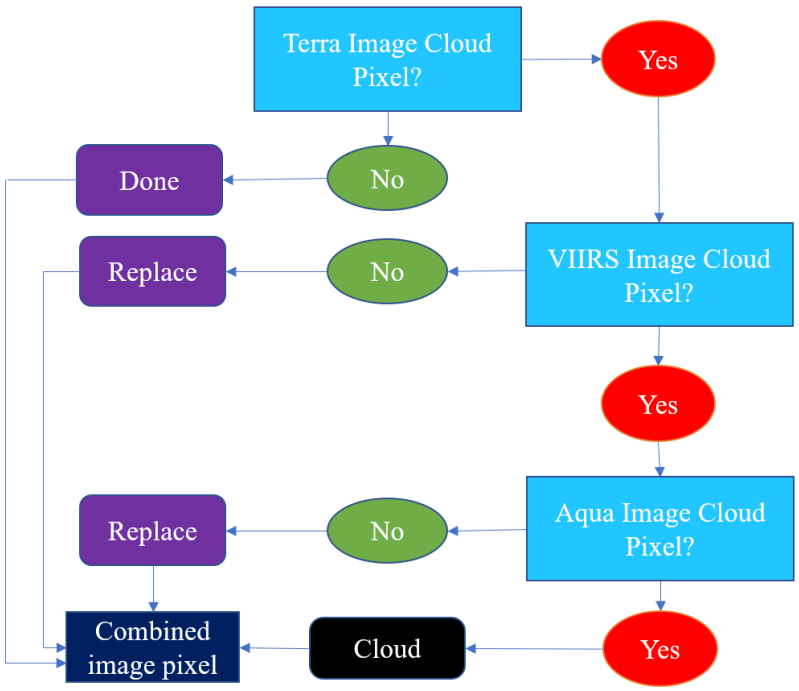

Figure 4.1: Diagram showing the cloud pixel replacement for Terra, Aqua and VIIRS

It was necessary to use the highest accuracy snow mapping estimates as possible. Aqua MODIS experienced a band 6 failure which impacts the snow and cloud mapping capability. Therefore, despite the restoration of band 6 sensors for Aqua, the SNOWMAP algorithm using Aqua exhibits lower accuracies than Terra and VIIRS (Key et al., 2013; Wang et al., 2009). Similarly, VIIRS also has lower reported accuracy than Terra (Chelamallu et al., 2014). This approach was adopted for years where VIIRS is available (2012-2019). Prior to 2012, a Terra Aqua combination (TAC) was adopted (Figure 4.2).

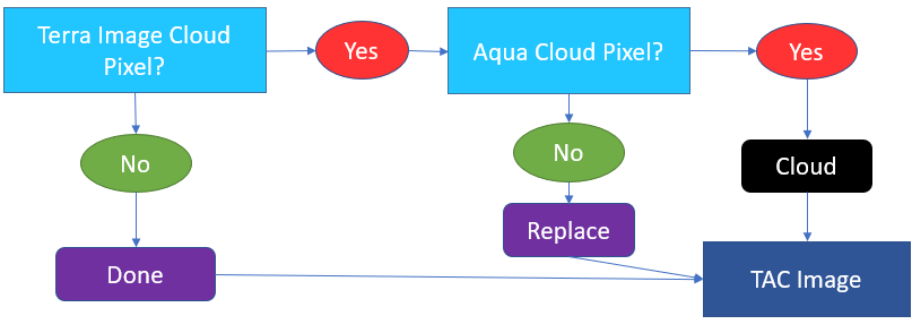

Figure 4.2: TAC cloud pixel replacement flow diagram

Having created a combined product of Terra, Aqua and VIIRS for 2012-2019 and a TAC for 2003-2011, an adjacent temporal deduction was performed to further mitigate cloud cover. This entails using the same function to replace same day pixels but applied to prior and subsequent days. Pixels were used from the day i-1 (previous day) followed by the subsequent day, i+1, to ensure a snow-covered pixel was not prematurely labeled as "no-snow" if snow melted during day i. This methodology was repeated for ATD +/-2 days if the pixel remained cloud-covered.

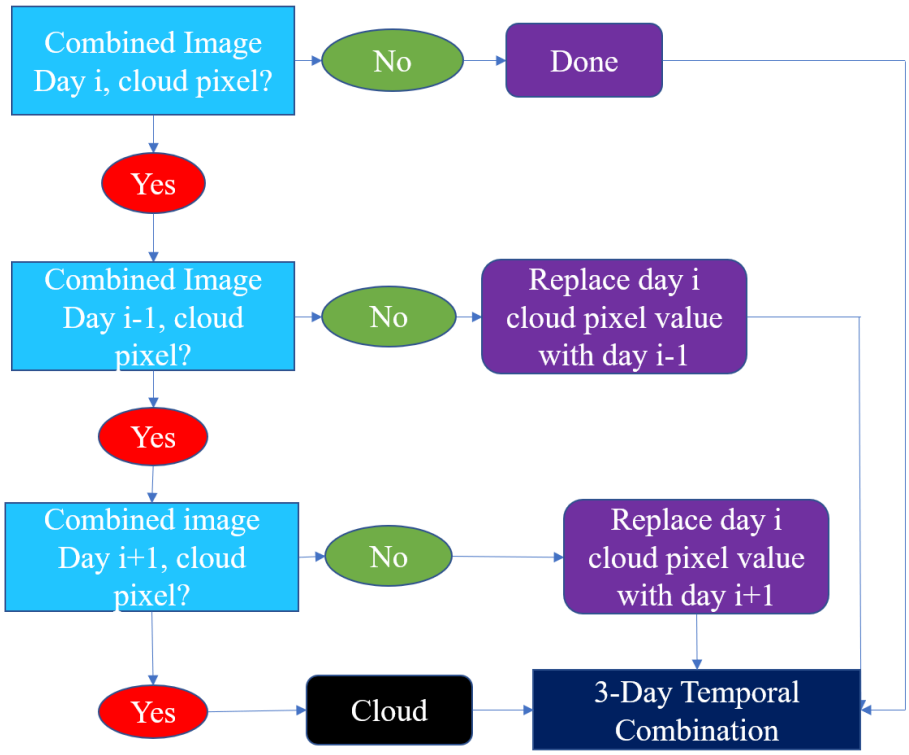

Figure 4.3 Flow chart for +/-1-day ATD for combined images

After a 2-day temporal filter was applied, a spatial filter was applied to the output images to further mitigate cloud contamination. Spatial filters have been used as part of a stepwise cloud removal process (Poggio & Gimona, 2015; Li, 2019). Some spatial filters incorporate terrain elevation and aspect as major drivers to the reclassification (Tong et al., 2009). Other spatial filters are done with using a majority-based approach, where a cloud pixel will be reclassified based on values of the nearest neighbors (Lindsay et al., 2015).

Some other approaches consist of snow and land-line rule-based approaches (Parajka & Broschl., 2008). In this study a 3x3 kernel (1500 x 1500 m) focal filter was applied to the 2-day temporally filtered images. Images were first reclassified as binary snow / no snow pixels based on a threshold of 50% snow cover. Meaning that pixels with a fractional snow cover >=50% were assumed to be snow and <50% no snow. This kernel uses the value of the nearest 8 pixels to interpolate the missing value. The spatial filter was added after the temporal filter to fill in as much of the large cloud coverage areas as possible prior to the spatial filter to maximize its effectiveness.

The last step for cloud mitigation is the implementation of the SNOWL method, proposed by Parajka et. al. 2012. The SNOWL method calculates mean elevation for all snow pixels and no snow pixels within a region (Parajka et al., 2012). These are then the "snow-line" and "land-line" elevations, cloud pixels above the snow-line elevation will be reclassified as snow and cloud pixels below the landline will be reclassified as land (Parajka et al., 2012). Pixels in between these two elevations are considered partially snow-covered and will be left as cloud for the purpose of this study. The accuracy of this procedure was higher for snow onset and offset and is effective and robust in mountainous regions (Parajka et al., 2012). Therefore, it is a fitting addition to the cloud mitigation methodology. The location of clouds is highly sensitive to this method. If cloud cover is focused at mid elevations, which is often the case in certain years, the snow line elevation estimation will be too high and snow cover will be underestimated. Images where cloud cover is greater than 25% throughout the whole area prior to this step will be excluded from the study, as another study using an elevation dependent interpolation method concluded that reliable cloud removal requires at least 70% of the image to be cloud free prior to the methods implementation (Gafurov & Bardossy, 2009). Figure 4.4 below shows a flow chart of this step in the methodology. This concludes the cloud-mitigation method, the overall steps are shown in figure 4.5.

Cloud cover will be extracted as a proportion of the area for each step in the methodology to compare the cloud mitigation throughout the entire methodology. Cloud

duration maps were also created where each pixel represents the number of days it was cloud covered. These were constructed for each year up to and after the SNOWL method for visual comparison for the efficacy of this method.

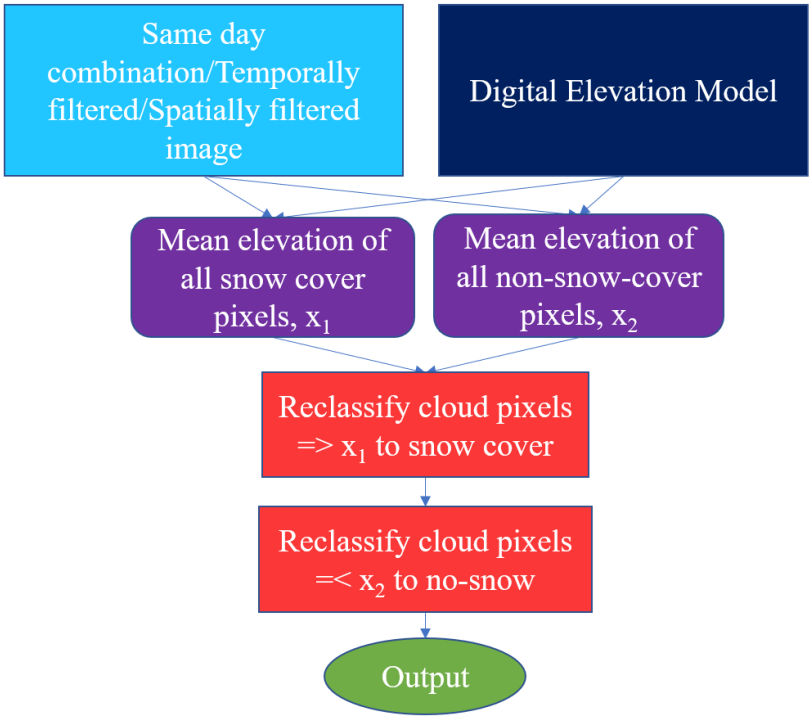

Figure 4.4: SNOWL reclassification of cloud covered pixels above and below the calculated elevations "snow-line" and land-line"

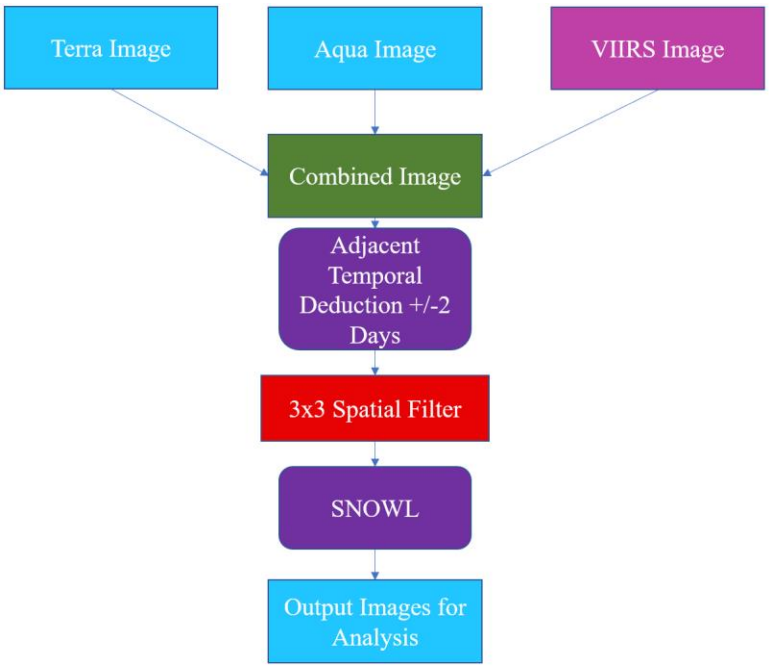

Figure 4.5: Overall methodology of the combined snow product data that combines the TAC, ATD and SNOWL methods to produce cloud-mitigated snow cover extent.

4.4 Evaluation of Cloud Mitigated Daily Snow Product

In situ snow measurements in this region were sparse and limited to 7 points throughout the area, mostly concentrated at medium to low elevation. Therefore, moderately high-resolution imagery was used ground-reference data to evaluate the moderate resolution (MODIS/VIIRS) product. A comparison study between MODIS FSC algorithm applied to Landsat ETM+ showed an adjusted R-square of 0.95 in an ordinary least square's regression and an RMSE of 10% in a mountain domain (Crawford, 2015). The disagreement between the two datasets was attributed to cirrus clouds, the aggressiveness of the MOD35_L2 cloud mask and thin patchy snow as this study was done during the off season in a mountain terrain (Crawford, 2015). Landsat also showed a lower FSC than MODIS in some cases, which was a result of a transient snow fall between the overpasses of MODIS and Landsat ETM+ (Crawford, 2015). Landsat-8 OLI has also been used for validation of cloud mitigation methods on MODIS products throughout the Tibetan Plateau by using a binary thresholding algorithm like that of the MODIS FSC SNOWMAP (Deng et al., 2015). This found R^2 values

ranging from 0.4-0.91 after a TAC, ATD, SNOWL and composite with AMSR2 was done (Deng et al., 2015). The agreement between the datasets also highly depends on type of land measured. For instance, grasslands have the highest R^2 at 0.91, whereas forested lands fall to 0.4 with this dataset (Deng et al., 2015). Therefore, the overall agreement of Landsat OLI and the MODIS product is relatively high. The largest differences between high resolution and moderate resolution snow mapping is that with high resolution it is easier to identify snow under forest canopies (Chokmani et al., 2010). In this case, a binary snow mapping approach is taken with a similar thresholding algorithm to SNOWMAP with an additional parameter targeting snow covered forests to assess agreement between high spatial resolution and the combined snow cover product.

Overall accuracy of MODIS products is between 85 and 99% in clear conditions, with identifying snow cover in forested regions being a limiting factor (Parajka et al., 2012). These areas exhibit a decrease in accuracy due to patchy or thin snow in underlying canopies as well as reflectance of snow changing in forested areas which requires high resolution to depict (Jain et al., 2008; Chaponniere et al., 2005). In forested areas under all-sky conditions, accuracy can be as low as 50% (Crawford, 2015). A series of level-2 Landsat-8 OLI products were used from 2013-2019 to compare with MODIS Terra/Aqua and VIIRS products separately as well for each step in the cloud mitigation methodology.

Although a topographic correction is usually a pre-processing step for rugged terrain, in this case it was not. Cosine correction (c-correction) is used for Landsat images to smooth images and correct reflection values (Wang et al., 2018). This method uses the solar zenith angle, solar azimuth, aspect, and slope to correct and remove effects of topographic shadows (Wang et al., 2018). However, after running a c-correction on the Landsat images, it was clear that the change in surface reflectance values for each individual band distorted data values. Since the data was being used to create indices (NDSI, NDVI), which can detect snow-cover in shadowed regions, applying a c-correction was not justified (Moreira et al., 2016). Research indicates that this method was 94% when compared to a GF-1 high resolution image acquired at the same time as the Landsat OLI image without topographic correction and only increased to 94.5% when topographic correction was implemented

(Wang et al., 2015; Wang et al., 2018). VIIRS and MODIS snow products assign "No Decision" to pixels with low illumination (solar zenith angle >70°) in the visible spectrum to minimize uncertainty of snow-cover pixels when cloud shadows or terrain shadows cause low reflectance (Hall et al., 2002; Riggs & Hall, 2015; Riggs et al., 2017). As mentioned earlier, these "No Decision" pixels will be changed to NA, which are removed for the evaluation to only measure agreement between snow-covered and land-covered pixels.

A threshold method for the normalized difference snow index (NDSI), normalized difference vegetation index (NDVI) and a normalized difference forest snow index (NDFSI) was used for snow extraction in Landsat-8 OLI images. NDFSI is calculated with the NIR band and the SWIR band (7). Using the NDFSI with NDSI and NDVI thresholding was chosen to minimize snow pixel false negatives in forest covered areas (Wang et al., 2015). This binary method mimics the MODIS SNOWMAP algorithm with the addition of the NDFSI to better distinguish snow cover in forested areas.

$$NDFSI = \frac{NIR-SWIR}{NIR+SWIR} \quad (5)$$

$$NDVI = \frac{NIR-Red}{NIR+Red} \quad (6)$$

$$NDSI = \frac{Visible-SWIR}{Visible+SWIR} \quad (7)$$

With the NDFSI, it is possible to distinguish snow covered forests as the NDFSI value is higher under these circumstances (Wang et al., 2018). A pixel is classified as snow initially if it has an NDSI value over 0.4 and a reflectance in the NIR above 11%. An NDSI cutoff of 0.4 corresponds with a 50% snow covered pixel (Nagler et al., 2016). The pixel will remain classified as snow cover if the green band reflectance is above 10% to reduce any false classifications of dark vegetation (Hall et al., 2001). The last threshold from SNOWMAP is the SWIR reflectance, as previously mentioned snow SWIR reflectance is about 0.20 or less and in some cases with low solar angels can range from 0.25-45 (Riggs & Hall, 2015). Thus, a threshold is placed so that any pixels with a SWIR > 0.45 are flagged as no snow. The temperature and elevation portions of the algorithm were not used in the binary snow map. These additional arguments for SNOWMAP are to reduce commission errors in warm coastal regions, subtropical forests and high reflective landcover such as salt flats and

omission errors in warm mountain regions (Riggs & Hall, 2015). Additional snow in forested regions are identified using the NDFSI.

To analyze the efficacy of using the NDFSI for detecting snow cover in forested regions, three dates throughout the off season in 2015 were chosen, April 20th, May 13th, and June 7th. This year was selected because it contained images from each month throughout the season that had minimal cloud cover. For each date 3 regions of interest were selected guided by the Landsat landcover classification image of Canada for selecting a snow, forest, and snow-covered forest regions of interest (ROI). These ROIs were not gathered from the exact same areas for each date and so the number of pixels selected for each ROI on each date varied. Figure 4.6 shows the NDVI-NDSI values for each class. A considerable number of snow-covered forest pixels are excluded from the SNOWMAP thresholding algorithm as they exhibit an NDSI lower than 0.4. However, figure 4.7 shows the values of NDVI-NDFSI, in these figures it is possible to visualize the differences in index values for these three classes as well as to see the number of forest snow pixels that would be included in the binary snow map using the NDFSI.

The first date, April 20th, shows a less clear boundary between open snow and snow-covered forests. During this period, snow cover is still prominent in the area and snow underneath the canopy will have similar reflectance characteristics to open snow cover. Conversely, the remaining dates show clear discrimination between the classes (Figure 4.6). This is because throughout the snow off season, the snow underneath canopies will become contaminated with dirt and dust that change allows for differences between open snow and snow-covered forests to be more separable. However, this also stretches the distribution of NDFSI values beyond the threshold of being classified as snow cover (Figure 4.7). This can be explained simply, as snow cover in forests becomes patchier the NDFSI value will be smaller and the pixel does not contain enough snow to be classified as such any longer. The NDSI of snow-covered forests are shown to have a wider range of values which is reflected by the mean values in table 4.3 from 0.3 near the end of the snow season to 0.6 at the start of the study period. Conversely, the mean of pure snow cover is stable at ~0.9 (Table 4.3).

Since the threshold of snow cover is NDSI > 0.4, snow cover under canopies would be largely underrepresented (Figure 4.6).

The disparity of these NDFSI values between snow covered forests and pure snow are utilized in the thresholding algorithm. The red lines throughout figure 4.6 and 4.7 show the thresholding values themselves. In figure 4.6 it is shown how much snow under the canopy would result in omission errors with the NDSI thresholding of MODIS SNOWMAP collection 5. Figure 4.7 shows the addition of forest snow covered pixels using the added NDFSI thresholding. Although the mean values between NDFSI and NDSI values do not show a significant difference, the figures displaying the data show the distribution of NDSI and NDFSI values of snow-covered forests (figure 4.6-4.7). From these ROIs and summary statistics, the decision to use the NDFSI in collaboration with the original thresholding of the SNOWMAP algorithm can be justified.

Table 4.3: Means and standard deviations of NDSI, NDVI and NDFSI for the three landcover types (snow, forest and snow covered forests)

	April 20th		*May 13th*		*May 22nd*		*June 7th*	
	n=1855		*n=1188*		*n=2280*		*n=425*	
Snow Covered Forest	**Mean**	**SD**	**Mean**	**SD**	**Mean**	**SD**	**Mean**	**SD**
NDSI	0.62	0.12	0.48	0.06	0.54	0.08	0.34	0.12
NDVI	0.11	0.08	0.12	0.02	0.15	0.03	0.22	0.04
NDFSI	0.68	0.08	0.56	0.05	0.66	0.05	0.53	0.07
Forest	*n=1870*		*n=1612*		*n=1457*		*n=1280*	
NDSI	-0.39	0.03	-0.51	0.04	-0.40	0.03	-0.32	0.03
NDVI	0.80	0.03	0.70	0.05	0.74	0.03	0.77	0.03
NDFSI	0.44	0.06	0.17	0.11	0.35	0.07	0.43	0.04
Snow	*n=5035*		*n=1936*		*n=1323*		*n=1960*	
NDSI	0.90	0.02	0.96	0.01	0.94	0.00	0.93	0.00
NDVI	-0.05	0.01	-0.11	0.00	-0.10	0.02	-0.08	0.00
NDFSI	0.89	0.02	0.95	0.01	0.93	0.00	0.92	0.01

This method was chosen for the ground-truth dataset to allow continuity between the MODIS SNOWMAP algorithm and the one shown here, but also to allow for added accuracy of forest snow mapping with the reference dataset. Decision rules for the Landsat-8 OLI

snow mapping algorithm is depicted in figure 4.9. The addition of NDFSI gives a better understanding of where MODIS, VIIRS and a combined product still have accuracy issues with forested landscapes. Snow covered forests NDSI are usually lower and therefore can be exempt in binary snow maps (Wang et al., 2018). Whereas, the NDFSI for these regions is high, within this dataset the mean value is 0.60 (Table 4.3). This additional index for thresholding binary snow maps have accuracies ranging from 93.5-94.5% (Wang et al, 2015; Wang et al., 2018). Figure 4.9 shows the binary snow map of the right hand and left-hand side of the thresholding algorithm to display the additional snow pixels captured with the use of the NDFSI threshold. Locations of these ROIs are available in Appendix A.

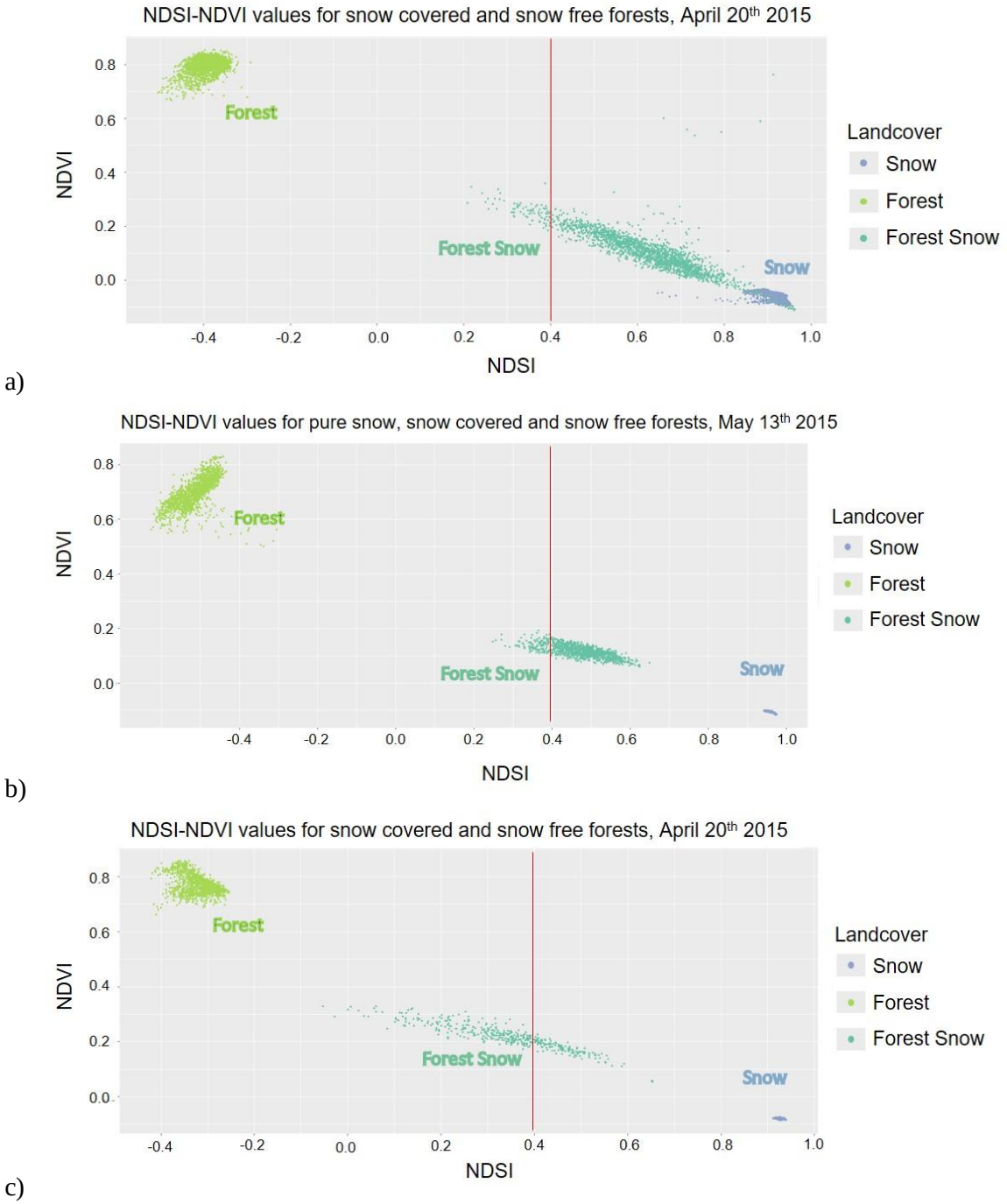

Figure 4.6: Landsat NDSI-NDVI values for forest cover, snow cover and snow covered forests for 3 ROIs, a-c red lines represent the base snow thresholding for MODIS SNOWMAP collection 6 for April 20th, May 13th and June 7th 2015

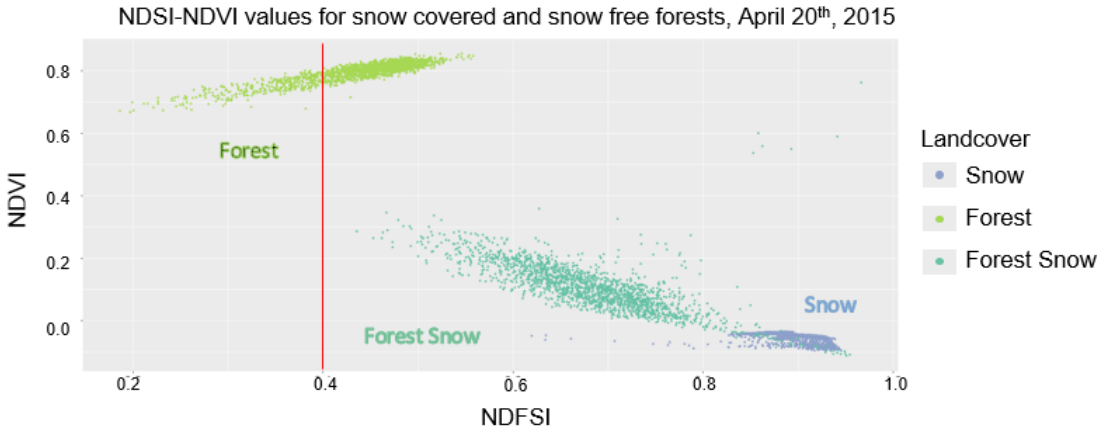

a)

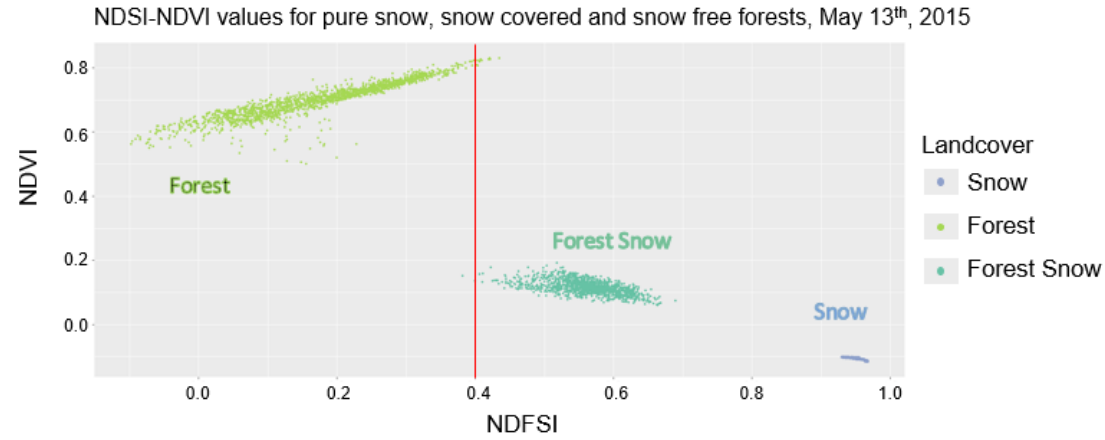

b)

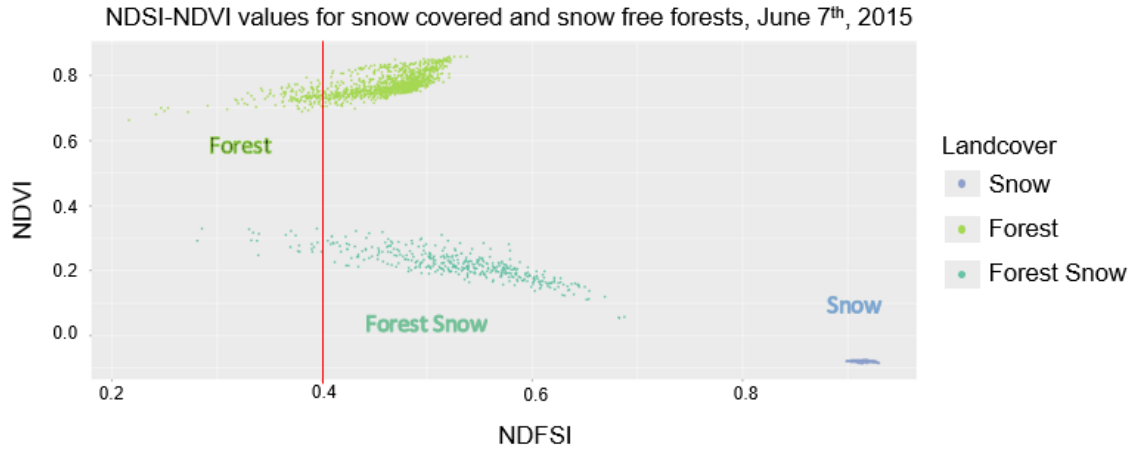

c)

Figure 4.7: NDFSI-NDVI values for forest cover, snow cover and snow covered forest for 3 ROIs, a-c show red lines representing snow thresholding values according to original SNOWMAP for April 20th, May 13th and June 7th 2015

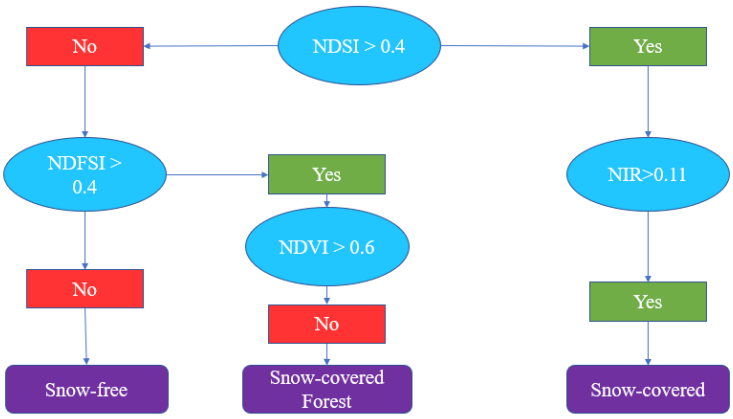

Figure 4.8: Adjusted decision rules for binary snow map of Landsat-8 OLI images (Wang et al., 2018)

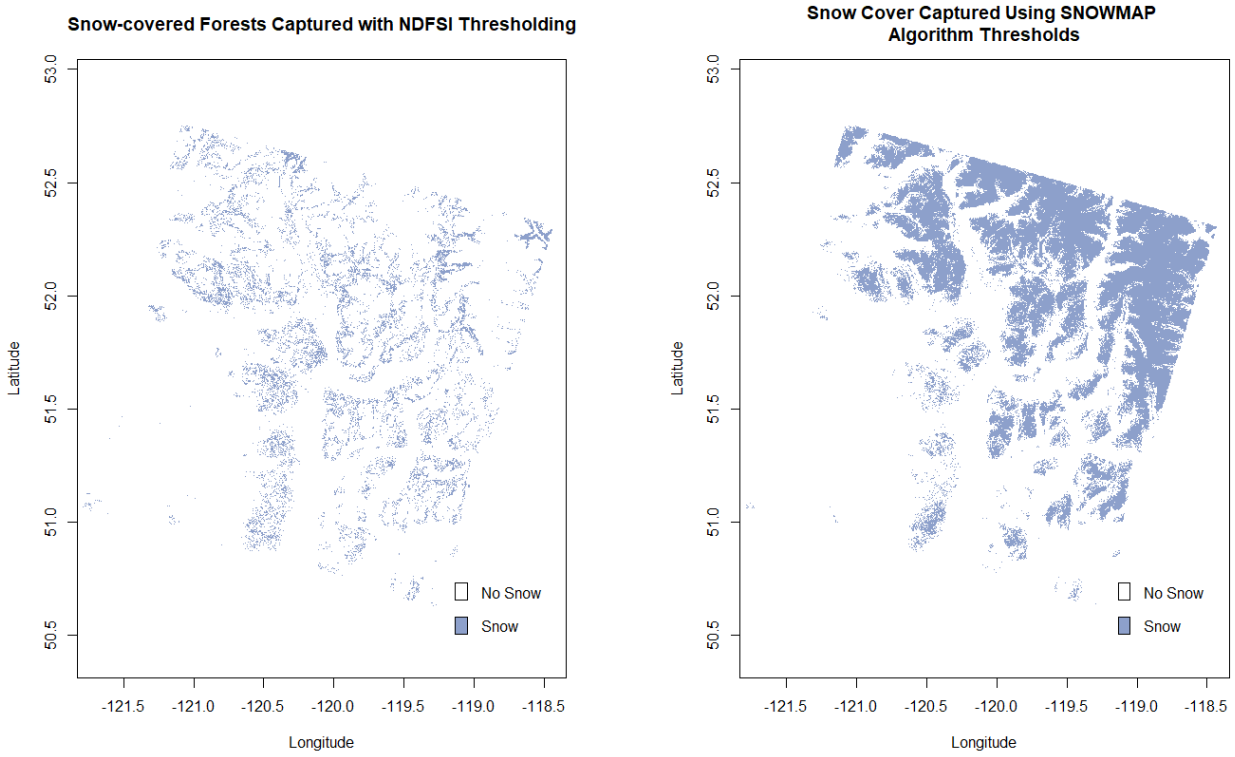

Figure 4.9: Left: Landsat snow cover using NDFSI thresholding with NDSI <0.4., Right: Landsat snow map using the MODIS thresholding with additional thresholding arguments of SWIR, green and NIR bands on April 20th, 2018

Only Landsat-8 OLI images that contained <20% cloud cover was used for the accuracy assessment from 2013 to 2019. The dataset consists of 18 images, locations of these images are provided in Appendix B. These images are gathered from rows 23 to 25 and paths 44 to 47. The remaining pre-processing steps include mosaicking images gathered on the same day, when available, co-registering them with the MODIS and VIIRS datasets and cropping them to the study region. Landsat-8 OLI contains a QA file where the cloud fraction mask (CF mask) was extracted. The function of mask (Fmask) is an object-based cloud and cloud shadow detection algorithm for Landsat imagery. While there are some known uncertainties within the cloud mask including misclassifying high reflectance landcover as cloud such as snow/ice, beaches, salt lakes and buildings (Zanter, 2019), the overall accuracy of the Fmask has been shown to be 96% (Zhu & Woodcock, 2012).

The binary snow mapping algorithm is applied to each Landsat-8 image and then the CF mask is applied. The Landsat images are then resampled to 500 m. The re-sampled Landsat data are used as the reference data in the computation of confusion matrices of the MODIS snow extent data that coincide with the Landsat OLI snow data. The MODIS snow data includes the Terra, Aqua, VIIRS, TAC, the combined product and the ATD for 1 and 2 days, the spatial filter and the SNOWL dataset. For each of the MODIS datasets, pixels flagged as anything above 100 (cloud, inland water, ocean etc.) will be changed to NA so the dataset includes only snow and no snow pixels, the remaining pixels have already been changed to reflect a binary snow map prior to the spatial filter step (Table 4.5). A threshold of 50% was implemented for the MODIS fractional snow datasets, pixels retaining a snow fraction of >50% are classified as snow. A systematic test in 10% increments found that pixels classified as snow with >=50% FSC had the highest agreement. All NA pixels are excluded from the confusion matrices, this includes cloud as masked by Landsat and clouds in all other datasets. Therefore, the number of points used for each agreement statistic will differ between datasets.

Table 4.4: MODIS and VIIRS flag value key (Riggs & Hall, 2015)

Flag	Value
NDSI	0-100
Missing Data	200
No Decision	201
Night	211
Inland Water	237
Ocean	239
Cloud	250
Detector Saturated	254
Fill	255

The confusion matrix statistics that are extracted from each table will be the sensitivity, specificity, overall and balanced accuracy. The commission and omission errors will both be calculated with other statistics given. Equations 8 through to 13 are the necessary calculations for each metric where TP is true positive, TN is true negative, FN is false negative, FP is false positive, and N is the number of observations.

$$Sensitivity = \frac{TP}{TP+FN} \tag{8}$$

$$Specificity = \frac{TN}{TN+FP} \tag{9}$$

$$Overall\ Accuracy = \frac{TP+TN}{TP+TN+FP+FN} \tag{10}$$

$$Balanced\ Accuracy = \frac{Sensitivity+Specificity}{2} \tag{11}$$

$$Type\ I\ Error = 1 - Sensitivity \tag{12}$$

$$Type\ II\ Error = 1 - Specificity \tag{13}$$

4.4.1 Snow Cover Analysis

Point data extracted from watersheds within the region were used to record the last day of snow (LDS) to analyze early snow melt patterns. This was done for within the individual watersheds analyzed in the study: South Thompson, Thompson, Okanagan, and Columbia. The snow proportions were extracted and summarized, for available data. In situ data gathered from the BC data portal automated snow collection and were used to determine whether the distributions of remote sensing derived LDS follow the same patterns as in situ

LDS. Climate teleconnection indices, the PDO, PNA and ONI, from the NOAA database were used to analyze the linear relationships between these indices and the LDS dataset. These indices were used because these are the main teleconnections that have been proven to have impacts on snow cover in this region (Fleming et al., 2010; Bevington et al., 2019; McClung, 2013). One article stated that the ONI and PDO are the most influential teleconnections in BC with respect to snow cover (Bevington et al., 2019). Another study stated that maximum snow depth measurements during El Nino were significantly lower than during La Nina years (McClung, 2013). The PNA was used as well as it is interconnected with variations in the ONI and it was stated to be a significant teleconnection on climatological variability in BC (Bevington et al., 2019). These relationships were tested with simple and multiple linear regression (MLR). For each 3-month interval, a simple linear regression with 200 m elevation intervals was done. This allows insight for how much LDS median variation within the 17-year dataset can be attributed to fluctuations in the ONI. This will also show which elevations are most susceptible to the ONI. The PDO and PNA were gathered for the study period (April 1st – June 30th), a multiple linear regression using both variables will be done for testing the significance of each variable on the off-dates for the same 200 m elevation intervals. These regression models are done for LDS datasets across the entire region and are not separated by watershed.

Chapter 5
Results

This study sets out to evaluate the patterns of snow cover in this region, using estimates of last day of snow (LDS). In addition, the study seeks to test associations in patterns observed with the Pacific Decadal Oscillation (PDO), Pacific North American teleconnection pattern (PNA) and the Oceanic Nino Index (ONI) on snow cover variability in this region through regression analysis. Contextually, the patterns of the snow offset date in this region over the 17-year dataset provides insights into climate variability. Although there are no clear trends in this period that show decreases in snow extent during the spring freshet in this region, it is important to note that this period is shorter than a typical 30-year climate record. Overall accuracy of the complete cloud mitigation method reached 96%. Each watershed LDS dataset showed similar patterns at various elevations. Regression models testing the explained variability of teleconnections on the LDS datasets vary depending on the elevation bands as well, with the PDO and ONI being the most influential over this region.

The chapter is divided into three sections. First, the results of the cloud mitigation efforts are presented. This is followed by an accuracy assessment of snow cover mapping. The third sections present the results of variations in snow cover extent in each basin and the links to teleconnection indices.

5.1 Cloud Mitigation

In this subsection, the progressive mitigation of cloud fraction from the Terra-Aqua Combined (TAC) method, the ATD method and the SNOWL methods are shown.

5.1.1 Terra Aqua Combined (TAC) and VIIRS combinations

One of the objectives of this study was to mitigate as much of the cloud cover as possible through the implementation of the multi-step methodology. The addition of VIIRS starting in 2012 has variable effects on the cloud fraction, reducing up to 25% cloud cover when compared to the TAC in some cases, notably April 4th, 2015. Figure 5.1 shows the

cloud fraction difference from the TAC to the combined product using VIIRS for the year 2015, the remaining years are presented in Appendix C. VIIRS overpass is only 30 minutes prior to Aqua, therefore, there were no expectations that this additional dataset would remove significant cloud cover. Cloud mitigation with the addition of VIIRS was only significant where the overcast was sparse. Therefore, it is possible that the additional data from VIIRS originate from the difference in cloud mask compared to MODIS as well as cloud movement.

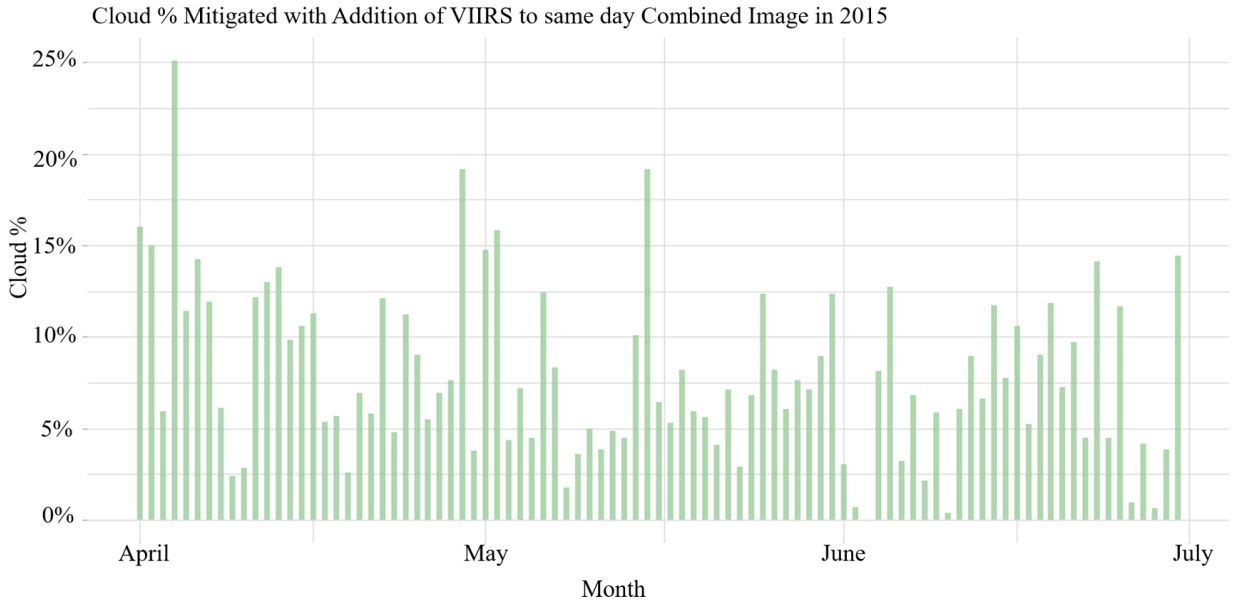

Figure 5.1: Cloud cover percentage mitigated through the addition of VIIRS to the same-day combination

5.1.2 The adjacent temporal deductions (ATD) method for +/- 2 days

The ATD of +/- 2 days was the most effective in mitigating cloud fraction. The most successful year for cloud mitigation was 2015. A summary of the cloud coverage improvements throughout the study period are provided in table 5.1. It is notable that the average cloud percentage in the year 2015 after the entire methodology has been implemented is at 0.2% (Table 5.1). Figure 5.2 below shows the cloud fraction for each step in the process in 2015, drastic variations in cloud cover for the combined product are areas where the ATD are the most effective. For example, mid-late June where TAC and the

combined product cloud fraction varied from 75% cloud cover to 50% repeatedly, applying ATD +/- 1 day mitigated nearly 50% of cloud cover (Figure 5.2). ATD +/- 2 days mitigated another 20% because of the differences in cloud fraction throughout that period. Early June is another example where original images and the combined product's cloud fraction was nearly 100% and was brought down to 20% after the ATD +/- 2 days (Figure 5.2).

Table 5.1: Average cloud cover percentage throughout the study period and throughout the methodology

	Terra	Aqua	TAC	VIIRS	Combined (Terra, Aqua, VIIRS)	TAC + ATD +/- 1 Day, Combined + ATD +/- 1 Day	TAC + ATD +/- 2 Day, Combined + ATD +/- 2 Day	TAC + ATD +/- 2 Day, Combined + ATD +/- 2 Day + SF	TAC + ATD +/- 2 Day, Combined + ATD +/- 2 Day + SF +SNOWL
2003	76.5	78.7	69.0	NULL	NULL	41.0	25.4	16.3	2.4
2004	63.0	66.0	53.6	NULL	NULL	26.3	15.2	9.5	1.4
2005	70.6	72.2	62.4	NULL	NULL	36.0	21.8	13.4	1.9
2006	69.5	71.9	61.4	NULL	NULL	32.0	18.3	11.0	1.6
2007	70.0	72.4	61.8	NULL	NULL	32.3	18.4	11.8	2.2
2008	77.8	79.6	70.8	NULL	NULL	40.7	24.4	15.1	2.1
2009	64.2	68.9	55.7	NULL	NULL	27.2	14.7	8.5	1.2
2010	76.7	79.0	68.0	NULL	NULL	38.4	24.6	15.4	2.4
2011	79.5	81.5	72.1	NULL	NULL	43.0	26.1	16.3	2.7
2012	80.3	81.7	73.0	75.2	64.2	33.1	18.1	18.1	2.5
2013	75.6	77.2	67.7	70.6	58.4	28.1	14.6	7.6	1.8
2014	75.1	79.0	67.0	72.5	57.7	23.3	10.4	4.5	0.7
2015	58.5	62.8	49.0	58.2	41.1	12.0	3.6	1.3	**0.2**
2016	65.4	68.9	57.0	66.3	50.5	19.7	8.2	4.1	0.8
2017	74.5	76.4	66.9	71.5	58.8	27.1	14.1	6.6	1.1
2018	68.4	71.8	60.9	65.3	52.4	22.4	11.1	5.5	1.0
2019	70.1	75.5	61.9	69.4	53.2	20.4	8.9	3.9	0.8
Average	71.5	74.3	63.4	68.6	54.5	29.6	16.3	9.9	1.6

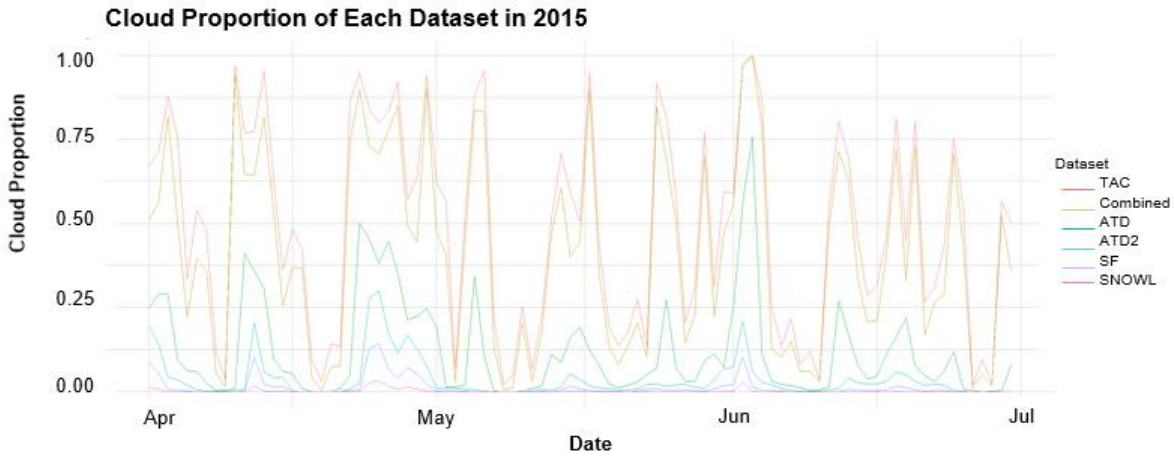

Figure 5.2: Proportion of cloud cover from April 1st to June 30th, 2015 for each step in the methodology

The spatial filter removed minimal cloud cover in most cases, however, there were instances shown in figure 5.2 above where the addition of the spatial filter brought the cloud fraction to 0%. This method is most effective where there are small gaps of cloud scattered throughout the images. This is because the kernel uses the average of surrounding pixels, so where there are large gaps of cloud only the edges of the gap will be filled. Where there are small gaps throughout the image, most of them will be interpolated by this method. This was the reasoning behind applying this portion of the methodology near the end of the process, in order to utilize the movement of clouds from the combination of the three satellite datasets as well as the ATD +/- 2 days to have the least amount of large cloud gaps as possible. Overall, throughout most years in the analysis this method has been successful in reducing significant cloud cover. In some cases (2014, 2015, 2017) cloud cover was mitigated to a maximum of 25% throughout the off-season. Whereas in the remaining years there are periods of time where cloud fraction remained as high as 75%, such as 2011 (Figure 5.3). The remaining visualizations of cloud fraction mitigation are presented in Appendix D.

5.1.3 Application of the SNOWL method to remove remaining cloud pixels

The SNOWL methodology mitigated a sizable portion of remaining cloud covered pixels in days where cloud cover was already below 25% after temporal and spatial filtering were done. In the cases where cloud cover is still in excess, such as 2011, the methodology does mitigate cloud cover but not entirely (figure 5.3). Days that display substantial amounts of cloud cover (>1%) throughout the entire region after the methodology is done will be removed from the snow cover proportion analysis. This is to ensure that uncertainty from cloud covered landcover is not prominent in the study.

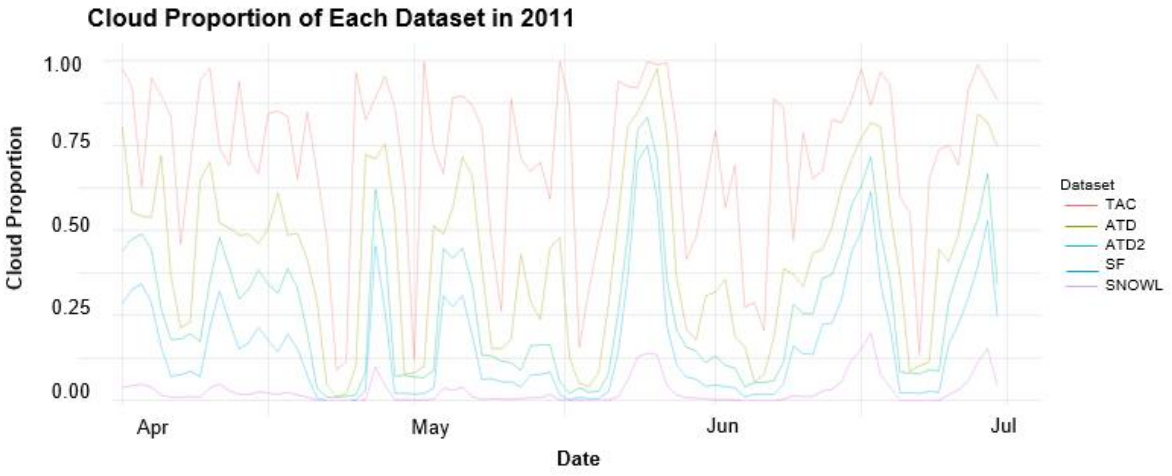

Figure 5.3: Proportion of cloud cover from April 1st to June 30th, 2011 for each step in the methodology

The locations at which clouds are the most prominent are important in understanding where the most uncertainties are throughout the region in respect to snow cover extent. The cloud duration map comparison allowed the visualization of the shift of cloud cover presence. Figure 5.4 below contains cloud duration maps for years where there was the most dramatic cloud mitigation with the combined product +ATD +/- 2 days +SF + SNOWL, in comparison to the combined product + ATD +/- 2 days + SF, where the value of each pixel represents the number of days that pixel was cloud covered in the 91-day period. These

images show a strong tendency for remaining cloud cover to be persistent mainly in the mountainous area of the study region.

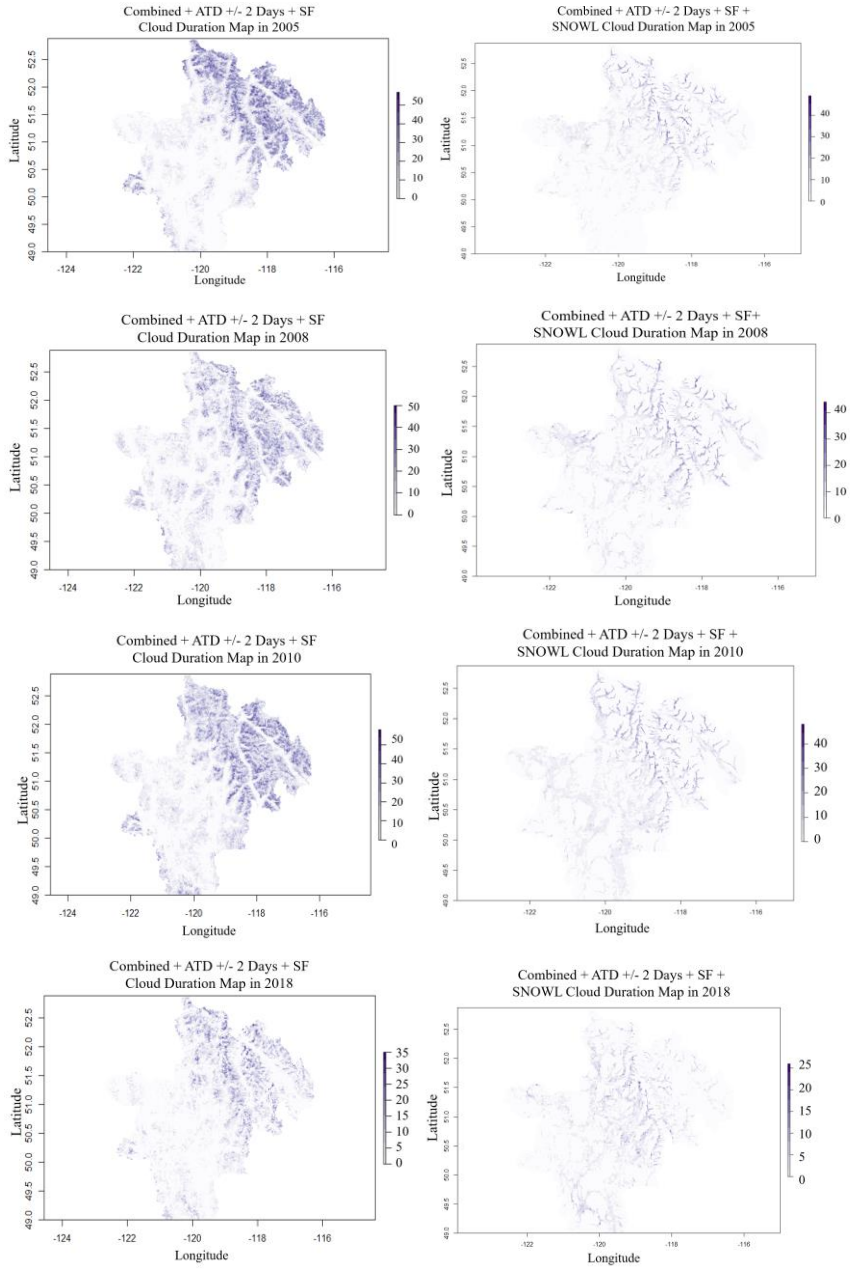

Figure 5.4 Cloud duration maps for 2005, 2008, 2010 and 2018 for TAC+ATD (left) and TAC+ATD+SNOWL (right) application, each pixel value is the number of days where it is classified as cloud cover

5.2 Accuracy Assessment of Combined Snow Cover Product (TAC+ATD+SF+SNOWL)

Confusion matrices accuracy metrics were calculated for the entirety of the images that coincided with Landsat-8 reference dataset but also for forested landcover separately. Understanding where the errors are concentrated throughout the methodology is important when assessing the accuracy of the overall products. Note that in subsequent tables, NA values are present where there weren't enough points in the specific dataset to compute a confusion matrix.

Table 5.2: Overall Accuracy (OA) for each step and separate datasets used throughout the validation dataset with highest daily accuracy in bold

Date	*Terra*	*Aqua*	*VIIRS*	*TAC*	*Combined*	*Combined + ATD*	*Combined + ATD 2 Day*	*Combined + ATD 2 Day + SF*	*Combined + ATD 2 Day + SF + SNOWL*
April 21st 2013	86.1	**87.3**	83.3	85.6	84.8	84.7	84.7	84.0	82.1
April 1st 2014	73.4	**75.0**	74.6	72.7	72.5	72.2	72.2	71.1	71.9
April 20th 2015	94.0	**94.1**	91.1	92.7	92.0	91.6	91.6	91.6	90.6
May13th 2015	87.8	**91.2**	89.1	87.7	87.1	83.5	83.7	83.7	85.4
May 22nd 2015	94.3	**94.3**	92.2	93.4	92.2	92.9	92.9	92.9	92.4
June 7th 2015	**99.4**	99.2	99.2	99.1	98.9	98.8	98.8	98.7	98.7
May 1st 2016	**92.2**	91.9	86.1	90.7	88.2	88.2	88.2	88.2	87.5
May 15th 2016	97.8	**98.4**	96.6	97.7	97.2	97.2	97.2	97.2	97.0
May 20th 2017	**92.8**	91.6	89.1	91.2	89.6	89.3	89.2	89.2	88.9
May 27th 2017	95.0	**95.3**	91.1	93.8	91.8	91.6	91.5	91.5	90.6
May 29th 2017	**90.2**	87.6	85.5	87.8	86.1	86.0	85.9	85.8	85.8
June 5th 2017	**98.1**	97.5	97.1	97.0	96.1	95.7	95.5	95.1	94.8
May 14th 2018	91.9	**92.9**	88.6	90.7	89.0	89.0	89.0	88.9	91.5
May 23rd 2018	**93.9**	92.9	89.0	92.5	90.4	90.0	90.0	90.0	89.8
June 24th 2018	NA	99.1	**99.5**	99.5	99.4	98.0	97.7	97.2	96.9
April 8th 2019	78.8	79.8	**80.7**	79.4	79.2	79.2	79.2	76.8	74.5
May 10th 2019	**91.9**	90.7	84.0	90.0	86.8	87.2	87.2	87.1	86.8
May 26th 2019	**91.3**	89.9	81.4	89.4	86.7	86.5	86.5	86.3	85.5

The overall accuracy throughout the dates are not significantly reduced for TAC or the combined product (table 5.2). The adjacent temporal deduction datasets also do not show significant decreases in agreement with the Landsat imagery. SNOWL, being the final method applied, will also adopt the misclassifications of the previous steps (TAC, ATD, spatial filter). The ATD is expected to have slightly less agreement with the Landsat images because of the seasonality of the study. ATD assumes that snow cover from the receding and preceding days have not changed, since this study focuses on the spring freshet, sometimes this may not be the case. Similarly, SNOWL is based on the mean elevation of snow and no-snow pixels. In complex landscapes such as this one, aspect and slope affect melt out of snow significantly (Erxleben et al., 2002). Thus, the slight reduction in accuracy after applying SNOWL can be attributed to pixels that are low (high) elevation but have north (south) facing slopes (Erxleben et al., 2002). Figure 5.5 below shows the number of data points from each dataset that are used in the computation of each confusion matrix. This gives an understanding of how much cloud mitigation is done within the Landsat-8 image coverage for each dataset. For the reference images used, there wasn't a significant increase in points when an ATD +/-2 day was put into place. This is because by this stage in the methodology, there were minimal cloud covered regions remaining in the image. It is important to note that not all images are taken from the exact same overpass in the study area, so there will be more data availability depending on the coverage of each reference image as well.

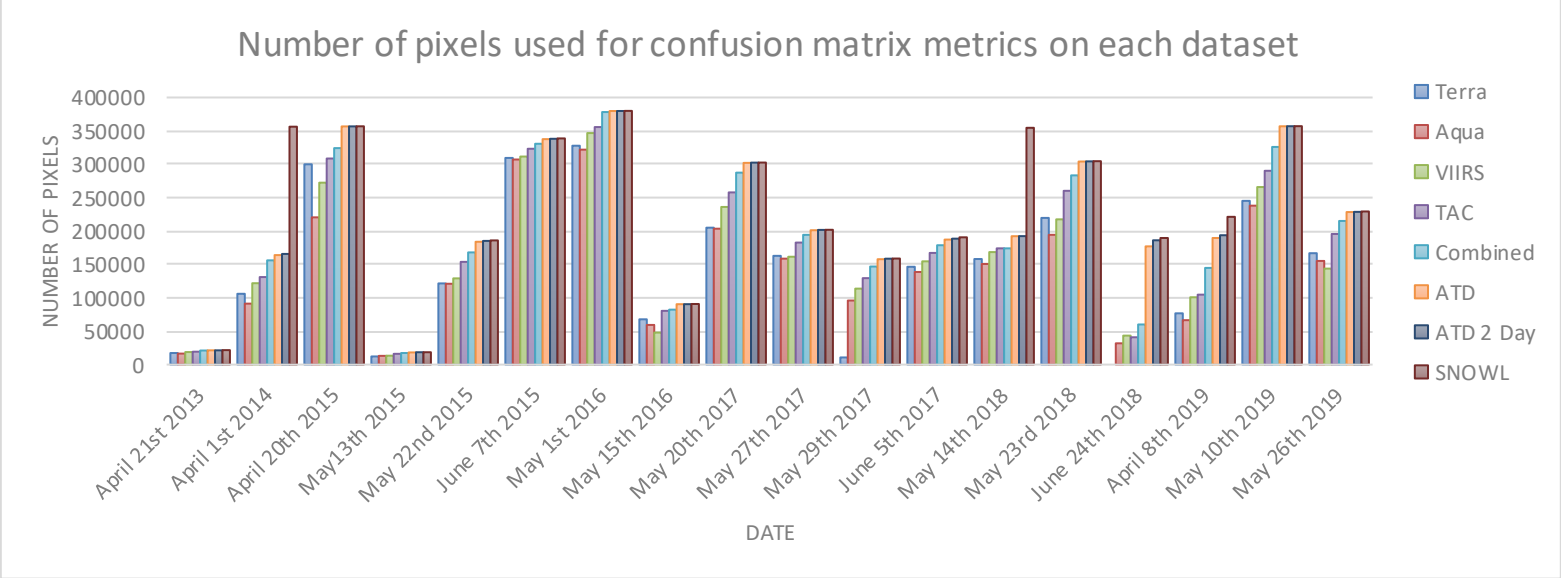

Figure 5.5: Bar graph showing the number of pixels used for the accuracy assessment on each date

June 24th, 2018 in the Landsat dataset was the only date where the ATD +/- 1 and 2 days made a large contribution to cloud mitigation. Table 5.2 shows that the overall accuracy decreased from 0.99 to 0.97. During this time of the year there will be minimal snow cover in the area, apart from the mountains. However, throughout the table the reduction in accuracy from the single datasets to the multi-day multi-satellite composites is limited to 2-8% adding about 20,000 points for ATD +/- 1 day and 21,165 for ATD +/- 2 days. These findings are like another study that found accuracy of ATD +/- 1 day to reach 96.3%, slightly lower than MODIS Terra by 0.7%. The amount of cloud cover mitigated in this study was not mentioned however (Gafurov & Bardossy, 2019).

A major limitation on snow cover mapping is identifying and correctly classifying snow cover in forested regions (Crawford, 2015). To analyze the accuracy in these areas, forested regions were separated for each date, the overall accuracy for forested regions in presented in table 5.3. Some dates show a dramatic decrease in accuracy for forested regions, while others remain above 90%. April 1st, 2014 and April 8th, 2019 are two notable dates as the accuracy drops from 72% and 79% to 58% and 68% respectively for the ATD +/- 1 day. These dates are at the beginning of the season, where Landsat-8 images tend to map more

snow cover in forested regions, especially with the NDFSI method than the SNOWMAP algorithm used in MODIS and VIIRS classification. Later dates throughout the season retain a relatively high OA partly because snow in forested regions has melted. To better understand these errors, an analysis of the spatial distribution of type I and type II errors is required (Figure 5.6).

Table 5.3: Overall Accuracy for each step in the methodology and each separate dataset throughout the validation dataset in forested regions exclusively with highest daily accuracy in bold

Date	*Terra*	*Aqua*	*VIIRS*	*TAC*	*Combined*	*Combined + ATD*	*Combined + ATD 2 Day*	*Combined + ATD 2 Day + SF*	*Combined + ATD 2 Day + SF + SNOWL*
April 21st 2013	**71.0**	64.5	76.5	70.6	74.5	74.4	74.4	74.9	74.4
April 1st 2014	56.6	56.1	**61.5**	56.3	58.5	58.7	58.6	58.9	76.0
April 20th 2015	90.0	**90.1**	86.3	88.3	87.1	86.2	86.2	86.3	85.0
May13th 2015	85.2	85.8	**86.2**	85.0	85.4	82.6	82.8	83.6	84.2
May 22nd 2015	**96.3**	95.7	94.5	95.3	94.3	94.5	94.5	94.4	94.3
June 7th 2015	**99.1**	98.8	98.9	98.8	98.6	98.6	98.6	98.5	98.8
May 1st 2016	**90.9**	89.9	83.7	88.6	85.0	85.0	85.0	84.9	84.3
May 15th 2016	97.2	**97.7**	96.7	97.0	96.8	96.9	96.9	97.0	97.3
May 20th 2017	**91.0**	88.2	86.4	88.6	86.7	86.3	86.3	86.1	86.1
May 27th 2017	**94.5**	**94.5**	90.5	93.0	90.3	90.0	90.0	89.9	89.2
May 29th 2017	**92.0**	87.8	88.0	88.6	87.6	87.3	87.2	87.1	87.3
June 5th 2017	**97.8**	96.6	96.1	96.5	95.4	94.9	94.8	94.5	94.3
May 14th 2018	88.7	**89.9**	84.7	87.0	84.7	84.6	84.6	84.6	86.3
May 23rd 2018	**94.9**	93.1	91.0	93.2	91.5	90.9	90.9	90.9	90.9
June 24th 2018	NA	**98.6**	NA	99.0	98.9	98.9	98.8	98.7	98.8
April 8th 2019	63.8	60.6	**66.6**	62.8	65.8	68.7	68.7	68.3	69.6
May 10th 2019	**90.2**	88.1	82.2	87.3	83.8	83.7	93.7	83.7	83.6
May 26th 2019	**93.8**	92.4	87.6	91.5	88.5	87.9	87.8	87.9	87.4

For a handful of dates selected to represent a spread throughout the season (April 1st – June 30th) in the accuracy dataset, accuracy maps were made to visualize the errors. Figure 5.6 depicts the false/true positives and false/true negative in both forested landcover and non-forested landcover. From these images, an overwhelming majority of false negatives are

occurring in forested landscapes, mostly confined to the tree-line area on mountains. The overall trend shows that there are significantly more omission errors in forested areas than commission errors. The exception for this is the two dates stated earlier. The best dates to analyze to assess the accuracy of the SNOWL step are April 1st, 2014 and May 14th, 2018 because these two dates have a significant increase in overlapping pixels to test between Landsat and the product. April 1st, 2014 agreement with Landsat from the combined product through to the SNOWL method decreases by a fraction of a percent (0.5%). On May 14th, 2018 the agreement between the product and Landsat increases from the ATD steps to the SNOWL step by 2.6%. The average agreement between Landsat and the combined + ATD + SF + SNOWL is 88.4% and reaches 98% (Table 5.3). It is expected that agreement with high resolution imagery would fluctuate given the study period and the variance with cloud fraction in each of these images. However, the slight decreases in accuracy as the images are progressed throughout the methodology is minimal. On average, there is a decrease in OA of 1% from the combined image through to the combined + ATD + SP + SNOWL product, but a 3% average decrease from the Terra snow product.

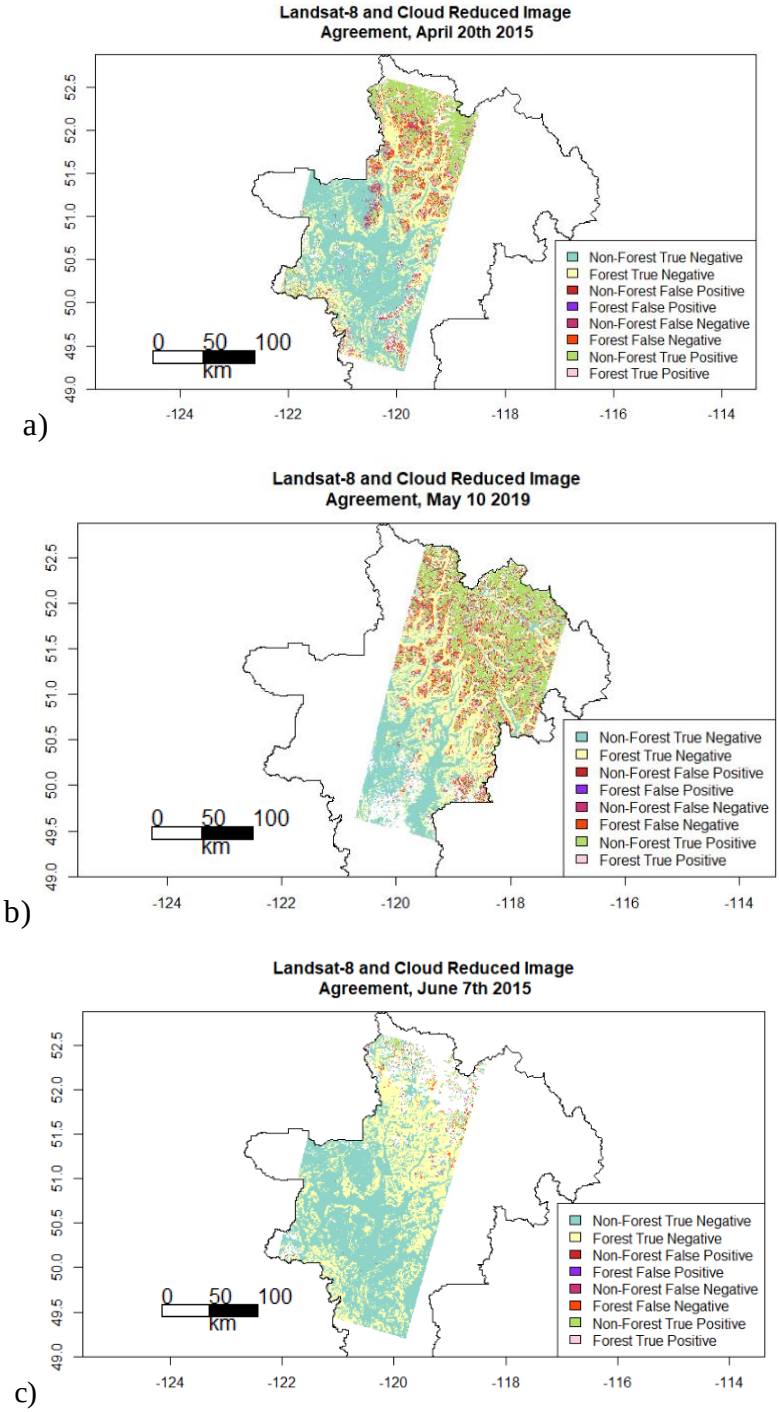

Figure 5.6: Accuracy maps showing the proportion of true/false positive to true/false negatives on (a) April 20th, 2015, (b) May 10th, 2019 and (c) June 7th, 2019 for both forested and non-forested areas

5.3 Snow cover

Understanding the variability and patterns of snow cover melt out in this region and the watersheds that resides within it, was one of the aims of this research. It has been shown that snow cover in the Northern Hemisphere is decreasing, especially in the off season (Brown & Mote., 2008; O'Leary et al., 2018; Derksen et al., 2014). In various mountain basins, snow duration maps have shown a decreasing trend, primarily focused in regions of low to mid elevation (Li et al., 2017). Because cloud cover persistence is variable throughout each year, snow cover duration maps were not created for this study. Instead, samples of pixels were taken from four watersheds within the study area. These watersheds consist of the South Thompson, Thompson, Columbia, and Okanagan watersheds. These watersheds are diverse in elevation, therefore the number of points gathered, and elevation bin sizes are not consistent throughout. For example, in the Thompson watershed, there are minimal areas above 2000 m.a.s.l. so this elevation was not sampled in this watershed. Likewise, in South Thompson, elevations below 1300 m.a.s.l. weren't included in this portion of analysis because many pixels below this elevation show that snow typically has melted prior to the start date of this study period (April 1st). Regions above 2300 m.a.s.l. were also excluded because these are presumably areas where permanent snow cover is present or melt out date is later than the last day in the study period (June 30th). Therefore, sampling between these watersheds does vary. Figure 5.7 shows the points gathered throughout the study region overlayed on the DEM used for reference. These points will be used to record the last day of snow (LDS) for each pixel throughout the study period. An LDS of 0 refers to a pixel melting out prior to the study period, and a value of 91 refers to a snow pixel remaining throughout the study period. The LDS is recorded as the last day where snow is present for a period >4 days consecutively. This is to reduce the error caused by false detection by one of the satellites that may carry over to the combined product or the ATD product.

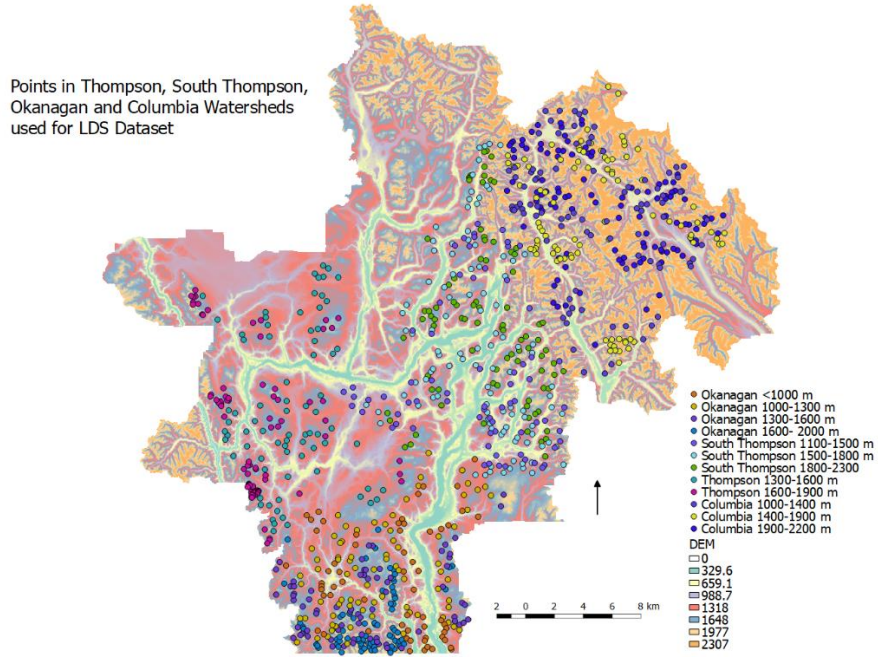

Figure 5.7: Distribution of points used for LDS analysis overlayed on DEM

Snow cover proportions were also extracted from all days where cloud was <1% of the entire study region. Snow proportions for the South Thompson watershed were also extracted where cloud was present for <1% of the watershed boundary, to analyze the variability of an individual watershed within the study region. These metrics are what will be analyzed to answer the key questions of this research.

5.3.1 Large Area Analysis: Full Thompson Okanagan Economic Region

To visualize this extracted dataset from the entire region, these points were input into a boxplot for ~300 m elevation bands. These boxplots are shown in figure 5.8. The points were sampled from 1200 to 2100 m.a.s.l. throughout the entire region.

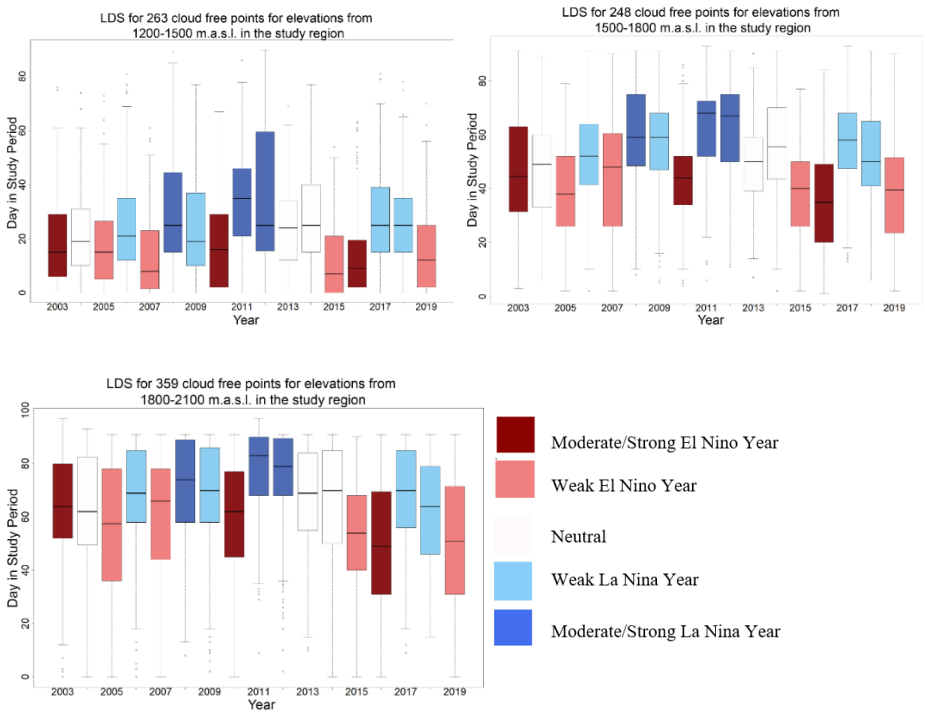

Figure 5.8: Distribution of LDS (boxplots) for the Thompson Okanagan region for 2003-2019 categorized by El Nino/La Nina strength., for the three elevation bands, 1200-1500 m.a.s.l., 1500-1800 m.a.s.l. and 1800-2100 m.a.s.l. between April 1st-June 30th

Figure 5.8 shows wide variability; however, the pattern remains consistent throughout for each of the elevation bands. For each of these figures, there is a wave-like pattern throughout the 17-year dataset in respect to the medians with later snow disappearance in the middle years and earlier disappearance in the later years. Several years show a positive skewness in these LDS boxplots. Positive (negative) skewness means that over half of the data points are lower (higher) than the average proportion of snow cover in these years. In the case of positive (negative) skewing, the median will be larger (smaller) than the average value. There is a positive skewness in later years in the boxplots (Figure 5.8), whereas earlier years exhibit a negative skewness. This means that in earlier years, more points are located below the average value, and in later years more points are located above the average value. The maximum and minimum values show a wide range, sometimes across the entire study period (1-91 days). Because of the variability of snow cover melt out and the various

influences on this process, this can be attributed to pixels having similar elevations but varying aspect, slope and landcover.

A supplementary dataset was gathered from in situ automated weather stations within the study region. This in situ data is open source and available via Aquarius Web Portal by the Provincial Government of British Columbia. From this database, LDS was recorded for points available as the day where snow depth is <3 cm. Unfortunately, there was no in situ data point within the study area where snow depth data was available from May 2003 to May 2019. Therefore, only four points were selected one from May 1st, 2004 and two more from May 1st, 2005. These points range from 1460 m to 1780 m in elevation. The threshold of 3 cm was adopted from other studies that have used similar thresholds for comparing snow cover from remote sensing observations to in situ ground measurements (Hori et al., 2017; Dong & Menzel, 2016). Interestingly, the snow depth measurements also follow the wave-like pattern from previous charts shown thus far (Figure 5.9). Peaks and troughs in snow depth in situ dataset coincide with the ONI phases.

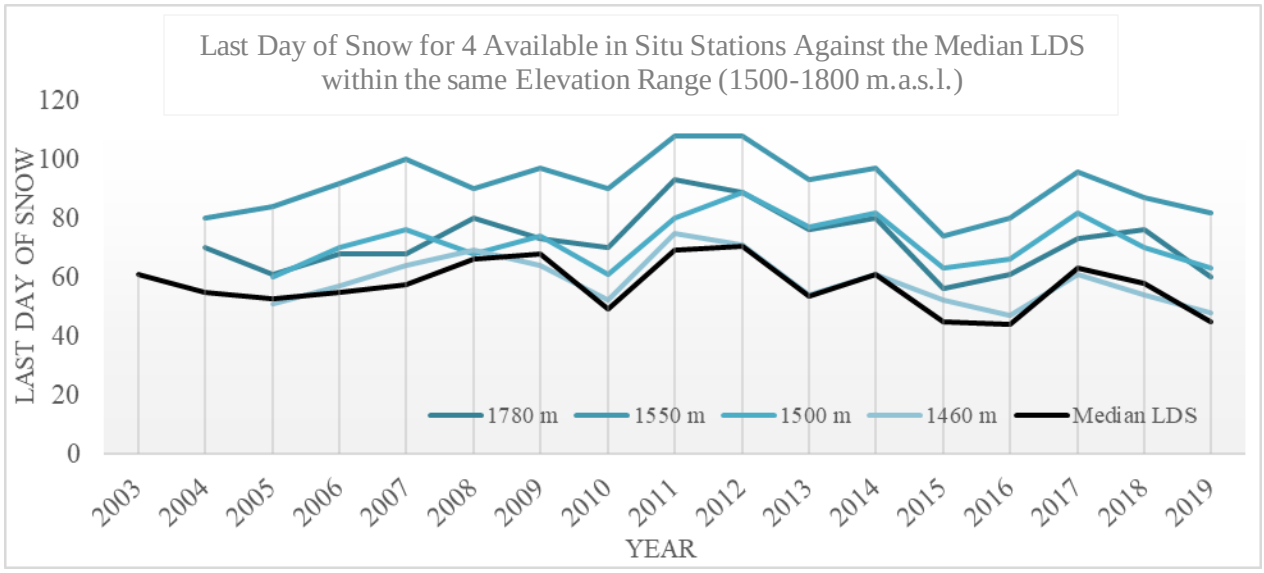

Figure 5.9: In situ LDS throughout the study period for 4 data points available from 2004/2005-2019

La Nina years are consistently higher in values in all three elevation bins. The peak value is consistently in 2011, where there was a strong La Nina (table 5.4). There are also differences in distribution, some years show a normal distribution of values whereas others are skewed. For instance, in 2007 at all elevations there is skewing within the dataset, low elevation in 2012 are also skewed (figure 5.8).

The wave-like pattern is present within the snow proportion dataset for the entire region as well, with the largest median value remaining at 2011 with a strong La Nina index and lowest values in 2010, 2015 and 2016 with a moderate to strong El Nino index (figure 5.10). However, this may due to the removal of snow proportion values on days where cloud cover >1%. The days still obstructed by clouds after the cloud mitigation process were not included in this calculation. This has a minor effect on the visualization and statistics of the extracted from the data.

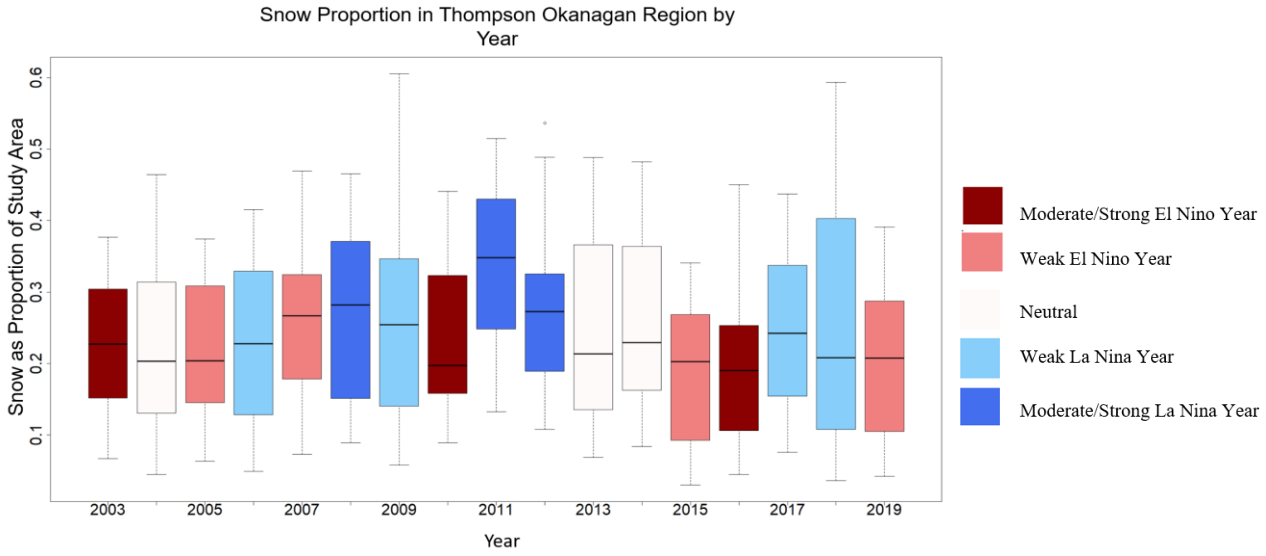

Figure 5.10: Total maximum snow cover extent proportions for the Thompson Okanagan region shown using boxplots for 2003-2019 categorized by El Nino/La Nina strength.

5.3.2 South Thompson Watershed

The South Thompson watershed is located within the Thompson Okanagan region, analyzing the patterns within a catchment is crucial in terms of water resources and

challenges that may face this area with increasing variability. Therefore, the above analyses were done within this watershed as Thompson Okanagan region contains the whole South Thompson watershed boundary. To start, points were sampled throughout the region at multiple elevations and then split off into elevation bands to create the LDS boxplots as shown earlier.

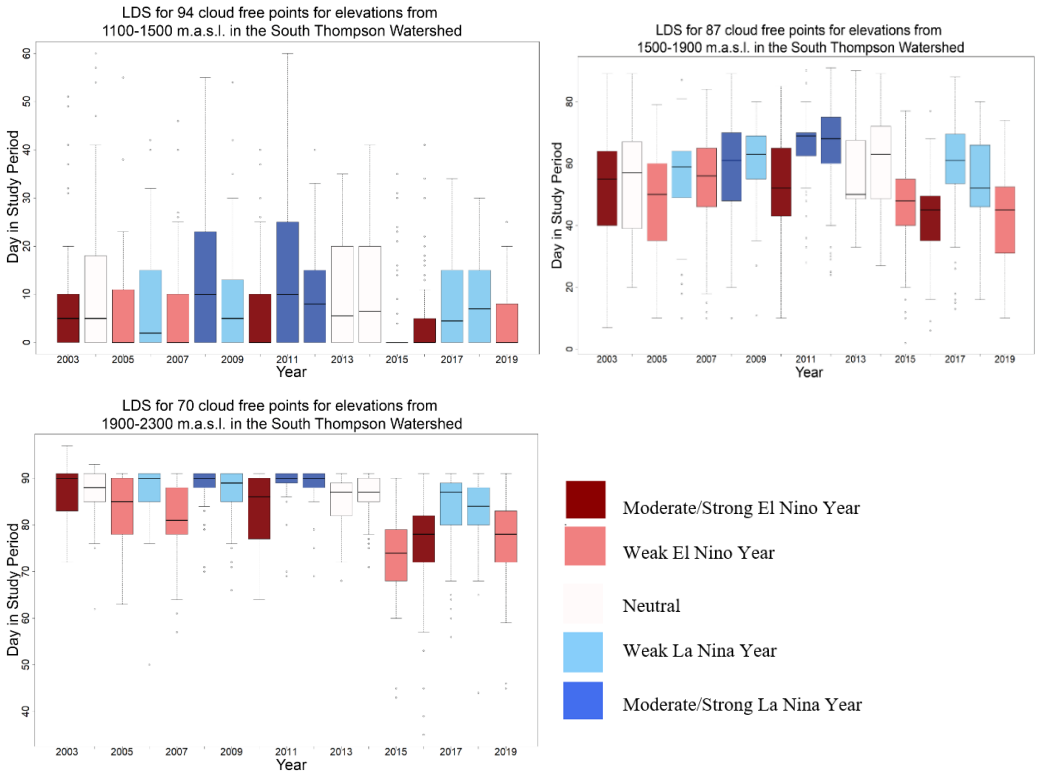

Figure 5.11: LDS distributions for 3 elevation bands (1100-1500 m.a.s.l., 1500-1800 m.a.s.l. and 1800-2300 m.a.sl.) throughout the South Thompson watershed from 2003-2019 categorized by El Nino/La Nina strength.

Overall, the trends in South Thompson follow the same patterns as the Thompson Okanagan region. For example, the years with the latest LDS median day are still the off-season of 2011 and 2012. The years with the lowest median value are 2015 and 2016 (Figure 5.11). The overall wave-like trend throughout the 17-year period is also present within this watershed. An interesting feature about this dataset is the high elevation dataset between 1900-2300 m.a.s.l. This collection of points, bound by the limit of the watershed, shows

several outliers. Average median values for El Nino and La Nina years were calculated for each elevation. Low elevation LDS average during El Nino years was 0 and 7 for La Nina years. Mid elevation average LDS median was 50 for El Nino years and 61 for La Nina years. High elevation LDS average for El Nino years was 81 and 90 for La Nina years.

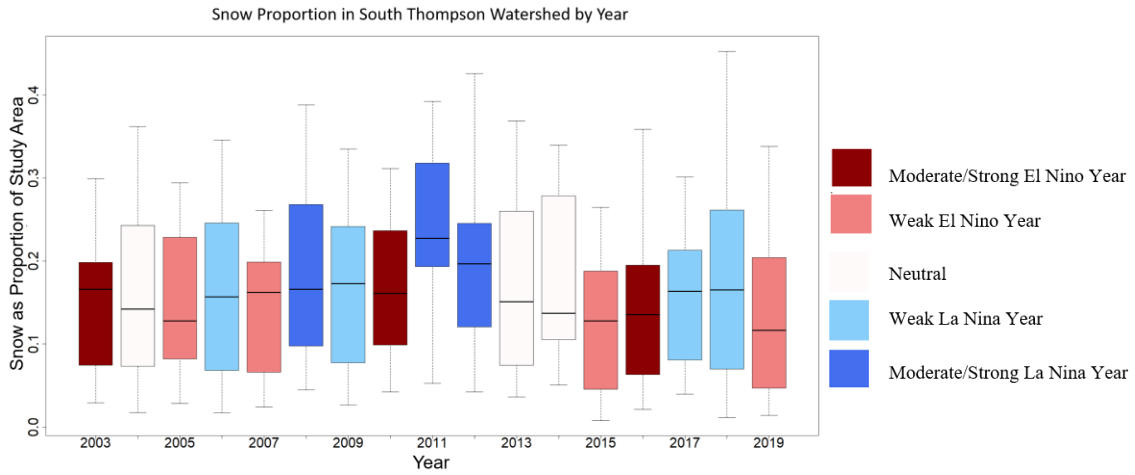

Figure 5.12: Boxplots of maximum snow cover fraction of the South Thompson watershed throughout the off season from 2003-2019 categorized by El Nino/La Nina strength.

The distributions of annual snow cover percentage in South Thompson are shown in figure 5.12. This pattern in this figure is the same as the LDS datasets for South Thompson, as well as the snow percentage distribution for the entire region of Thompson Okanagan (figure 5.10). Days where cloud cover exceed 1% were removed from the visualization of this boxplot.

5.3.3 Thompson Watershed

The Thompson watershed is located west of South Thompson. This region does not have the range of elevation as other watersheds in this region, therefore the elevation bands and points collected were limited. This area experiences a rain shadow from the coastal mountains in British Columbia. As such, snow cover will disappear earlier in the season than the study period. Although this region is still snow covered for the winter, the rain shadow effect characterized by dry/warm descending air on the leeward side of the Coastal

mountains, cause this region to experience lower precipitation (Thorne & Woo, 2011). Due to these characteristics, the points gathered here range from 1300 m.a.s.l. to 1900 m.a.s.l., shown in the figures below are the boxplots representing LDS for these points (figure 5.13). Average median values for El Nino and La Nina values were calculated. For low-mid elevations El Nino years showed an LDS of 6.5 and 16 for La Nina years. For high elevations El Nino LDS was 27.5 and La Nina 50.

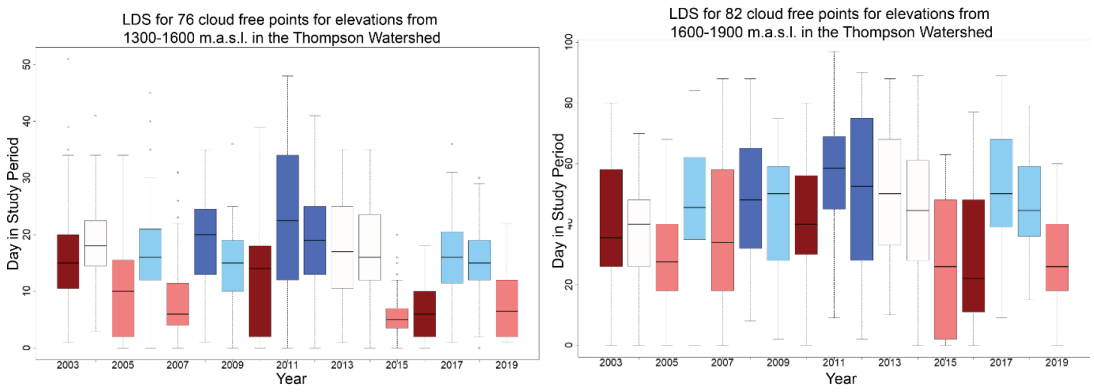

Figure 5.13: LDS distributions (boxplots) for two elevation bands (1300-1600 m.a.s.l. and 1600-1900 m.a.s.l.) in the Thompson watershed categorized by El Nino/La Nina strength.

There is more variability in this dataset in comparison to previous boxplots, more notably at lower elevations. This could be in part due to the relatively low relief in this region in comparison to other watersheds in the study area. However, the peaks in LDS remain in 2011, 2017 and 2018. While the lowest values remain in 2003, 2015, 2016 and 2019 as shown in previous datasets. These values are more pronounced in this watershed, due to reasons stated above.

5.3.4 Okanagan Watershed

The Okanagan watershed is located south of the South Thompson and Thompson watersheds. This watershed is part of the Okanagan Basin, extending into the United States. Points gathered throughout this watershed range from 1000-2300 m.a.s.l. The boxplots of LDS distributions are shown below in figure 5.14. The overall trends resemble the previous plots; however, they show greater variability and exaggerated values in this region. Average

median El Nino LDS for low elevation was 1.5 and 23 for La Nina. Mid elevation El Nino was 25.5 and 45 for La Nina. High elevation average median LDS for El Nino years was 42 and 61 for La Nina.

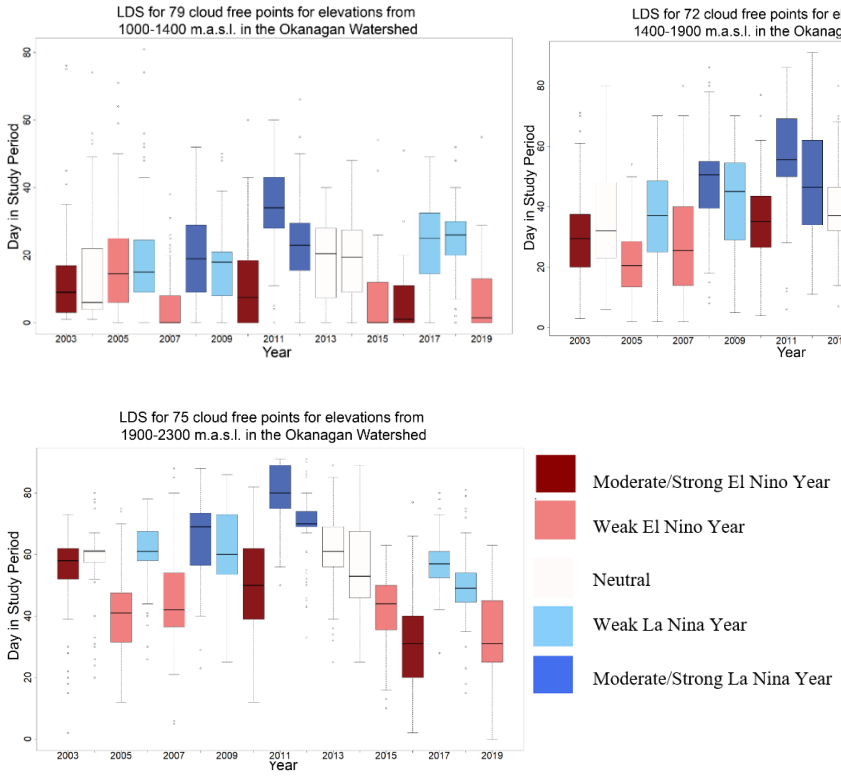

Figure 5.14: LDS distributions (boxplots) set for 3 elevation bands (1000-1400 m.a.sl., 1400-1900 m.a.sl. and 1900-2300 m.a.sl.) in Okanagan watershed categorized by El Nino/La Nina strength.

5.3.5 Columbia Watershed

The Columbia watershed is the final watershed in the region that was analyzed for the LDS dataset. This region contains part of the Rocky Mountains of BC and therefore is the watershed with the highest elevation in the study region. This means there will be greater topographic effects on the dataset meaning greater variation in distributions of LDS due to effects of slope and aspect. This region also shows to have longer lasting snow cover at the same elevations as previous watersheds. Figure 5.15 below shows the LDS distributions for

three elevation bands. The average median LDS at low elevations for El Nino years was 28 and 46 during La Nina years. Mid elevations for El Nino years was 45 compared to 63 for La Nina years. High elevations El Nino years average median LDS was 62.5 and 75 for La Nina years.

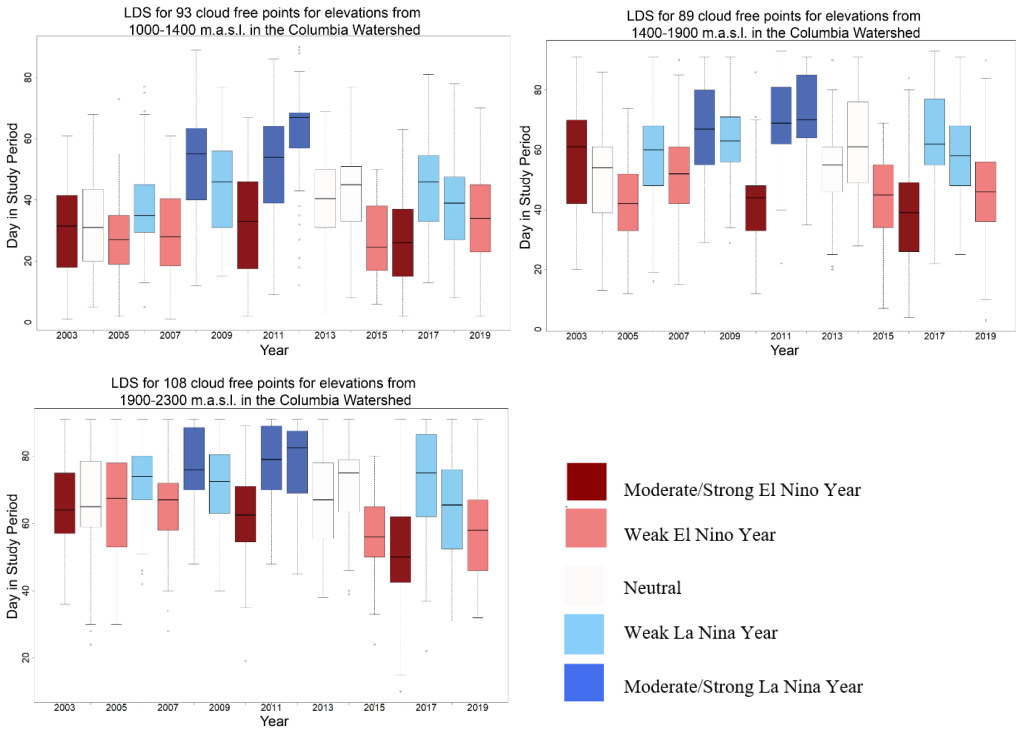

Figure 5.15: LDS distributions (boxplots) for 3 elevation bands (1000-1400 m.a.sl., 1400-1900 m.a.sl. and 1900-2300 m.a.sl.) in Columbia watershed categorized by El Nino/La Nina strength.

Comparing the same elevation bin of 1000-1400 m.a.s.l for Columbia and Okanagan watersheds, the Okanagan watershed has overall earlier disappearance of snow than Columbia, but still follow the same pattern. These variations are expected with the differences in elevation, aspect, and topographic relief between these two watersheds.

5.3.6 Simple and Multiple Linear Regression for LDS datasets

Simple and multiple linear regression were used to determine the strength of the relationships between the PDO, PNA and ONI with the LDS dataset throughout the study region. Linear regression is a statistical procedure whereby explanatory variables are used to

predict the outcome of a dependent variable (Gromping, 2009). Simple and multiple linear regression are distinguished by having one or more explanatory variables, respectively (Li et al., 2018). The LDS dataset was tested for normality using the Shapiro test and visualized using QQ-plots. Linearity, homogeneity of residuals and independence of residual errors were all assumptions that were tested for prior to applying these techniques to the dataset, these were reasonably satisfied, and the plots are available in Appendix E.

Phases in the ONI, PDO and PNA affect the severity of the cold season throughout snow dominated basins (Shabbar, 2014; Bevington et al., 2019; Griesbauer & George, 2019). Throughout the watersheds investigated, we see these effects clearly. As medians and distributions of LDS for El Nino years are lower and La Nina years are much higher during the study period. However, it is not clear to what extent these atmospheric connections dominate variations in the snow off season in this region. To better understand this relationship in the study area, linear regression models were created to specifically test the effects of each of the mentioned indices. The main objective here is to understand how much of the variation within the LDS datasets are explained through phases and severity of the ONI, PDO and PNA and whether each index is statistically significant in the equation.

The overall medians for six elevations bands of 200 m were extracted for each year in the study period. These bands are <1000 m, 1000-1200 m, 1200-1400 m, 1400-1600 m, 1600-1800 m, and 1800-2000 m. The multiple linear regression was used for the PDO and PNA by averaging the values, found in table 5.5, and using that average as the explanatory variable with the LDS dataset being the dependent variable. The simple linear regression model was used for each 3-month interval of the ONI from December-June. The ONI averages were the explanatory variables with the LDS remaining the dependent variable. Since it is established that the individual watersheds follow the same overall pattern, LDS points from the entire area were used in this piece.

Table 5.4: ONI severity by year in the study period (April 1st – June 30th) (NOAA, 2020).

Year	ONI	Intensity	DJF	FMA	AMJ
2003	**El Nino**	**Moderate**	**0.9**	**0.4**	**-0.3**
2004	Neutral	N/A	0.4	0.2	0.2
2005	El Nino	Weak	0.6	0.4	0.3
2006	La Nina	Weak	-0.8	-0.5	0.0
2007	El Nino	Weak	0.7	0	-0.3
2008	**La Nina**	**Strong**	**-1.6**	**-1.2**	**-0.8**
2009	La Nina	Weak	-0.8	-0.5	0.1
2010	**El Nino**	**Moderate**	**1.5**	**0.9**	**-0.1**
2011	**La Nina**	**Strong**	**-1.4**	**-0.8**	**-0.5**
2012	**La Nina**	**Moderate**	**-0.8**	**-0.5**	**-0.2**
2013	Neutral	N/A	-0.4	-0.2	-0.3
2014	Neutral	N/A	-0.4	-0.2	0.3
2015	El Nino	Weak	0.6	0.6	1
2016	**El Nino**	**Very Strong**	**2.5**	**1.7**	**0.5**
2017	La Nina	Weak	-0.3	0.1	0.4
2018	La Nina	Weak	-0.9	-0.6	-0.1
2019	El Nino	Weak	0.8	0.8	0.6

Table 5.5: Monthly PNA index and PDO index throughout the study period (April 1st – June 30th) (NOAA, 2020)

	PNA April	PNA May	PNA June	PDO Index
2003	0.14	-2.2	-0.6	0.5993
2004	0.51	-1.76	-0.37	0.2471
2005	1.28	1.74	0.29	0.2945
2006	0.45	-1.27	-1.06	0.0585
2007	1.25	-0.06	-0.38	-0.1606
2008	-0.97	1.33	-1.75	-0.979
2009	0.21	-0.58	0.35	-0.4662
2010	1.54	-0.93	-0.2	-0.6209
2011	-1.59	0.19	0.22	-1.4458
2012	0.15	-0.42	-0.5	-1.2326
2013	-1.56	-0.36	-0.43	-0.6036
2014	0.25	-0.76	-1.46	1.1313
2015	-0.15	-0.16	-0.17	1.5746
2016	0.87	-1.06	-0.7	1.3134
2017	0.4	-0.31	1.01	0.538
2018	-0.91	-1.34	0.51	0.2309
2019	-0.61	-0.29	0.12	0.6504

Table 5.6: MLR results for median LDS from 2003-2019 and the explanatory variables: PDO and PNA.

Elevation	Variable	Coefficient Significance	R^2 value	Adj R^2	F stat
<1000m	PNA	0.47	0.57**	0.51	9.29
	PDO	0.0007			
1000-1200 m	PNA	0.27	0.64**	0.59	12.63
	PDO	0.0001			
1200-1400 m	PNA	0.96	0.51**	0.44	7.38
	PDO	0.0001			
1400-1600 m	PNA	0.66	0.62**	0.57	11.61
	PDO	0.0002			
1600-1800 m	PNA	0.83	0.54**	0.48	8.32
	PDO	0.001			
1800-2000 m	PNA	0.69	0.57**	0.51	9.38
	PDO	0.0008			

** Model Significance <0.01

The MLR results are presented in table 5.6 using the averaged values presented in table 5.5. The overall findings here suggest that the PNA and LDS datasets do not have strong relationship as the p-value is not statistically significant. However, the PDO is always statistically significant. The F-statistic also shows that these predictors do have a relationship with the LDS dataset, the critical F-statistics for a significance value of 0.05 and 14 degrees of freedom (df) is 2.48. The F-statistic is used in conjunction with the p-value, but it tests the joint significance of all predictors. Therefore, a significant F-statistic in this case suggests that only the PDO is contributing to the relationship since the PNA has a very large p-value throughout the table. Since the lowest F-statistic is 8.3, there is a statistically significant relationship between the PDO and the LDS datasets. Collinearity between PNA and PDO were tested for and at -0.11, it further indicates that the PNA is not contributing to the model. Also, the R^2 values are stable throughout the elevation bands, the lowest being 64%% between 1000-1200 m, when adjusted for all variables drops to 59%. This suggests that the addition of the PNA variable to the model is not contributing to the variability explained in the MLR. This test shows that there is a statistically significant relationship between the PDO and the LDS dataset.

Table 5.7: Simple linear regression results for each 3-month interval of ONI (December-June) (explanatory) to the LDS medians in various elevation bands (dependent). Bold values indicate where the R^2 value reached its highest

	Elevation	<1000 m	1000-1200 m	1200-1400 m	1400-1600 m	1600-1800 m	1800-2000 m
DJF	R^2 value	0.55**	0.53**	0.36**	0.34**	0.2	0.28*
	F stat	18.19	17.42	8.47	7.57	3.84	5.96
JFM	R^2 value	0.60**	0.56**	0.39**	0.38	0.24*	0.31*
	F stat	22.83	19.18	8.77	8.99	4.61	6.78
FMA	R^2 value	0.69**	0.60**	0.46**	0.44**	0.29**	0.36**
	F stat	33.02	22.82	12.92	11.62	6.1	8.65
MAM	**R^2 value**	**0.78****	**0.69****	**0.60****	**0.62****	**0.44****	**0.50****
	F stat	52.89	33.54	22.5	24.18	11.94	14.77
AMJ	R^2 value	0.61**	0.52**	0.62**	0.67**	0.53**	0.54**
	F stat	23.2	16.09	24.22	30.72	16.61	17.63

*Significance value <0.05
** Significance value <0.01

The simple linear regression results are presented in table 5.7. There is always a statistically significant relationship between the explanatory and dependent variables, where the explanatory variables are the ONI values for each of the 3-month intervals and the dependent variables are the LDS medians at each elevation bin. Thus, each of these regression models do differ and there hasn't been model selection throughout this process. The main justification for choosing linear over non-linear models was that the main goal here is to understand how much variability is explained by the teleconnections analyzed. The data also satisfied the assumptions and conditions for linear modeling. Linear modeling has also been used in the past to explain relationships between large scale teleconnections and snow timing such as snow offset dates, snow duration, and snow onset dates (Bevington et al., 2019). There is a general trend in R^2 values as well, as elevation increases the R^2 value begins to decrease. The largest R^2 values are in the March-April-May (MAM) monthly interval, reaching 78%. The F-statistics throughout each model is also statistically significant. An F-statistic > 1.97 is considered significant with 15 df and a significance value of 0.05. The F-statistics are also the highest during the MAM monthly interval. There is a pattern in

the strength of the relationship between the LDS dataset and the ONI, as elevation increases, the R^2 value begins to decrease. The strongest relationship is during MAM, at low elevations. This suggests that the strongest relationship between ONI and PDO is at mid-low elevations and at high elevations these relationships decrease. Also, note that the alpha level chosen was 0.05, relating to the probability of a type 1 error occurring. Most of the linear regression models shown here have a p-value below this significance value. Therefore, we can be confident about these relationships with a 5% chance of falsely rejecting the null hypothesis.

Chapter 6
Discussion

The aims and objectives of this study were to understand the dynamics and overall patterns of snow patterns during the spring freshet in Thompson-Okanagan whilst retaining as much temporal and spatial resolution as possible. This chapter is divided into three sections, the analysis of LDS variability, limitations, and future work.

6.1 Snow cover analysis

6.1.1 LDS Variations

In general, the median for last day of snow follows patterns of the PDO and ONI closely. The patterns of skewness throughout LDS boxplots suggest that there are variations within the dataset for each year. This is potentially caused by the point selection, aspect and slope affect the timing and duration of snowmelt. Depending on the landcover, whether it is forest covered or bare land exposed to direct radiation also influence snowmelt. Forest cover will cause faster melt out of snow cover. It is also more difficult to capture snow covered pixels within these areas because of the spatial resolution and the spectral differences of snow and forest covered snow. Various aspects and slope at these high elevations can affect the snow duration. Steeper and north facing slopes are favorable for longer snow duration in high elevations, whereas gradual and south facing slopes are more exposed to direct radiation and therefore will melt out faster (Pepin et al., 2015; Chaponniere et al., 2005). This can also explain why the distribution of each year within the datasets show a wide range in values (Figure 5.8-5.15). More pronounced at high elevations where the entire study region is plotted (Figure 5.8).

Throughout the individual watersheds, the LDS patterns closely resemble that of the LDS for the entire region. However, the variations in elevation band sampling reveals more insight when individual watersheds are analyzed. The South Thompson watershed low elevation (1100-1500 m) sampling shows extremely low values in comparison to the Okanagan and Columbia watersheds sampled at nearly the same elevation interval (1000-

1400 m) (Figure 5.11, Figure 5.14 & Figure 5.15). The South Thompson watershed is located to the west of Columbia and is characterized by lower overall relief which provides less topographic shadowing effects on the low elevation pixels. This could cause low elevation pixels in South Thompson to melt out at a fast rate. Okanagan also has relatively low relief in comparison to Columbia, LDS for low elevations in Okanagan are closer to that of South Thompson but have a wider range of values. This is potentially caused by the microclimate of this southern region of BC. Overall, the melt patterns throughout the study region consistently show similar patterns. Although, when analyzing the individual watersheds, the patterns are more extreme with the maximum and minimum of LDS medians in each elevation bands being reduced considerably. This suggests that the microclimate affecting snow melt varies depending on specific domain including variations in temperatures, ground temperature, and patterns of rainfall during the spring freshet.

6.1.2 Teleconnection and LDS Data Analysis

The wave-like patterns visible throughout the LDS boxplots (Figures 5.8-5.15) correspond with variations of the ONI and PDO. Studies have drawn connections between large scale atmospheric circulation patterns and their effects on snow cover extent in the western Canada (Moor & Scott, 2006; Mote et al., 2005; Thorne & Moo, 2011; Islam et al., 2017; Fleming & Whitfield, 2010). The ONI is a climatic pattern where the temperature of the equatorial Pacific is warmer or cooler than normal for a period longer than 5 consecutive months, leading to warmer or cooler temperatures in the parts of the Northern Hemisphere (Shabbar, 2014). These periods are classified as El Nino, above normal temperatures or La Nina, below normal temperatures (Bevington et al., 2019; Shabbar, 2014; Griesbauer & George, 2019). The 17-year study period contains 7 El Nino years, 7 La Nina years and 3 neutral years. El Nino years are characterized by above-normal temperatures, paired with reduced precipitation (Bevington et al., 2019; Shabbar, 2014; Griesbauer & George, 2019). La Nina years are the opposite, where temperatures are lower than normal and there is an increase in precipitation in North America (Bevington et al., 2019; Shabbar, 2014; Griesbauer & George, 2019). The PDO also plays a role in variability over this region, as

positive phases in the PDO correspond with warmer temperatures over the west coast, and negative phases with cooler temperatures (Shabbar, 2014). The PNA also affects this region, with positive phases in the PNA indicate above normal temperatures in the west and the inverse (Shrestha et al., 2015; Bevington et al., 2019). The effects of PNA are enhanced in western Canada by the El Nino via adiabatic heating causing Rossby waves that increase PNA circulation (Bevington et al., 2019; Thorne & Woo, 2011). Therefore, the fluctuations in LDS can be attributed in part to the ONI, PDO and PNA.

The regression models were used to assess the extent of the relationship between the teleconnection patterns and the LDS dataset. The PNA did not show a statistically significant impact on the LDS dataset. This was also shown to be true in other studies (Bevington et al., 2019; Thorne & Woo, 2011). The PDO was always significant, which was also the conclusion was other studies using regression analysis with PDO and snow off-dates and snow duration (Bevington et al., 2019). R^2 values for the MLR with PDO and PNA reached 64% at low-mid elevations (1000-1200 m). ONI was consistently statistically significant, with R^2 values increasing in the JFM months onward. Studies have shown that the ONI begins to influence snow duration and snow off-dates starting in January (Bevington et al., 2019; Griesbauer & George, 2019). However, the largest values are in FMA and MAM at mid-low elevations, reaching 78%. Similar patterns are found in other studies, which conclude that teleconnections have less influence on high elevations (Bevington et al., 2019; McClung, 2013).

The warmest years in the study period appear to be 2015 and 2016. These years were paired with a strongly positive PDO at 1.57 and 1.31, respectively (Table 5.5). Again, a strong positive PDO like this would signify overall warming of the region, with strong relationships between both the PDO and ONI with LDS datasets, it explains why these years have visibly lower LDS medians throughout all elevations (Bevington et al., 2019; Mote et al., 2005). The LDS shows that the coldest years were 2011 and 2012 where there were strong/moderate La Nina events in effect. The PDO during these years were also strongly negative at -1.44 and -1.23 (Table 5.5). Therefore, the PDO and ONI have major implications for the LDS dataset, and overall snow cover variability throughout the spring freshet in the

Thompson-Okanagan region. However, there are other factors to take into consideration when linking the LDS to large-scale atmospheric circulation patterns like the ONI and PDO, such as the metrics used to calculate the indices themselves. It should be noted that the PDO is calculated as a monthly spatial average of SST, usually taken between October-March when there is the most variability (NOAA, 2020). The ONI is calculated using a monthly moving average of SST and then comparing this 5-month average to the 30-year average (NOAA, 2020). The PNA is measured by winds and pressure patterns anomalies (NOAA, 2020). Thus, all these patterns are measured by identifying anomalies from previous records and average SST and atmospheric pressure heights, this could ultimately affect the indices and their relationship with the LDS in these linear regression models. These findings suggest that increased variability of teleconnections will likely impact this region.

6.1.3 LDS and Landcover Change

Another pattern noticeable with these boxplots is the distribution of values in 2017 and 2018 La Nina years compared to other La Nina years have slightly earlier melt out date medians, notably mid-elevations in the South Thompson watershed (Figure 5.11). An important thing to note about this period were massive forest fires. Southern interior BC experienced 26,869 km^2 of land ravaged by forest fires (Bevington et al., 2019). Nearly 40% of the forest cover change in this region from 1917-2017 is attributed to forest fires in 2017 (Bevington et al., 2019; Luckman & Kavanagh, 2000). These changes in forest land in the region affects snow cover duration and accumulation, as forest cover decreases snow accumulation will increase with the decrease in loss by interception. These changes also bring an increased areal extent of snow cover is exposed to direct radiation, ablation, and redistribution via blowing snow (Moore & Scott, 2006; Schelker et al., 2012; Greene et al., 1999). Thus, this could partially be the reason 2017-2018 La Nina years and 2019 El Nino had slightly earlier LDS than the other La Nina/El Nino years in the study period. Clear cutting in Southern BC is also cause for reduction in forest cover as well as the Pine Beetle infestation (Picketts et al., 2012; Li et al., 2018). These patterns of deforestation began before the study period, therefore the baseline for snow cover patterns prior to these changes in

landcover are not available (Taylor et al., 2012). The effects of these landcover change in this area have been studied to assess changes in peak and low river and baseflow (Winkler et al., 2015). These have shown and earlier peak flow, and a low spring and summer flow (Winkler et al., 2015). This means that landcover change, notably forest cover decreases have changed the timing of snow melt to be earlier (Winkler et al., 2015).

6.1.4 Potential Implications

El Nino years cost the Canadian economy billions of dollars in GDP due to loss of water resources leading to crop yield decreases due to drought, decrease in heating needs, snow recreation, and tourism (Shabbar, 2014; Strum & Goldstein, 2017). In this study, we can assign numeric significance to how much earlier snow will melt during an El Nino year in comparison to La Nina years. Each median LDS for each watershed studied and elevation bin acquired showed a significant difference between El Nino and La Nina LDS. At higher elevations, these differences were smaller than at mid-low elevations, as is expected from the regression models where we see the decrease of R^2 values with an increase in elevation. However, at mid-low elevations (900-1300 m.a.s.l. the differences average ~23 days, meaning that El Nino years are associated with a decrease in snow days by this margin at elevations between 800-1300 m.a.sl. in comparison with La Nina years. At mid elevations (1300-1800 m.a.s.l.) the average decrease in median LDS is ~18 days and at high elevations (1800-2300 m.a.sl.) it is ~13 days. There is a decline in LDS differences as elevation decreases because of the weakening relationship between ONI and snow off-dates at higher elevations (Bevington et al., 2019; McClung, 2013). Unfortunately, with only 3 neutral years in the study, there are not enough years to have an accurate baseline LDS, so these comparisons are between La Nina and El Nino years. This significantly earlier melt out of snow cover has impacts on peak flows in the region and causes low flows during the late spring and summer seasons (Winkler et al., 2017).

6.2 Limitations

The cloud filling methodology mitigated up to 90% of cloud cover in some cases, with an average of 3% decrease in accuracy from original Terra snow products. The accuracy throughout the methodology did not show extreme fluctuations. After each additional methodology was applied to the images, the accuracy declines were very minimal in most cases. It is suspected that as we move through each step, the additional pixels used to test accuracy do not increase drastically. However, even in cases where ATD have increased pixels under investigations, only a 2% decline in accuracy is shown. The reason there are declines in accuracy as opposed to increases, is because of the seasonality of the study. With ATD in a study during the spring freshet, inaccuracies will arise when snow melt occurs on a day where that pixel is cloud covered because it will be assigned as snow if it had been classified as snow the previous day. This is more prominent issue with ATD. However, a 2% decrease in accuracy is a good margin with the addition of over 20,000 pixels (Table 5.3). SNOWL showed a drastic increase in points used on April 1st, 2014 and May 14th, 2018 (Figure 5.5). On May 14th, the accuracy increased by ~2% from the ATD accuracy and April 1st remained the same. This shows that SNOWL is robust and accurate throughout the spring freshet in this region.

The accuracy assessment was done for forested and non-forested land separately as well, to better understand where the inaccuracies are concentrated. Many studies report on the inability to accurately classify snow cover in forested regions (Wang et al., 2011; Tait, 2000; Czyzowska-Wisniewski, 2015). The findings here corroborate these assertions, as forested region showed lower accuracies across all methodologies almost consistently (Table 5.3). Errors in forested regions can also be caused in part by thin patchy snow underneath the canopy (Hall, 2007). In these cases, for 500 m resolution it will be extremely difficult to identify this snow cover. Underlying vegetation will also change the reflectance properties of snow, SNOWMAP is sensitive to these changes and likely will erroneously flag these pixels as “no snow” (Wang et al., 2011; Chokmani et al., 2010). Interestingly, there were some days where accuracy in forested regions were higher than the whole area, notably June 24th, 2017 and May 26th, 2019. A possible explanation for this is that both dates are late in the season.

Nearly the end of June snow cover is expected to be almost entirely limited to upper limits in the mountains where there is minimal vegetation (Rayne & Forest, 2016). It was noted that 2019 was a year of minimal snow cover in the region and thus the end of May in 2019 could be explained with the same reasoning. Accuracy results for a couple of dates in early April were surprisingly low as well. Snow cover during April will be present in forest covered regions, where the largest inaccuracies occur. Since the method for classifying snow cover in Landsat images were tailored to better represent snow covered forests, it is understandable that the MODIS algorithm at a much larger spatial resolution would fall short of this.

There is a slight lag in overpass times Terra, Aqua and VIIRS and Landsat-8. Therefore, it is possible that the snow cover in these forested regions were in fact snow covered and by the time Landsat-8 had gathered data in the region that snow was no longer present. This is especially true in forested regions when considering sensible heat exchange from vegetation, this heat could quickly melt snow surrounding vegetation (Kim et al., 2017). Other main reasons why we see inaccuracies are the confusion of snow and cirrus clouds and thin patchy snow which are reported problems in most research concerning snow cover (Dietz, 2012; Parajka et al., 2010; Hall et al., 2019). Though the MODIS cloud mask is very conservative and overestimates cloud cover, in some cases high cirrus clouds can be misclassified as snow (Hall et al., 2019; Dong, 2018). Patchy snow throughout the season is a major source for omission errors for moderate resolution like MODIS (Jain et al., 2008; Parajka et al., 2012; Crawford, 2015). This is because these areas are often the transitional zones from snow cover to non-snow-covered regions. These regions often exhibit characteristics of patchy, thin, and often dirty snow that is affecting the retrieval of snow at moderate resolutions (Crawford, 2015; Dietz, 2012). These misclassifications in the original satellite images could transfer over to the main product throughout the methodology. However, the overall accuracies are within the same range as other studies when conducting multi-step methodologies (Parajka et al., 2012). The forest cover accuracy also shows the same range as other studies between ~60-98% agreement with high resolution imagery when considering snow-covered forests (Crawford, 2015).

This cloud mitigation methodology allowed for the successful creation of the LDS dataset to analyze snow patterns in the Thompson Okanagan region. The LDS datasets do provide a good understanding of variability at various elevations throughout the 4 watersheds studied in the region. The LDS dataset is sensitive to transient snow fall. However, the methodology to extract the LDS is robust as it is recorded as the last day where snow is present for >4 days consecutively. The study period was only 17-years and therefore no conclusions could be made about climate change in the region. Nevertheless, the findings show that there are variations within the LDS dataset that can be attributed to teleconnection patterns. Further investigation using this methodology in coming years would assist in understanding potential climate change impacts on the region. Spatial resolution is a major limitation in remote sensing. In a forest covered region such as Thompson-Okanagan, this limitation caused errors in snow mapping under forest canopies, patchy and thin snow, and dirty snow (Hall, 2007; Jain et al., 2008 & Chaponniere et al., 2005). Yet, forest covered regions exclusively still reached up to 98% accuracy when comparing to high resolution imagery. Therefore, by mitigating cloud cover in the region, it was possible to extract valuable insights on snow patterns which would not be possible without the multi-step cloud mitigation methodology.

The use of MODIS and VIIRS resampled to 500 m resolution, and daily temporal resolution are limited by their availability. However, moderate resolution is essential when measuring snow offset dates in a region with complex topography such as Thompson Okanagan. Increased variability of snow cover is associated with changes in aspect, slope, vegetation cover and rain events (Erxleben et al., 2002). Thus, to increase certainty of the LDS dataset it can be argued that this spatial scale is required. Also, given the timing of the study daily temporal resolution is required because the focus is to understand the daily changes in snow offset date as they are associated with changes in phase of atmospheric circulation patterns.

6.3 Future work

Further research includes further developing the method presented with additional steps for cloud mitigation. Applying the method in other regions to test robustness, specifically in mountain regions for the implementation of SNOWL. The addition of VIIRS to TAC could also be applied in any study to mitigate cloud cover contamination. Published works of recently developed cloud-gap-filled snow cover products using Terra/Aqua and VIIRS show that this is a viable method to mitigate cloud contamination (Hall et al., 2019). Land cover change is a major source of snow cover variability in this region (Winkler et al., 2017). Analysis of land cover change within the period in this study would be beneficial to better solidifying the relationship between snow cover variability and clear-cutting forests, forest cover change via Pine Beetle infestation and forest fires as well. The addition of Sentinel-1 (SAR) instrument measurements in conjunction with visible-infrared imagery would mitigate all cloud cover, as SAR observations use large wavelengths that are unaffected by cloud cover. An application of this methodology could be to continue to monitor snow cover variability in climate sensitive regions such as Thompson-Okanagan.

Snow water equivalent (SWE) data would be an asset to stakeholders in the area. However, there is a relationship between SWE and snow depth to snow cover given that the deeper the snowpack, the more time it will take to melt. Given this relationship, it can be argued that snow cover extent and LDS are still valuable and critical components to water resource management. In the past, visible infrared remote sensing has been used to construct snow depletion curves with daily temporal resolution (Winkler et al., 2015). From the cloud mitigated product, this is a potential avenue for future research in the region.

Chapter 7
Conclusion

This study investigated the snow offset dates in Thompson-Okanagan, southern BC from 2003-2019. Using visible infrared remote sensing imagery has major cloud coverage. Therefore, the objective was to perform a multi-step cloud mitigation method and measure the accuracy and success of the procedure. Snow cover melt out was measured by the metric of LDS taken at various elevations throughout the 4 watersheds within the region. The key findings and potential implications are summarized below.

Multi-step cloud removal processes are popular throughout the literature for studying snow cover (Parajka et al., 2012; Lindsay et al., 2015; Hüsler et al., 2014; Li et al., 2017). This multi-step methodology mitigated up to 90% of cloud cover in some cases, leaving an average annual cloud coverage of 0.2-2.4% (Table 5.1). Remaining cloud cover is exclusively present at mid-elevations where SNOWL leaves pixels assumed to be "partly snow-covered" as clouds. Accuracy was retained throughout these processes, decreasing by an average of 3% by the end of multi-step methodology, but reaching agreement of 98%. These misclassifications are presumably attributed to the presence of cirrus clouds and misclassification in the snow product data themselves, thin and patchy snow during the offset. The forest cover snow inaccuracies were shown, and most false negatives were present in forested regions. The issues with measuring snow cover using visible remote sensing are present throughout the literature as the spectral signature of snow changes for dirty, thin, patchy snow and snow cover in forests (Li et al., 2019). This multi-step methodology can be used in other mountainous regions, notably regions that do not experience polar night since all satellite imagery used was visible infrared. Although the accuracies with comparison to high resolution imagery was stable in this environment, accuracy may vary in distinct locations. Reproducibility of this methodology can be done in any region as all data is opensource and all software used is as well. Although the cloud mitigation methodology did not completely remove cloud cover for each year, it was

successful in removing a majority of cloud cover to create the LDS datasets throughout the four watersheds investigated.

Snow cover analysis throughout the four individual watersheds investigated in the region show a similar pattern. The wave like trend in the LDS dataset coincide with major fluctuations in the ONI. ONI and PDO fluctuations explain up to 78% and 64% of variability in the low-mid elevation snow cover melt out dates, respectively. Results from the MLR showed the PNA had no statistically significant relationship with the LDS datasets. Studies within this region have shown comparable results when attributing fluctuations in snow cover to large teleconnection pattems (Bevington et al., 2019). It is also shown that on average throughout the region El Nino years will influence the melt out of snow to be ~23 days earlier than the average La Nina year at low elevations, ~18 days at mid elevations and ~13 days at high elevations.

These changes in snowmelt affect flow regimes, as was found in other studies (Winkler et al., 2015). Flow regimes affect the crop yield in the region, which is crucial for the wine industry in Okanagan as well (Caprio & Quamme, 2002; Picketts et al., 2012). Aquatic habitat could also be impacted by changing flow regimes; however, this is not a simple linear relationship. Further research is required to conclude the impact of offset flow regimes on fish habitat, specifically salmon production in this region (Bradford et al., 2011). Earlier snowmelt is linked to low baseflow in the summer season, this dryness could increase risk of forest fires in the Thompson-Okanagan region (Berman et al., 2018). This area is already experiencing increased forest loss from forest fires, pine beetle infestation and clear cutting (Winkler et al., 2017; Schelker et al., 2013). Forest fire risk and snow offset date is linked, as earlier snowmelt increases variability and area burned during the summer seasons in western regions (Westerling, 2016). In mountainous regions, the inverse can occur as well, as forest fires increase, they melt snow in higher elevations leading to decreases in water availability and fueling larger fires and area burned (Westerling, 2016). This relationship has large impacts on the economy, forest fires in 2004 reduced revenue by 3% for tourism in southern BC specifically in the winery district (Statistics Canada, 2017). Further investigations on the economic impacts of reduced snow cover during El Nino events are

required. However, a study showed a decrease in the Canadian economy by almost $4 billion due to an El Nino event in 1997-98 (Shabbar, 2014). These losses are attributed to crop loss from drought, heating industry losses, recreational revenue loss from lack of wintertime snow, ice wine industry losses and Salmon fishery loss (Shabbar, 2014).

There was no distinct downward trend in median LDS in the four individual watersheds studied within Thompson-Okanagan. Climate studies have shown earlier snow melt in the springtime and decreasing overall snow extent in the northern hemisphere (Sturm & Goldstein, 2017). Although we don't see this trend with the LDS datasets from this study or from the in situ data gathered from the stations available, this study was done on a 17-year dataset, and therefore is not a long enough timeframe to draw conclusions about recent climate change impacts on the region. The short dataset is due to availability of data. In this region, historical snow cover data such as the NOAA CDR would bring about too many uncertainties given that it masks out mountain ranges and has a coarse temporal resolution at the start of the record (1966) and coarse spatial resolution. As stated previously, daily temporal resolution is ideal for a study focusing on the spring freshet period and moderate spatial resolution is as well when focusing on regional scale fluctuations of snow offset date. Studies done using regional climate models predict variations in this area with a changing climate, including increased precipitation as rain instead of snow, a possible transition into a pluvial region, decreased water availability, increased forest fires and increased risk of flooding (Islam et al., 2019; Harder et al., 2015; Winkler et al., 2017). Thus, the findings in this study pertain mostly to variations in snow melt out dates via large atmospheric teleconnections and potentially land cover change. With increased anthropogenic forcing, the patterns and relationships derived between LDS and teleconnections could fluctuate especially given that the effects of climate change on ONI and PDO are still under investigation (Collins et al., 2010). These changes may in part be attributed to climate change but continuing this study in the future is necessary to establish this connection.

References

Bales, R. C., Glaser, S. D., & Bayen, A. M. (2018). Multi-spatial-scale observational studies of the Sierra Nevada snowpack using wireless-sensor networks and multi-platform remote-sensing data [Unpublished doctoral dissertation/master's thesis] UC Berkeley.

Barsi, J. A., Lee, K., Kvaran, G., Markham, B. L., & Pedelty, J. A. (2014). The Spectral Response of the Landsat-8 Operational Land Imager. *Remote Sensing*, *6*, 10232–10251. https://doi.org/10.3390/rs61010232

Beacham, T. D., & Withler, R. E. (2017). Population structure of sea-type and lake- type sockeye salmon and kokanee in the Fraser River and Columbia River drainages. *PLOS One*, 1–17. https://doi.org/10.5061/dryad.3g824.

Berman, E. E., Bolton, D. K., Coops, N. C., Mityok, Z. K., Stenhouse, G. B., & Moore, R. D. (Dan. (2018). Daily estimates of Landsat fractional snow cover driven by MODIS and dynamic time-warping. *Remote Sensing of Environment*, *216*, 635–646. https://doi.org/10.1016/j.rse.2018.07.029

Bernhardt, M., Schulz, K., Liston, G. E., & Zängl, G. (2012). The influence of lateral snow redistribution processes on snow melt and sublimation in alpine regions. *Journal of Hydrology*, *424–425*, 196–206. https://doi.org/10.1016/j.jhydrol.2012.01.001

Bevington, A. R., Gleason, H. E., Foord, V. N., Floyd, W. C., & Griesbauer, H. P. (2019). Regional influence of ocean – atmosphere teleconnections on the timing and duration of MODIS-derived snow cover in British Columbia, Canada, *The Cryosphere, 13*, 2693-2712. https://doi.org/10.5194/tc-13-2693-2019

Bhatti, A. M., Koike, T., & Shrestha, M. (2016). Climate change impact assessment on mountain snow hydrology by water and energy budget-based distributed hydrological model. *Journal of Hydrology*, *543*, 523–541. https://doi.org/10.1016/j.jhydrol.2016.10.025

Bormann, K. J. (2018). Estimating snow-cover trends from space. *Nature Climate Change*, *8*, 924-936. https://doi.org/10.1038/s41558-018-0318-3

Bradford, M.J., Higgins, J.K., Sneep, J. (2011). Test of an environmental flow release in a British Columbia river: does more water mean more fish? *Freshwater Biology*, 2119–2134. https://doi.org/10.1111/j.1365-2427.2011.02633.x

Brown, R. D., & Derksen, C. (2013). Is Eurasian October snow cover extent increasing? *Environmental Research Letters, 8*. https://doi.org/10.1088/1748-9326/8/2/024006

Brown, R. D., & Robinson, D. A. (2011). Northern Hemisphere spring snow cover variability and change over 1922 – 2010 including an assessment of uncertainty. *The Cryosphere*, 219–229. https://doi.org/10.5194/tc-5-219-2011

Brown, R. D., Mote, P. W. (2008). The Response of Northern Hemisphere Snow Cover to a Changing Climate. *Journal of Climate*, *22*, 2124–2145. https://doi.org/10.1175/2008JCLI2665.1

Brown, R., Derksen, C., & Wang, L. (2007). Assessment of spring snow cover duration variability over northern Canada from satellite datasets. *Remote Sensing of Environment, 111*, 367–381. https://doi.org/10.1016/j.rse.2006.09.035

Brown, R., Derksen, C., & Wang, L. (2010). A multi - data set analysis of variability and change in Arctic spring snow cover extent, 1967 – 2008. *Journal of Geophysical Research, 115*. https://doi.org/10.1029/2010JD013975

Caprio, J. M., & Quamme, H. A. (2002). Weather conditions associated with grape production in the Okanagan Valley of British Columbia and potential impact of climate change. *Canadian Journal of Plant Science,* 755-765.

Carey, S. K., & Pomeroy, J. W. (2009). Progress in Canadian Snow and Frozen Ground Hydrology, 2003-2007. *Canadian Water Resources Journal, 34(2)*, 127–138.

Chaponnière, A., Maisongrande, P., Duchemin, B., Hanich, L., Boulet, G., Escadafal, R., & Elouaddat, S. (2005). A combined high and low spatial resolution approach for mapping snow covered areas in the Atlas mountains. *International Journal of Remote Sensing*, *26*(13), 2755–2777. https://doi.org/10.1080/01431160500117758

Chelamallu, H. P., Venkataraman, G., & Murti, M. V. R. (2014). Accuracy assessment of MODIS / Terra snow cover product for parts of Indian Himalayas. *Geocarto International, 29*(6), 592–608. https://doi.org/10.1080/10106049.2013.819041

Chen, B., Member, S., Huang, B., Member, A., Chen, L., & Xu, B. (2017). Spatially and Temporally Weighted Regression : A Novel Method to Produce Continuous Cloud-Free Landsat Imagery. *IEEE Transactions on Geoscience and Remote Sensing*, *55*(1), 27–37. https://doi.org/10.1109/TGRS.2016.2580576

Chokmani, K., Dever, K., Bernier, M., Gauthier, Y., Chokmani, K., Dever, K., … Paquet, L. (2010). Adaptation of the SNOWMAP algorithm for snow mapping over eastern Canada using Landsat-TM imagery Adaptation of the SNOWMAP algorithm for snow mapping over eastern Canada using Landsat-TM imagery. *Hydrological Sciences Journal, 55(4), 6667*. https://doi.org/10.1080/02626661003747374

Church, M., & Ryder, J. M. (n.d.). Physiography of British Columbia, 17–46.

Collins, M. et al., (2010). The impact of global warming on the tropical Pacific Ocean and El Nino. *Nature Geoscience, 3*, 391-397. https://doi.org/10.1038/ngeo868

Cotton, W.R., & Anthes, R.A. (1992). Chapter 12 The Influence of Mountains on Airflow, Clouds and Precipitation. *International Geophysics, 44*, 788-870. https://doi.org/10.1016/S0074-6142(08)60551-3.

Crawford, C. J. (2015). MODIS Terra Collection 6 fractional snow cover validation in mountainous terrain during spring snowmelt using Landsat TM and ETM +. *Hydrological Processes, 29*, 128–138. https://doi.org/10.1002/hyp.10134

Czyzowska-Wisniewski, E. H., van Leeuwen, W. J. D., Hirschboeck, K. K., Marsh, S. E., & Wisniewski, W. T. (2015). Fractional snow cover estimation in complex alpine-forested environments using an artificial neural network. *Remote Sensing of Environment, 156*, 403–417. https://doi.org/10.1016/j.rse.2014.09.026

Dedieu, J. P., Carlson, B. Z., Bigot, S., Sirguey, P., Vionnet, V., & Choler, P. (2016). On the importance of high-resolution time series of optical imagery for quantifying the effects of snow cover duration on alpine plant habitat. *Remote Sensing, 8*(6). https://doi.org/10.3390/rs8060481

Dedieu, J. P., Lessard-Fontaine, A., Ravazzani, G., Cremonese, E., Shalpykova, G., & Beniston, M. (2014). Shifting mountain snow patterns in a changing climate from remote

sensing retrieval. *Science of the Total Environment*, *493*, 1267–1279. https://doi.org/10.1016/j.scitotenv.2014.04.078

Deng, J., Huang, X., Feng, Q., Ma, X., & Liang, T. (2015). Toward improved daily cloud-free fractional snow cover mapping with multi-source remote sensing data in China. *Remote Sensing*, *7*(6), 6986–7006. https://doi.org/10.3390/rs70606986

Derksen, C., & Brown, R. (2012). Spring snow cover extent reductions in the 2008 – 2012 period exceeding climate model projections. *Geophysical Research Letters*, *39*, 1–6. https://doi.org/10.1029/2012GL053387

Derksen, C., Smith, S. L., Sharp, M., & Brown, L. (2012). Variability and change in the Canadian cryosphere. *Climatic Change*. https://doi.org/10.1007/s10584-012-0470-0

Derksen, L. R. M. P. J. K. C. (2014). Interpreting observed northern hemisphere snow trends with large ensembles of climate simulations. *Climate Dynamics*, *43*, 345–359. https://doi.org/10.1007/s00382-013-1954-y

Dietz, A. J., Kuenzer, C., Gessner, U., & Dech, S. (2012). Remote sensing of snow - a review of available methods. *International Journal of Remote Sensing*, *33*(13), 4094–4134. https://doi.org/10.1080/01431161.2011.640964

Dong, C. (2018). Remote sensing, hydrological modeling and in situ observations in snow cover research: A review. *Journal of Hydrology*, *561*, 573–583. https://doi.org/10.1016/j.jhydrol.2018.04.027

Dong, C., & Menzel, L. (2016). Producing cloud-free MODIS snow cover products with conditional probability interpolation and meteorological data. *Remote Sensing of Environment*, *186*, 439–451. https://doi.org/10.1016/j.rse.2016.09.019

Dong, T., Liu, J., Qian, B., Zhao, T., Jing, Q., Geng, X., … Shang, J. (2016). Estimating winter wheat biomass by assimilating leaf area index derived from fusion of Landsat-8 and MODIS data. *International Journal of Applied Earth Observation and Geoinformation*, *49*, 63–74. https://doi.org/10.1016/j.jag.2016.02.001

Dore, M. H. I. (2005). Climate change and changes in global precipitation patterns: What do we know ? *Environment International*, *31*, 1167–1181. https://doi.org/10.1016/j.envint.2005.03.004

Eckerstorfer, M., Bühler, Y., Frauenfelder, R., & Malnes, E. (2016). Remote sensing of snow avalanches: Recent advances, potential, and limitations. *Cold Regions Science and Technology*, *121*, 126–140. https://doi.org/10.1016/j.coldregions.2015.11.001

Elliott, G. P., & Petruccelli, C. A. (2018). Tree recruitment at the treeline across the Continental Divide in the Northern Rocky Mountains, USA : the role of spring snow and autumn climate. *Plant Ecology & Diversity*, *11*(3), 319–333. https://doi.org/10.1080/17550874.2018.1487475

Engebretson, C. (2020). Landsat 8-9 Operational Land Imager (OLI) - Thermal Infrared Sensor (TIRS) Collection 2 Level 2 (L2) Data Format Control Book (DFCB) September 2020 Operational Land Imager (OLI) - Thermal Infrared Sensor (TIRS) Data Format Control Book (DFCB. *U.S. Geological Survey*, *2*.

Erxleben, J., Elder, K., & Davis, R. (2002). Comparison of spatial interpolation methods for estimating snow distribution in the Colorado Rocky Mountains. *Hydrological Processes*, *16*(18), 3627–3649. https://doi.org/10.1002/hyp.1239

Fleming, S. W., & Whitfield, P. H. (2010). Spatiotemporal mapping of ENSO and PDO surface meteorological signals in British Columbia , Yukon , and southeast Alaska Spatiotemporal Mapping of ENSO and PDO Surface Meteorological Signals in British Columbia , Yukon , and Southeast Alaska. *Atmosphere-Ocean, 48(2),* 122-131. https://doi.org/10.3137/AO1107.2010

Glantz, M. H., & Ramirez, I. J. (2020). Reviewing the Oceanic Nino Index (ONI) to Enhance Societal Readiness for El Nino's Impacts. *Int J Disaster Risk Sci, 11*, 394–403. https://doi.org/10.1007/s13753-020-00275-w

Gafurov, A., Bardossy, A. (2009). Cloud removal methodology from MODIS snow cover product. *Hydrology and Earth System Sciences, 13*, 1361–1373.

Gao, Y., Xie, H., Yao, T., & Xue, C. (2010). Integrated assessment on multi-temporal and multi-sensor combinations for reducing cloud obscuration of MODIS snow cover products of the Paci fi c Northwest USA. *Remote Sensing of Environment*, *114*(8), 1662–1675. https://doi.org/10.1016/j.rse.2010.02.017

Greene, E. M., Liston, G. E., & Pielke, R. A. (1999). Relationships between landscape , snowcover depletion , and regional weather and climate. *Hydrological Processes, 13*, 2453–2466.

Grömping, U. (2009). Variable Importance Assessment in Regression: Linear Regression versus Random Forest. *The American Statistician, 63*(4), 308-319. Retrieved January 6, 2021, from http://www.jstor.org/stable/25652309

Gwangyong, C., Robinson, A.D.,& Sinkyu, K. (2010). Changing Northern Hemisphere Snow Seasons. *American Meteorological Society,* 5305–5310. https://doi.org/10.1175/2010JCLI3644.1

Hall, D. K., Riggs, G. A., & Barton, J. S. (2001). Algorithm Theoretical Basis Document (ATBD) for the MODIS Snow and Sea Ice-Mapping Algorithms. Retrieved from https://modis-snow-ice.gsfc.nasa.gov/?c=atbd&t=atbd

Hall, D. K., Riggs, G. A., Digirolamo, N. E., & Román, M. O. (2019). MODIS Cloud-Gap Filled Snow-Cover Product : Advantages and Uncertainties. *Hydrology and Earth System Sciences*, 1–23.

Hall, D. K., Riggs, G. A., Digirolamo, N. E., Román, M. O., & Hall, C. D. K. (2019). Evaluation of MODIS and VIIRS cloud-gap-filled snow-cover products for production of an Earth science data record. *Hydrology and Earth System Sciences,* 5227–5241.

Hall, D. K., Riggs, G. A., Salomonson, V. V, DiGirolamo, N. E., & Bayr, K. J. (2002). MODIS snow-cover products. *Remote Sensing of Environment*, *83*(1–2), 181–194. https://doi.org/10.1016/S0034-4257(02)00095-0

Harder, P., Pomeroy, J. W., & Westbrook, C. J. (2015). Hydrological resilience of a Canadian Rockies headwaters basin subject to changing climate, extreme weather, and forest management. *Hydrological Processes, 3924*, 3905–3924. https://doi.org/10.1002/hyp.10596

Hedrick A.R., Marks, D., Havens, S., Robertson, M., Johnson, M., Sandusky, M., et al. (2018). Direct Insertion of NASA Airborne Snow Observatory-Derived Snow Depth Time Series Into the iSnobal Energy Balance Snow Model. *Water Resources Researche*, 8045–8063. https://doi.org/10.1029/2018WR023190

Hernández-henríquez, M. A., Déry, S. J., & Derksen, C. (2015). Polar amplification and elevation-dependence in trends of Northern Hemisphere snow cover extent, 1971 – 2014. *Environmental Research Letters*, *10*(4), 44010. https://doi.org/10.1088/1748-9326/10/4/044010

Hori, M., Sugiura, K., Kobayashi, K., Aoki, T., Tanikawa, T., Kuchiki, K., … Enomoto, H. (2017). A 38-year (1978–2015) Northern Hemisphere daily snow cover extent product derived using consistent objective criteria from satellite-borne optical sensors. *Remote Sensing of Environment*, *191*, 402–418. https://doi.org/10.1016/j.rse.2017.01.023

Hüsler, F., Jonas, T., Riffler, M., Musial, J. P., & Wunderle, S. (2014). A satellite-based snow cover climatology (1985-2011) for the European Alps derived from AVHRR data. *Cryosphere*, *8*(1), 73–90. https://doi.org/10.5194/tc-8-73-2014

Huss, M., Bookhagen, B., Huggel, C., Jacobsen, D., Bradley, R. S., Clague, J. J., & Vuille, M. (2013). Earth's Future Toward mountains without permanent snow and ice Earth ' s Future. *AGU Earth's Future,5,* 418–435. https://doi.org/10.1002/eft2.207

Islam, U. S., Dery, J.S, & Werner, A. T. (2017). Future Climate Change Impacts on Snow and Water Resources of the Fraser River Basin , British Columbia. *Journal of Hydrometeorology*, 473–496. https://doi.org/10.1175/JHM-D-16-0012.1

J. Schelker, L. Kuglerová, K. Eklöf, K. Bishop, H. Laudon. (2013). Hydrological effects of clear-cutting in a boreal forest – Snowpack dynamics, snowmelt and streamflow responses. *Journal of Hydrology*, 484, 105-114, ISSN 0022-1694, https://doi.org/10.1016/j.jhydrol.2013.01.015.

Jain, S. K., Goswami, A., & Saraf, A. K. (2008). Accuracy assessment of MODIS, NOAA and IRS data in snow cover mapping under Himalayan conditions. *International Journal of Remote Sensing*, *29*(20), 5863–5878. https://doi.org/10.1080/01431160801908129

Kang, H., D., Shi, Z., Huilin, G., Dery J., S. (2014). On the Changing Contribution of Snow to the Hydrology of the Fraser River Basin , Canada. *Journal of Hydrometeorology*, 1344–1365. https://doi.org/10.1175/JHM-D-13-0120.1

Key, J. R., Mahoney, R., Liu, Y., Romanov, P., Tschudi, M., Appel, I., … Meade, P. (2013). Snow and ice products from Suomi NPP VIIRS. *Journal of Geophysical Research: Atmospheres*, *118*, 816–830. https://doi.org/10.1002/2013JD020459

Kienzle, S. W., Nemeth, M. W., Byrne, J. M., & Macdonald, R. J. (2012). Simulating the hydrological impacts of climate change in the upper North Saskatchewan River basin , Alberta , Canada. *Journal of Hydrology*, *412–413*, 76–89. https://doi.org/10.1016/j.jhydrol.2011.01.058

Kim, D., Ray, R. L., & Choi, M. (2017). Simulations of energy balance components at snow-dominated montane watershed by land surface models. *Environmental Earth Sciences*, *76*(9), 1–17. https://doi.org/10.1007/s12665-017-6655-0

Klock, R., & Mullock, J. (2001). The Weather of British Columbia. *NAV Canada*.

Lapp, S., Byrne, J., Townshend, I., & Kienzle, S. (2005). Climate warming impacts on snowpack accumulation in an alpine watershed. *International Journal of Climatology, 536*, 521–536. https://doi.org/10.1002/joc.1140

Lehning, M., Grünewald, T., & Schirmer, M. (2011). Mountain snow distribution governed by an altitudinal gradient and terrain roughness. *Geophysical Research Letters*, *38*(19), 1–5. https://doi.org/10.1029/2011GL048927

Li, J., & Roy, D. P. (2017). A Global Analysis of Sentinel-2A, Sentinel-2B and Landsat-8 Data Revisit Intervals and Implications for Terrestrial Monitoring. *Remote Sensing*. https://doi.org/10.3390/rs9090902

Li, Q., Wei, X., Yang, X., Giles-hansen, K., Zhang, M., & Liu, W. (2018). Topography significantly influencing low flows in snow-dominated watersheds. *Hydrology and Earth System Science*,*22*, 1947–1956.

Li, X., Fu, W., Shen, H., Huang, C., & Zhang, L. (2017). Monitoring snow cover variability (2000 – 2014) in the Hengduan Mountains based on cloud-removed MODIS products with an adaptive spatio-temporal weighted method. *Journal of Hydrology*, *551*, 314–327. https://doi.org/10.1016/j.jhydrol.2017.05.049

Li, X., Jing, Y., Shen, H., & Zhang, L. (2019). The recent developments in cloud removal approaches of MODIS snow cover product. *Hydrology and Earth System Science*, *23*, 2401–2416.

Li, Y. (2019). Developing Daily Cloud - Free Snow Composite Products From MODIS and IMS for the Tienshan Mountains. *Earth and Space Science*, *6*, 266-275. https://doi.org/10.1029/2018EA000460

Liao, C. (2017). A Spatio-Temporal Data Fusion Model for Generating NDVI Time Series in Heterogeneous Regions, (30 m). *Remote Sensing*, 1–28. https://doi.org/10.3390/rs9111125

Lindsay, C., Zhu, J., Miller, A. E., Kirchner, P., & Wilson, T. L. (2015). Deriving snow cover metrics for Alaska from MODIS. *Remote Sensing*, *7*(10), 12961–12985. https://doi.org/10.3390/rs71012961

Liston, G. E. (1999). Interrelationships among Snow Distribution , Snowmelt , and Snow Cover Depletion : Implications for Atmospheric , Hydrologic , and Ecologic Modeling. *J. Applied Meteorology*,*38*,1474–1487.https://doi.org/10.1175/1520-0450

Liston, G. E., & Elder, K. (2006). A Distributed Snow-Evolution Modeling System (SnowModel). *Journal of Hydrometeorology*, *7*(6), 1259–1276. https://doi.org/10.1175/JHM548.1

Lopez-Burgos, H. Y. G. & M. C. (2013). Reducing cloud obscuration of MODIS snow cover area products by combining spatio-temporal techniques with a probability of snow Solid Earth. *Hydrology and Earth System Sciences*, 1809–1823. https://doi.org/10.5194/hess-17-1809-2013

Marty, C., & Blanchet, J. (2012). Long-term changes in annual maximum snow depth and snowfall in Switzerland based on extreme value statistics. *Climate Change*, 705–721. https://doi.org/10.1007/s10584-011-0159-9

Mcclung, D. M. (2013). The effects of El Nino and La Nina on snow and avalanche patterns in British Columbia, Canada, and central Chile. *Journal of Glaciology*, *59*(216), 783–792. https://doi.org/10.3189/2013JoG12J192

Merritt, W. S., Alila, Y., Barton, M., Taylor, B., Cohen, S., & Neilsen, D. (2006). Hydrologic response to scenarios of climate change in sub watersheds of the Okanagan basin, British Columbia. *Journal of Hydrology*, *326*, 79–108. https://doi.org/10.1016/j.jhydrol.2005.10.025

Metsämäki, S., Böttcher, K., Pulliainen, J., Luojus, K., Cohen, J., Takala, M., … Koponen, S. (2018). The accuracy of snow melt-off day derived from optical and microwave

radiometer data — A study for Europe. *Remote Sensing of Environment, 211,* 1–12. https://doi.org/10.1016/j.rse.2018.03.029
Miller, S. D., Straka, W., Mills, S. P., Elvidge, C. D., Lee, T. F., Solbrig, J., … Weiss, S. C. (2013). Illuminating the Capabilities of the Suomi National Polar-Orbiting Partnership (NPP) Visible Infrared Imaging Radiometer Suite (VIIRS) Day/Night Band. *Remote Sensing, 5,* 6717–6766. https://doi.org/10.3390/rs5126717
Minder, J. R., Letcher, T. W., & Skiles, S. M. (2016). An evaluation of high-resolution regional climate model simulations of snow cover and albedo over the Rocky Mountains, with implications for the simulated snow-albedo feedback. *J. Geophys. Res. Atmos, 121,* 9069–9088. https://doi.org/10.1002/2016JD024995.Received
Moore, R. D., & Scott, D. F. (2006). Camp Creek Revisited: Streamflow Changes Following Salvage Harvesting in a Medium-Sized, Snowmelt- Dominated Catchment. *Canadian Water Resources Journal, 30,* 331–344. https://doi.org/10.4296/cwrj3004331
Moreira, E. P., & Formaggio, A. R. (2016). Topographic effect on spectral vegetation indices from Landsat TM data: Is topographic correction necessary? *Bol. Cienc. Geod., 4*, 95–107. http://dx.doi.org/10.1590/S1982-21702016000100006
Morriss, B. F., Ochs, E., Deeb, E. J., Newman, S. D., Daly, S. F., & Gagnon, J. J. (2016). Remote Sensing of Environment Persistence-based temporal fi ltering for MODIS snow products. *Remote Sensing of Environment, 175,* 130–137. https://doi.org/10.1016/j.rse.2015.12.030
Mote, P. W., Rupp, D. E., Li, S., Sharp, D. J., Otto, F., Uhe, P. F., … Allen, M. R. (2016). Perspectives on the causes of exceptionally low 2015 snowpack in the western United States. *Geophysical Research Letters, 43,* 980–988. https://doi.org/10.1002/2016GL069965.Received
Mudryk, L. R. (2017). Snow cover response to temperature in observational. *Geophysical Research Letters, 44,* 919-926. https://doi.org/10.1002/2016GL071789
Nagler, T., Rott, H., Ripper, E., Bippus, G., & Hetzenecker, M. (2016). Advancements for snowmelt monitoring by means of Sentinel-1 SAR. *Remote Sensing, 8*(4), 1–17. https://doi.org/10.3390/rs8040348
Niwano, M., Aoki, T., Kuchiki, K., Hosaka, M., & Kodama, Y. (2012). Snow Metamorphism and Albedo Process (SMAP) model for climate studies : Model validation using meteorological and snow impurity data measured at Sapporo , Japan. *Journal of Geophysical Research, 117*, 1–18. https://doi.org/10.1029/2011JF002239
NOAA (National Oceanic and Atmospheric Administration) (2020) Retrieved December 12, 2020, from https://origin.cpc.ncep.noaa.gov/products/analysis_monitoring/ensostuff/ONI_v5.php
NOAA (National Oceanic and Atmospheric Administration) (2020) Retrieved December 12, 2020, from https://www.ncdc.noaa.gov/teleconnections/pna/
O'Leary, D., Hall, D., Medler, M., & Flower, A. (2018). Quantifying the early snowmelt event of 2015 in the Cascade Mountains, USA by developing and validating MODIS-based snowmelt timing maps. *Earth Science, 12*(4), 693–710. https://doi.org/10.1007/s11707-018-0719-7
Parajka, J., Holko, L., Kostka, Z., & Blöschl, G. (2012). MODIS snow cover mapping accuracy in a small mountain catchment - Comparison between open and forest sites.

Hydrology and Earth System Sciences, *16*(7), 2365–2377. https://doi.org/10.5194/hess-16-2365-2012

Parajka, J., Pepe, M., Rampini, A., Rossi, S., & Blöschl, G. (2010). A regional snow-line method for estimating snow cover from MODIS during cloud cover. *Journal of Hydrology*, *381*(3–4), 203–212. https://doi.org/10.1016/j.jhydrol.2009.11.042

Park, N., Bellaire, S., Jamieson, B., Thumlert, S., Goodrich, J., & Statham, G. (2016). Cold Regions Science and Technology Analysis of long-term weather, snow, and avalanche data at Glacier. *Cold Regions Science and Technology*, *121*, 118–125. https://doi.org/10.1016/j.coldregions.2015.10.010

Paul, F., Winsvold, S. H., Kääb, A., Nagler, T., & Schwaizer, G. (2016). Glacier remote sensing using Sentinel-2. part II: Mapping glacier extents and surface facies, and comparison to Landsat 8. *Remote Sensing*, *8*(7). https://doi.org/10.3390/rs8070575

Pederson, G. T., Betancourt, J. L., & Mccabe, G. J. (2013). Regional patterns and proximal causes of the recent snowpack decline in the Rocky Mountains, U. S. *Geophysical Research Letters*, *40*, 1811–1816. https://doi.org/10.1002/grl.50424

Pepin, N., Bradley, R. S., Diaz, H. F., Baraer, M., Caceres, E. B., Forsythe, N., … Yang, D. Q. (2015). Elevation-dependent warming in mountain regions of the world. *Nature Climate Change*, *5*(5), 424–430. https://doi.org/10.1038/nclimate2563

Picketts, I. A. N. M., Curry, J., & Rapaport, E. (2012). Community Adaptation to Climate Change : Environmental Planners ' Knowledge and Experiences in British Columbia , Canada. *Journal of Environmental Policy & Planning*, *14*(2), 119–137.

Poggio, L., & Gimona, A. (2015). International Journal of Applied Earth Observation and Geoinformation Sequence-based mapping approach to spatio-temporal snow patterns from MODIS time-series applied to Scotland. *International Journal of Applied Earth Observations and Geoinformation*, *34*, 122–135. https://doi.org/10.1016/j.jag.2014.08.005

Pollock, E. W., & Bush, A. B. G. (2013). Changes in Snow Mass Balance in the Canadian Rocky Mountains Caused by CO 2 Rise: Regional Atmosphere Model Results. *Atmosphere-Ocean*, *5*, 505–521.

Pomeroy, J. W., & Bru, E. (1990). Physical Properties of Snow.

Rangwala, I., & Miller, J. R. (2012). Climate change in mountains: a review of elevation-dependent warming and its probable causes. *Climatic Change*, *114*, 527–547. https://doi.org/10.1007/s10584-012-0419-3

Rey D., Neuhäuser M. (2011) Wilcoxon-Signed-Rank Test. In: Lovric M. (eds) International Encyclopedia of Statistical Science. *Springer, Berlin, Heidelberg*. https://doi.org/10.1007/978-3-642-04898-2_616

Riggs, G. A., & Hall, D. K. (2015). MODIS Snow Products Collection 6 User Guide.

Riggs, G. A., Hall, D. K., & Román, M. O. (2017). Overview of NASA ' s MODIS and Visible Infrared Imaging Radiometer Suite (VIIRS) snow-cover Earth System Data Records. *Earth System Science Data*, *9*, 765–777.

Robinson, D. A., Dewey, K. F., & Heim, R. R. (1993). Global Snow Cover Monitoring: An Update. *Bulletin of the American Meteorological Society*, *74*(9), 1689–1696. https://doi.org/10.1175/1520-0477(1993)074<1689:GSCMAU>2.0.CO;2

Romanov, P., Gutman, G., & Csiszar, I. (2000). Automated Monitoring of Snow Cover over North America with Multispectral Satellite Data. *Journal of Applied Meteorology*, *39*(11), 1866–1880. https://doi.org/10.1175/1520-0450(2000)039<1866:AMOSCO>2.0.CO;2

Roy, A., Royer, A., & Turcotte, R. (2010). Improvement of springtime streamflow simulations in a boreal environment by incorporating snow-covered area derived from remote sensing data. *Journal of Hydrology*, *390*(1–2), 35–44. https://doi.org/10.1016/j.jhydrol.2010.06.027

Saavedra, F. A., Kampf, S. K., Fassnacht, R., & Sibold, J. S. (2017). A snow climatology of the Andes Mountains from MODIS snow cover data. *International Journal of Climatology*, *1539*, 1526–1539. https://doi.org/10.1002/joc.4795

Schelker, J., Kuglerová, L., Eklöf, K., Bishop, K., & Laudon, H. (2013). Hydrological effects of clear-cutting in a boreal forest – Snowpack dynamics , snowmelt and streamflow responses. *Journal of Hydrology*, *484*, 105–114. https://doi.org/10.1016/j.jhydrol.2013.01.015

Schnorbus, M., Werner, A., & Bennett, K. (2014). Impacts of climate change in three hydrologic regimes in British Columbia , Canada. *Hydrological Processes*, *1189*, 1170–1189. https://doi.org/10.1002/hyp.9661

Shabbar, A. (2014). The impact of El Niño-Southern Oscillation on the Canadian climate Advances in Geosciences The impact of El Ni no-Southern Oscillation on the Canadian climate. *Environment and Climate Change*. https://doi.org/10.5194/adgeo-6-149-2006

Shrestha, R. R., Schnorbus, M. A., Cannon, A. J. (2015). A Dynamical Climate Model – Driven Hydrologic Prediction System for the Fraser River , Canada, (2013), 1273–1292. https://doi.org/10.1175/JHM-D-14-0167.1

Shrestha, R. R., Schnorbus, M. A., Werner, A. T., & Berland, A. J. (2012). Modelling spatial and temporal variability of hydrologic impacts of climate change in the Fraser River basin , British. *Hydrological Processes*, *26*, 1841–1861. https://doi.org/10.1002/hyp.9283

Smith, R. S., Scherer, R. A., & Dobson, D. A. (2008). snowmelt in the south-central interior of British Columbia. *BC Journal of Ecosystems and Management*, *9*(1), 57–70.

Solberg, R., Koren, H., & Amlien, J. (2006). A review of optical snow cover algorithms. *Nork Regnesentral*.

Statistics Canada. 2017. *Thompson--Okanagan [Economic region], British Columbia and British Columbia [Province]* (table). *Census Profile*. 2016 Census. Statistics Canada Catalogue no. 98-316-X2016001.Ottawa.Released November 29, 2017.https://www12.statcan.gc.ca/census-recensement/2016/dppd/prof/index.cfm?Lang=E (accessed December 7, 2020).

Sturm, M., M.A. Goldstein, and C. Parr (2017), Water and life from snow: A trillion-dollar science question, *Water Resources, 53*, 3534-3544, doi 10.1002/2017WR020840

Sulla-Menashe, D., & Friedl, M. A. (2018). User Guide to Collection 6 MODIS Land Cover (MCD12Q1 and MCD12C1) Product. Retrieved from https://lpdaac.usgs.gov/documents/101/MCD12_User_Guide_V6.pdf

Tait, A. B., Hall, D. K., Foster, J. L., & Armstrong, R. L. (2000). Utilizing multiple datasets for snow-cover mapping. *Remote Sensing of Environment*, *72*(1), 111–126. https://doi.org/10.1016/S0034-4257(99)00099-1

Tan, T. C., Ho, S. C., Chong, S. M., & Easa, A. M. (2017). Reconstructing SWE using remote sensing snow cover data and distributed snowmelt model. *International Food Research Journal*, *24*(1), 318–326. https://doi.org/10.1002/hyp

Tang, Z., Wang, X., Wang, J., Wang, X., Li, H., & Jiang, Z. (2017). Spatiotemporal Variation of Snow Cover in Tianshan Mountains , Central Asia , Based on Cloud-Free Product, 2001-2005, *Remote sensing*, *9*, 2001–2015. https://doi.org/10.3390/rs9101045

Taylor S.W., Carroll, A.L., Alfaro, R.I., Safranyik, L. (2006). Chapter 2 Forest, Climate and Mountain Pine Beetle Outbreak Dynamic in Western Canada. *Natural Resources Canada*.

Thorne, R., & Woo, M. (2011). Streamflow response to climatic variability in a complex mountainous environment : Fraser River Basin , British Columbia , Canada, *Hydrological Processes*, *3085*(August), 3076–3085. https://doi.org/10.1002/hyp.8225

Tong, J. (2009). Interrelationships between MODIS / Terra remotely sensed snow cover and the hydrometeorology of the Quesnel River Basin , British Columbia , Canada, *Hydrology and Earth Sciences*, *13*, (2003), 1439–1452.

Tribe, S. (2005). Eocene paleo-physiography and drainage directions, southern Interior Plateau , British, *Canadian Journal Earth Science*, *42*, 215–230. https://doi.org/10.1139/E04-062

Viviroli, D., Dürr, H. H., Messerli, B., Meybeck, M., & Weingartner, R. (2007). Mountains of the world, water towers for humanity: Typology, mapping, and global significance. *Water Resources Research*, *43*(7), 1–13. https://doi.org/10.1029/2006WR005653

Wang, L., Toose, P., Brown, R., & Derksen, C. (2016). Frequency and distribution of winter melt events from passive microwave satellite data in the pan-Arctic , 1988 – 2013, *The Cryosphere*, *10*, 2589–2602. https://doi.org/10.5194/tc-10-2589-2016

Wang, L., Wolken, G. J., Sharp, M. J., Howell, S. E. L., Derksen, C., Brown, R. D., … Cole, J. (2011). Integrated pan - Arctic melt onset detection from satellite active and passive microwave measurements, 2000 – 2009, *Journal of Geophysical Research Atmospheres*, *116*, 2000–2009. https://doi.org/10.1029/2011JD016256

Wang, X., Wang, J., Che, T., Huang, X., Hao, X., & Li, H. (2018). Snow Cover Mapping for Complex Mountainous Forested Environments Based on a Multi-Index Technique, *Applied Earth Observations and Remote Sensing*, *11*(5), 1433–1441.

Wang, X., Wang, J., Jiang, Z., Li, H., & Hao, X. (2015). An Effective Method for Snow-Cover Mapping of Dense Coniferous Forests in the Upper Heihe River Basin Using Landsat Operational Land Imager Data, *Remote Sensing*,*7*, 17246–17257. https://doi.org/10.3390/rs71215882

Wang, X., Xie, H., Liang, T., & Huang, X. (2009). Comparison and validation of MODIS standard and new combination of Terra and Aqua snow cover products in northern Xinjiang , China, *Hydrological Processes*, *42*, 419–429. https://doi.org/10.1002/hyp

Wang, Z., Schaaf, C. B., Sun, Q., Kim, J., Erb, A. M., Gao, F., … Papuga, S. A. (2017). Monitoring land surface albedo and vegetation dynamics using high spatial and temporal resolution synthetic time series from Landsat and the MODIS BRDF/NBAR/albedo

product. *International Journal of Applied Earth Observation and Geoinformation*, *59*, 104–117. https://doi.org/10.1016/j.jag.2017.03.008

Westerling, A. L. (2016). Increasing western US forest wildfire activity: sensitivity to changes in the timing of spring. *Philosophical Transactions B*.

Wilson AM, Jetz W (2016) Remotely Sensed High-Resolution Global Cloud Dynamics for Predicting Ecosystem and Biodiversity Distributions. *PLoS Biol* 14(3): e1002415. doi:10.1371/journal.pbio.1002415

Winkler, R D., Spittlehouse, D., Boon, S., & Zimonick, B. (2015). Forest disturbance effects on snow and water yield in interior British Columbia. *Hydrology Research*, 521–532. https://doi.org/10.2166/nh.2014.016

Winkler, R., Spittlehouse, D., & Boon, S. (2017). Streamflow response to clear - cut logging on British Columbia's Okanagan Plateau, *Ecohydrology,* 1–15. https://doi.org/10.1002/eco.1836

Xu, Y., Ramanathan, V., & Washington, W. M. (2015). Observed high-altitude warming and snow cover retreat over Tibet and the Himalayas enhanced by black carbon aerosols. *Atmospheric Chemistry and Physics Discussions*, *15*(13), 19079–19109. https://doi.org/10.5194/acpd-15-19079-2015

Xue, H., Wang, J., Xiao, Z., Chen, P., & Liu, Y. (2014). Combining MODIS and AMSR-E observations to improve MCD43A3 short-time snow-covered Albedo estimation. *Hydrological Processes*, *28*(3), 570–580. https://doi.org/10.1002/hyp.9570

Zeinivand, H., & Smedt, F. De. (2010). Prediction of snowmelt floods with a distributed hydrological model using a physical snow mass and energy balance approach, *Natural Hazards, 54*, 451–468. https://doi.org/10.1007/s11069-009-9478-9

Zheng, Z., Molotch, N. P., Oroza, C. A., Conklin, M. H., & Bales, R. C. (2018). Spatial snow water equivalent estimation for mountainous areas using wireless-sensor networks and remote-sensing products. *Remote Sensing of Environment*, *215*, 44–56. https://doi.org/10.1016/j.rse.2018.05.029

Zhu, Z., & Woodcock C. E., (2012). Object-baes cloud and cloud shadow detection in Landsat imagery. *Remote Sensing of Environment, 118*, 83-94. https://doi.org/10.1016/j.rse.2011.10.028

Appendix A

Locations of ROIs for NDFSI analysis

Regions of Interest on April 20th, 2015 on Landsat OLI True Color Composite

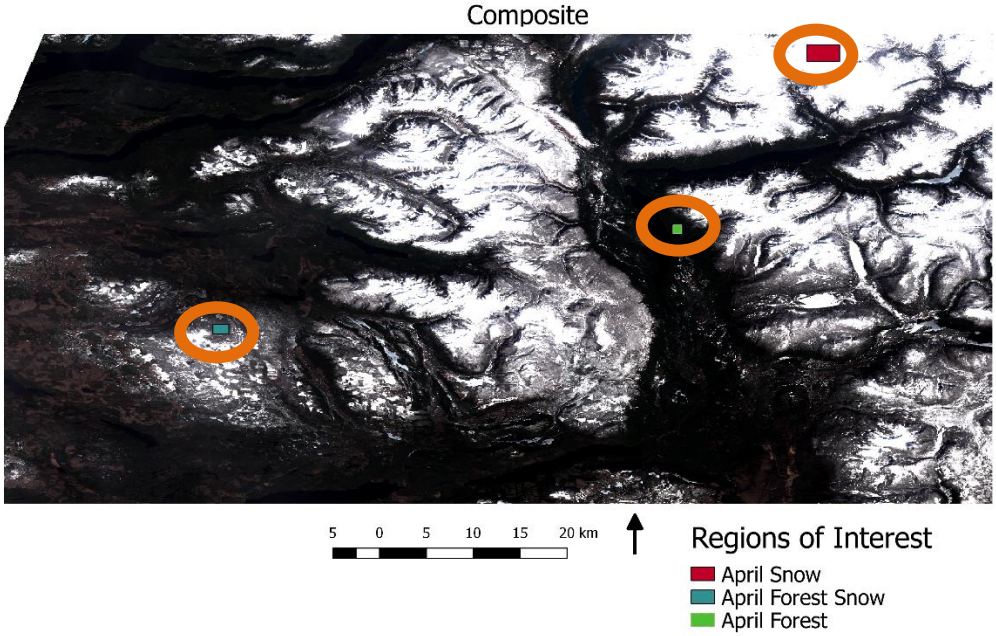

Regions of Interest on May 13th, 2015 on Landsat OLI True Color Composite

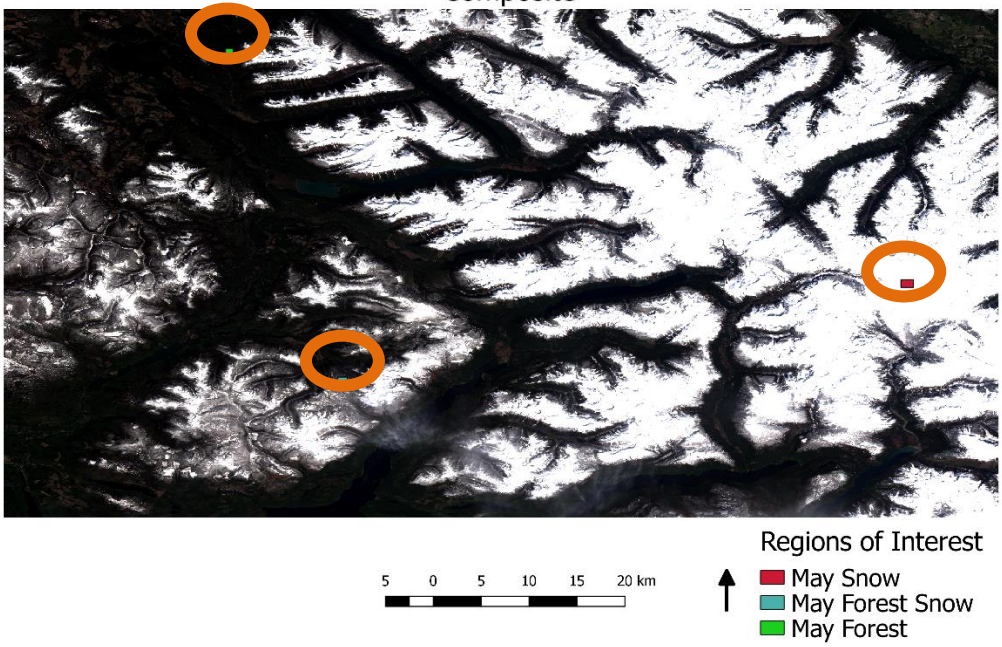

Regions of Interest on June 7th, 2015 on Landsat OLI True Color Composite

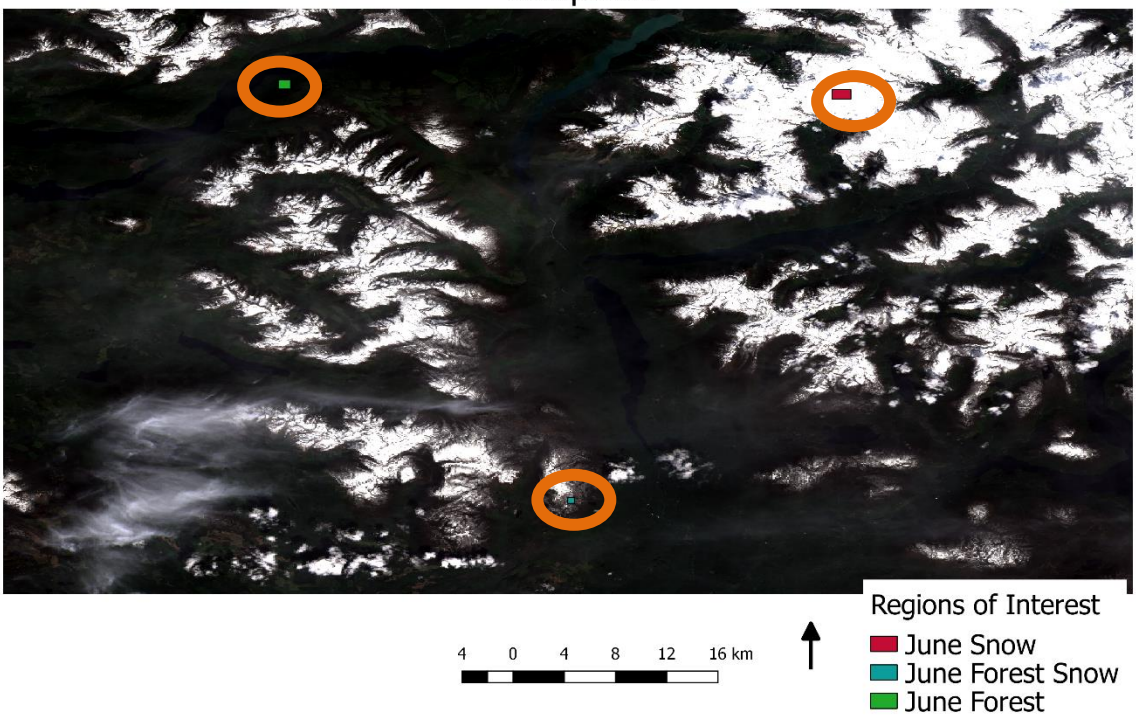

Appendix B

Locations of available Landsat-8 OLI images

Locations for dates: April 21st, 2013, May 13th, 2015, May 15th, 2016

Path 47, Row 23

Location for dates: April 1st, 2014, April 20th, 2015, June 7th, 2015,

Path 46, Row 24

Location for dates: May 22nd, 2015, May 24th, 2016, May 27th, 2017, May 14th, 2018

Path 46, Row 23

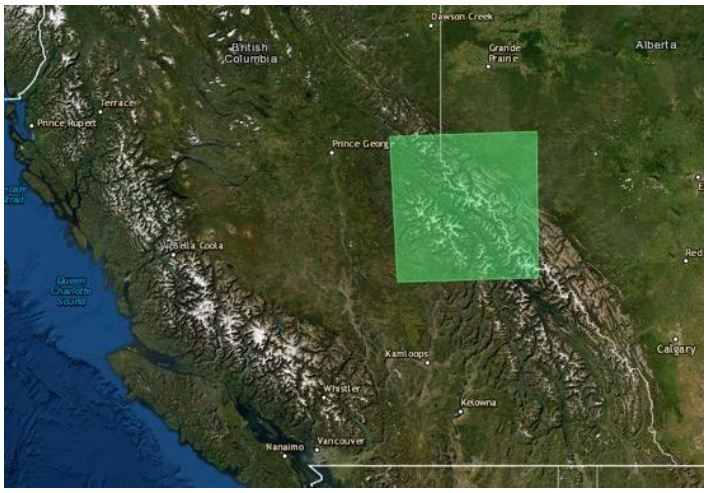

Location for dates: May 1st, 2016, May 20th, 2017, May 23rd, 2018, April 8th, 2019, May 10th, 2019, May 26th, 2019

Path 45, Row 24

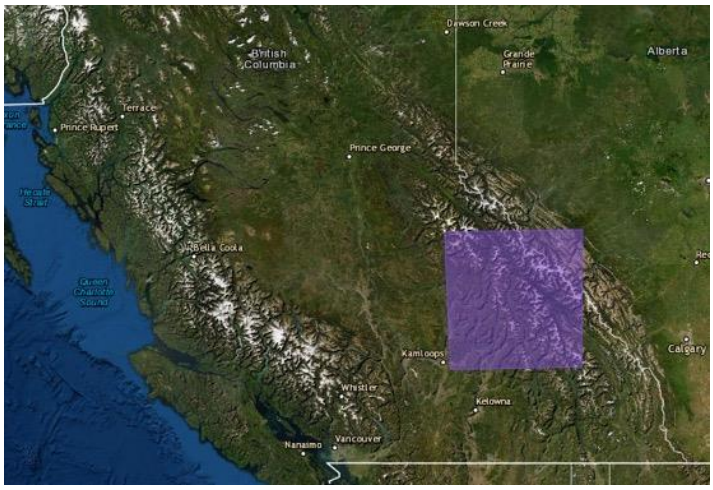

Location for dates: May 29th, 2017

Path 44, Row 24

Location for dates: June 5th, 2017, June 24th, 2018

Path 45, Row 25

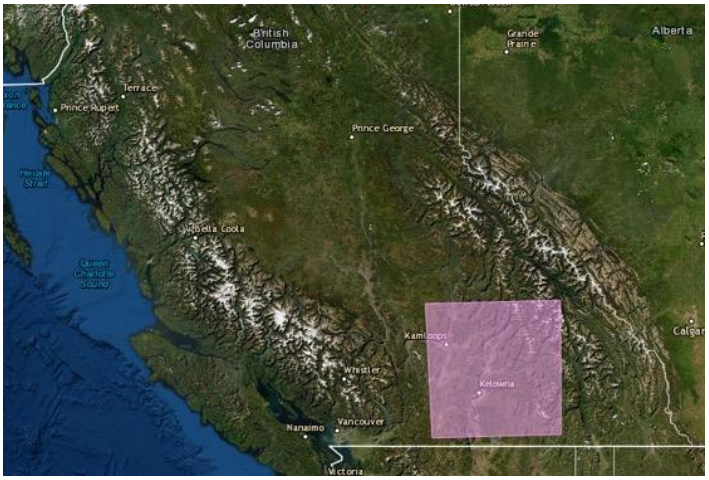

Appendix C

Annual VIIRS reduction graphs

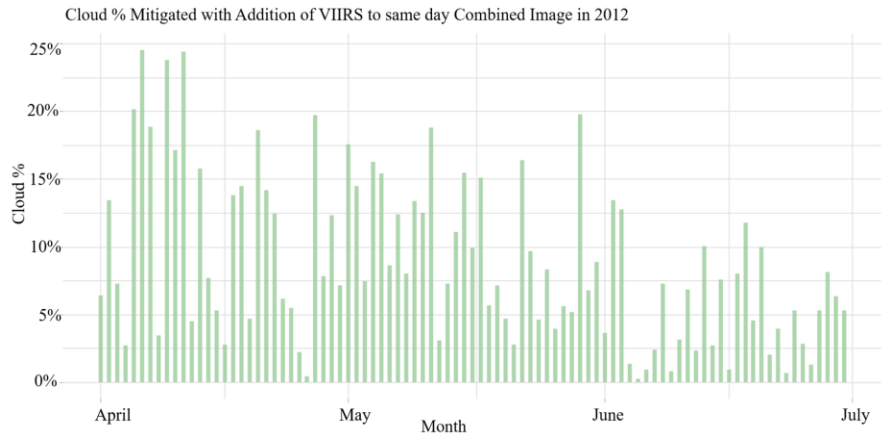

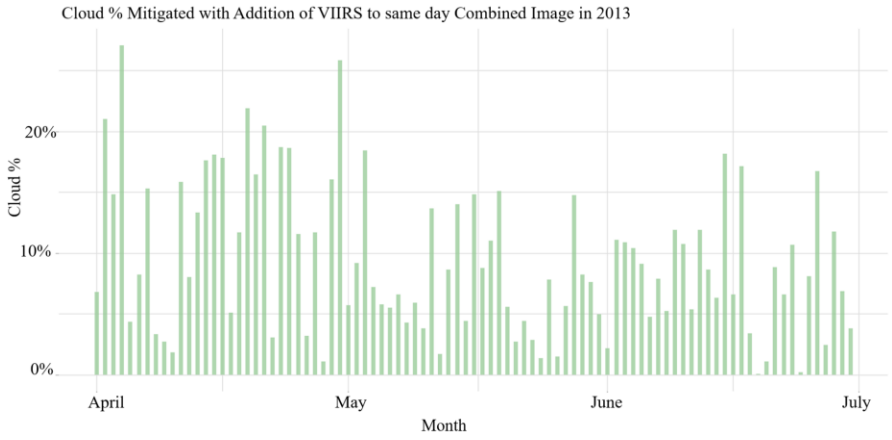

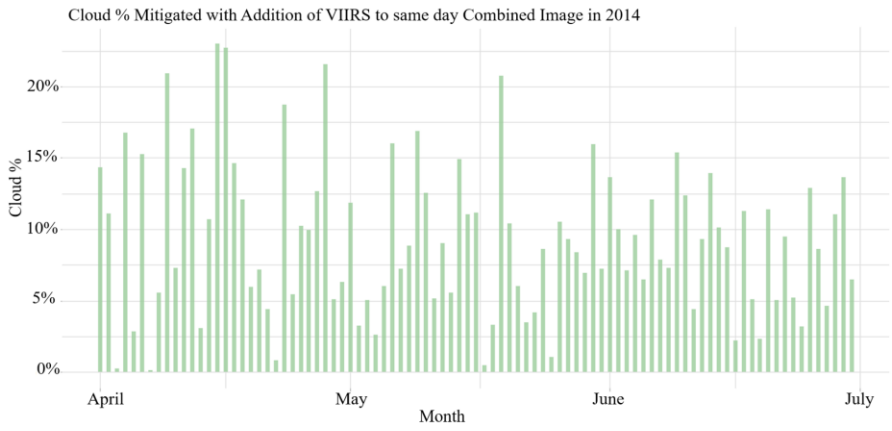

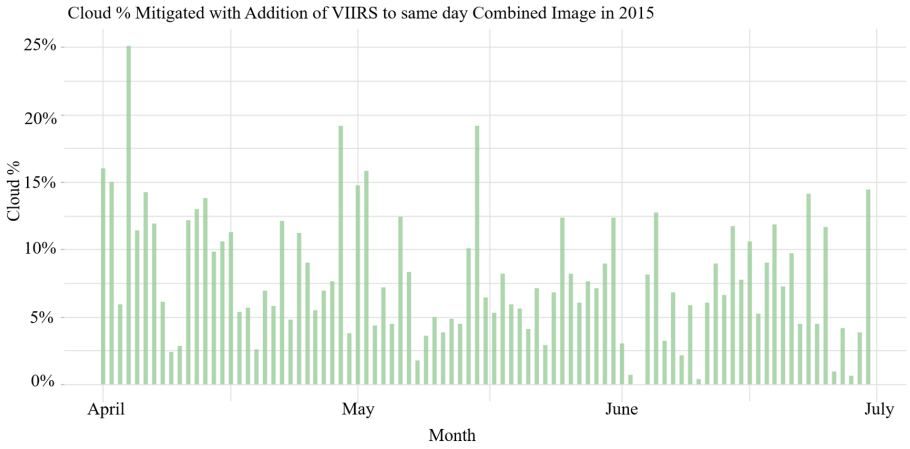
Cloud % Mitigated with Addition of VIIRS to same day Combined Image in 2015
25%
20%
15%
10%
5%
0%
Cloud %
April
May
June
July
Month

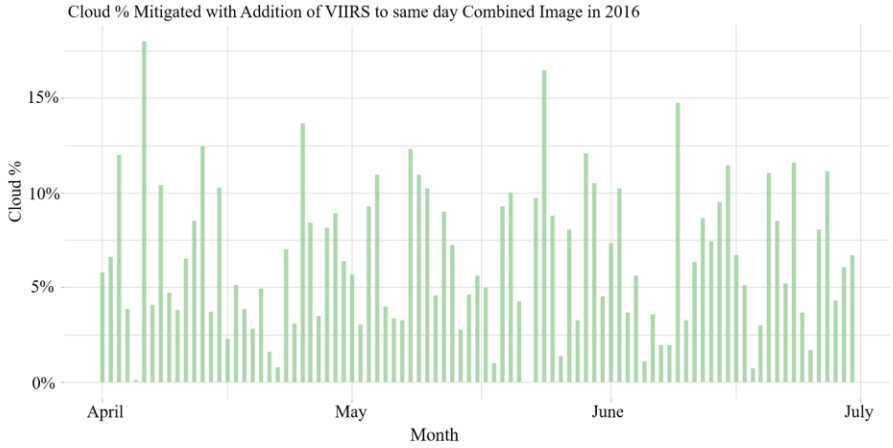
Cloud % Mitigated with Addition of VIIRS to same day Combined Image in 2016
15%
10%
5%
0%
Cloud %
April
May
June
July
Month

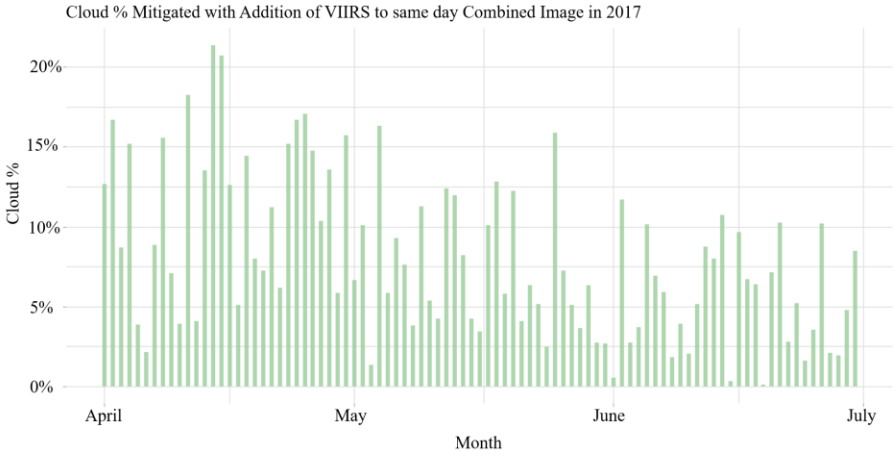
Cloud % Mitigated with Addition of VIIRS to same day Combined Image in 2017
20%
15%
10%
5%
0%
Cloud %
April
May
June
July
Month

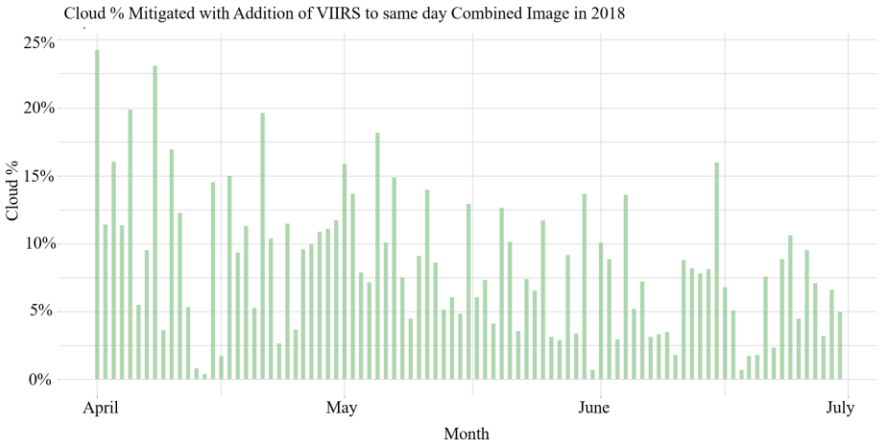
Cloud % Mitigated with Addition of VIIRS to same day Combined Image in 2018
25%
20%
15%
10%
5%
0%
Cloud %
April
May
June
July
Month

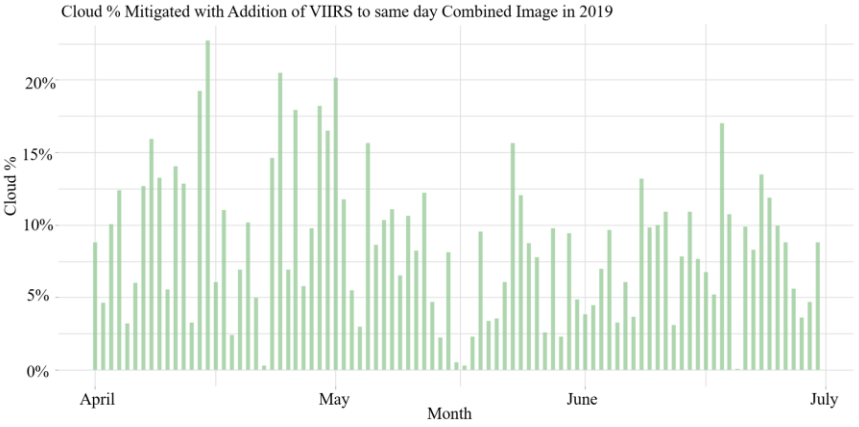
Cloud % Mitigated with Addition of VIIRS to same day Combined Image in 2019
20%
15%
10%
5%
0%
Cloud %
April
May
June
July
Month

Appendix D

Cloud proportion graphs for each year in the study period

2003

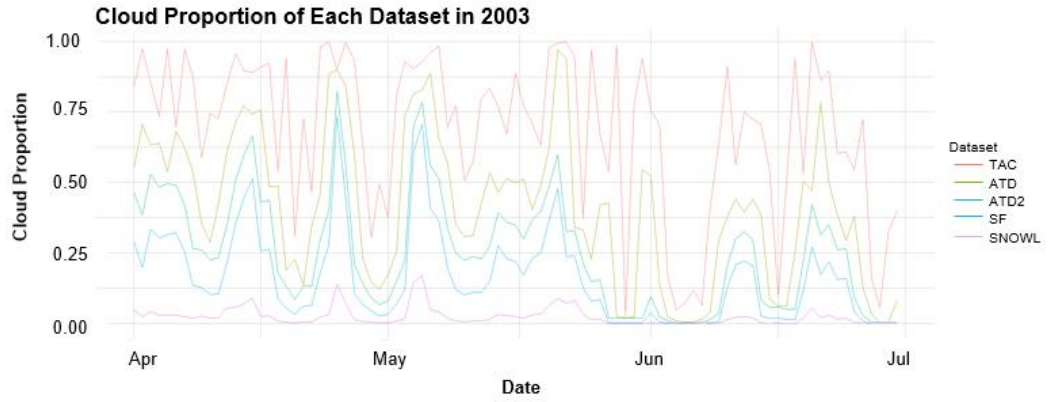

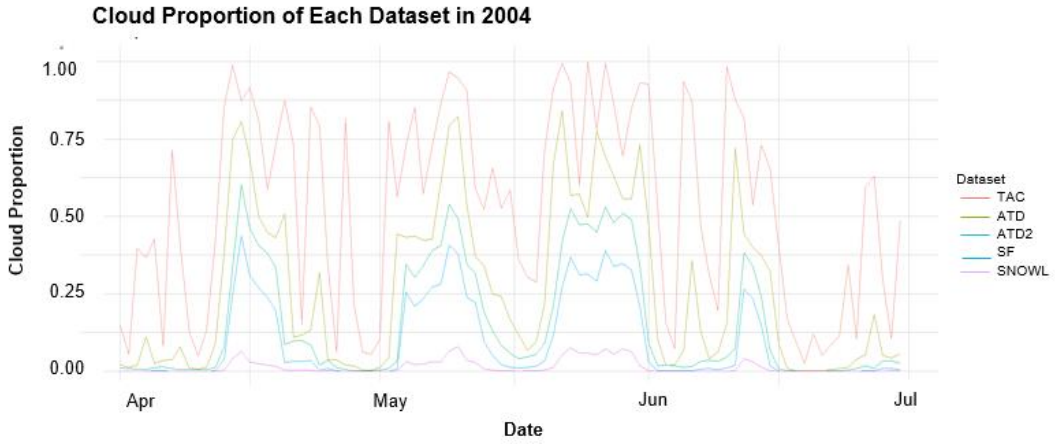

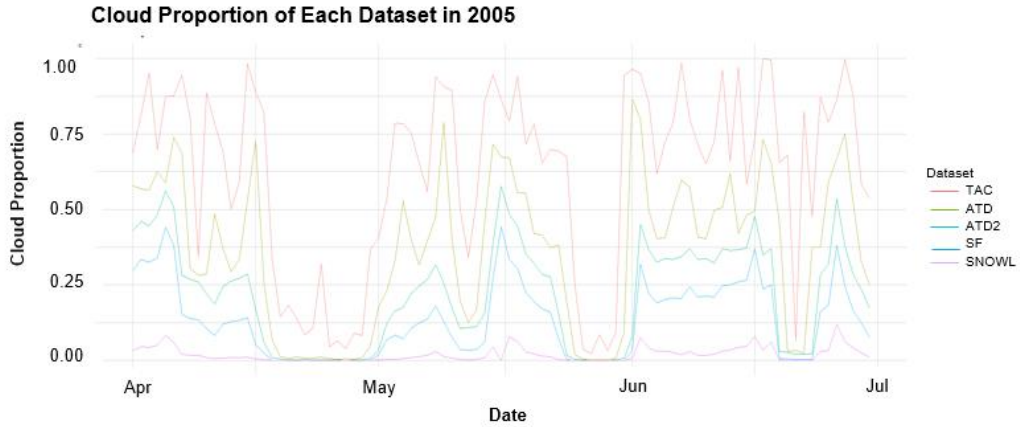

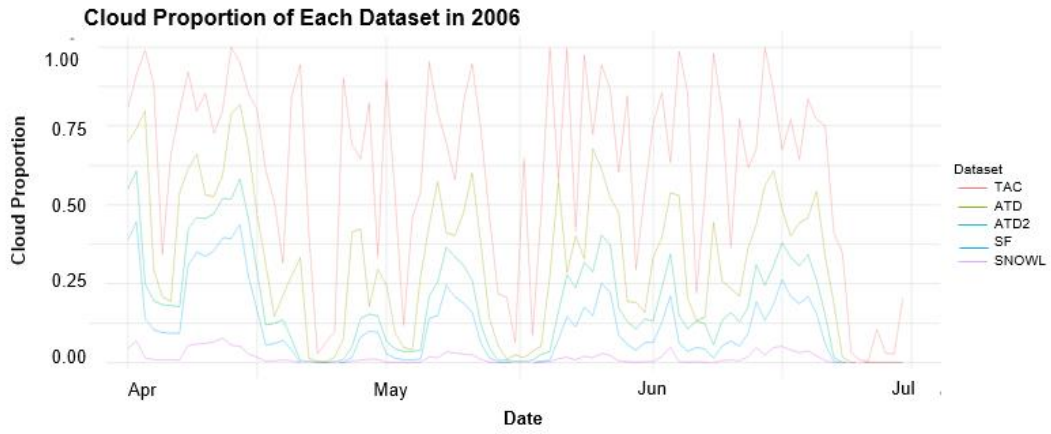
Cloud Proportion of Each Dataset in 2006
Cloud Proportion
1.00
0.75
0.50
0.25
0.00
Apr
May
Jun
Jul
Date
Dataset
TAC
ATD
ATD2
SF
SNOWL

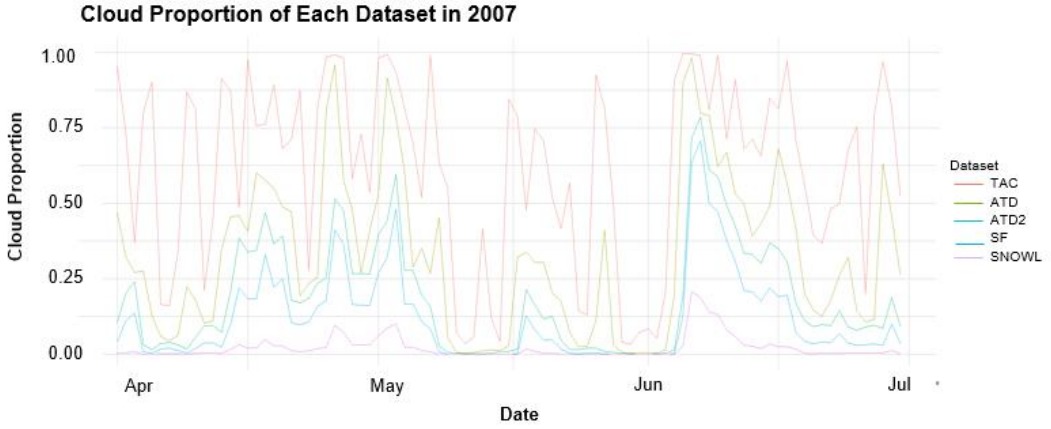
Cloud Proportion of Each Dataset in 2007
Cloud Proportion
1.00
0.75
0.50
0.25
0.00
Apr
May
Jun
Jul
Date
Dataset
TAC
ATD
ATD2
SF
SNOWL

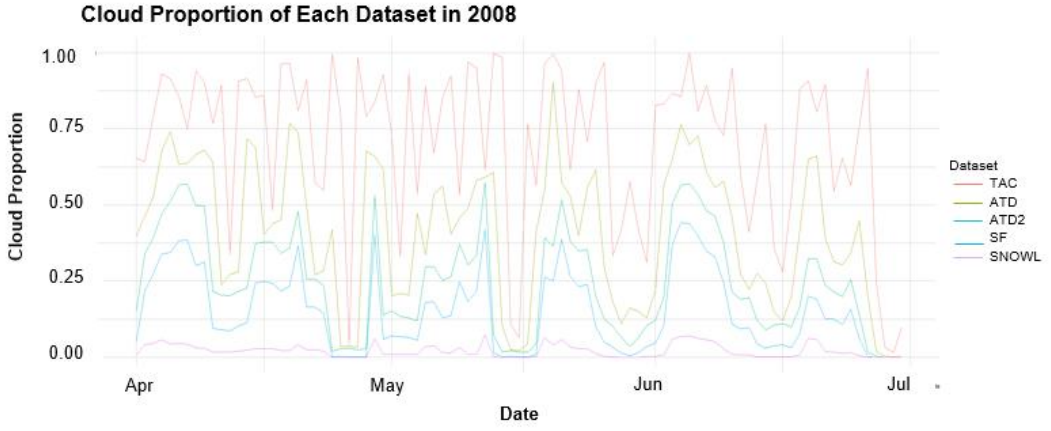
Cloud Proportion of Each Dataset in 2008
Cloud Proportion
1.00
0.75
0.50
0.25
0.00
Apr
May
Jun
Jul
Date
Dataset
TAC
ATD
ATD2
SF
SNOWL

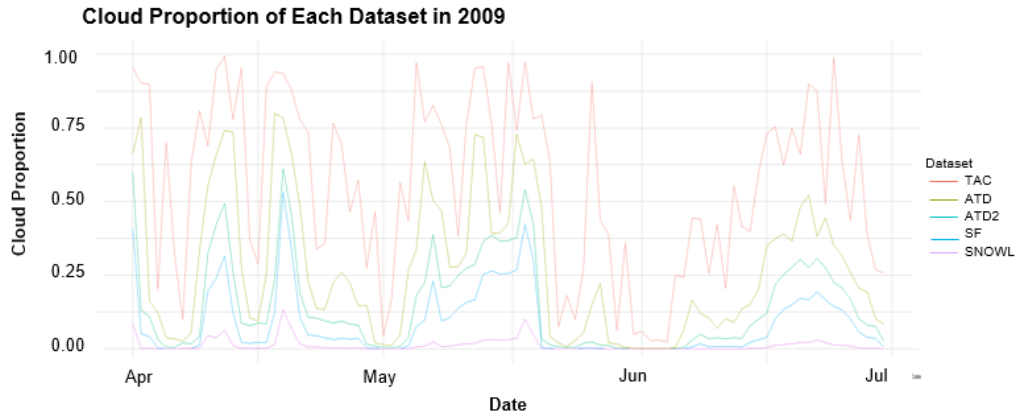
Cloud Proportion of Each Dataset in 2009
Cloud Proportion
1.00
0.75
0.50
0.25
0.00
Apr
May
Jun
Jul
Date
Dataset
TAC
ATD
ATD2
SF
SNOWL

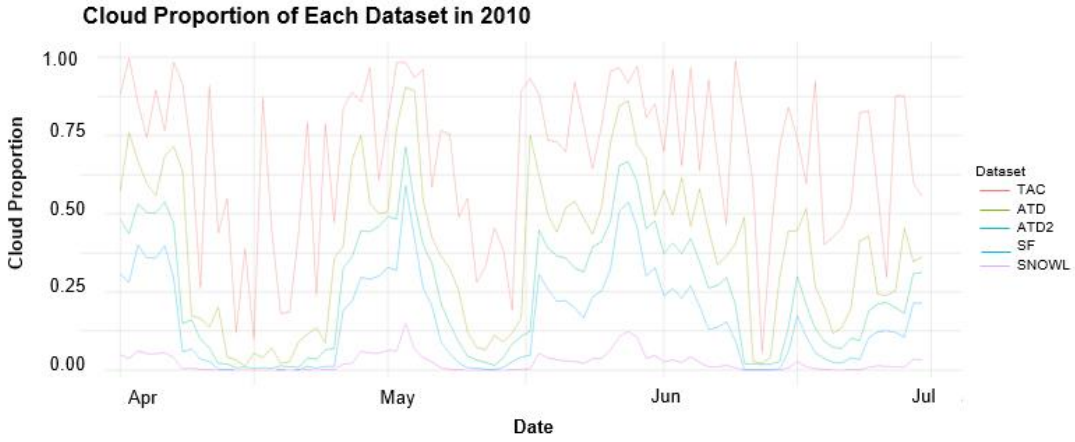
Cloud Proportion of Each Dataset in 2010
Cloud Proportion
1.00
0.75
0.50
0.25
0.00
Apr
May
Jun
Jul
Date
Dataset
TAC
ATD
ATD2
SF
SNOWL

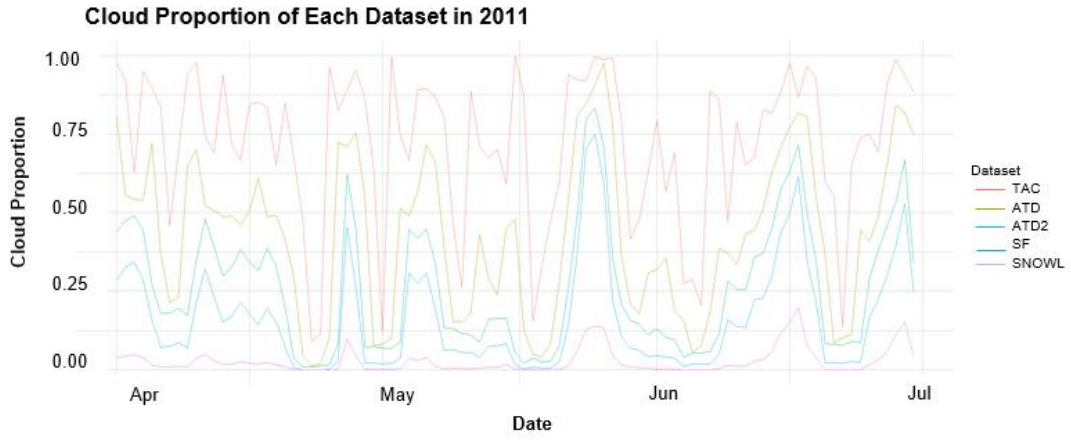
Cloud Proportion of Each Dataset in 2011
Cloud Proportion
1.00
0.75
0.50
0.25
0.00
Apr
May
Jun
Jul
Date
Dataset
TAC
ATD
ATD2
SF
SNOWL

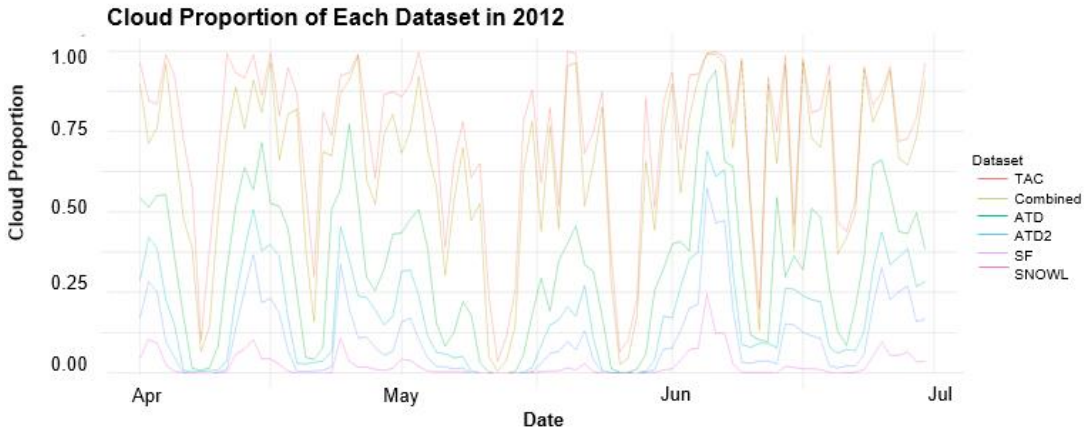
Cloud Proportion of Each Dataset in 2012
Cloud Proportion
1.00
0.75
0.50
0.25
0.00
Apr
May
Jun
Jul
Date
Dataset
TAC
Combined
ATD
ATD2
SF
SNOWL

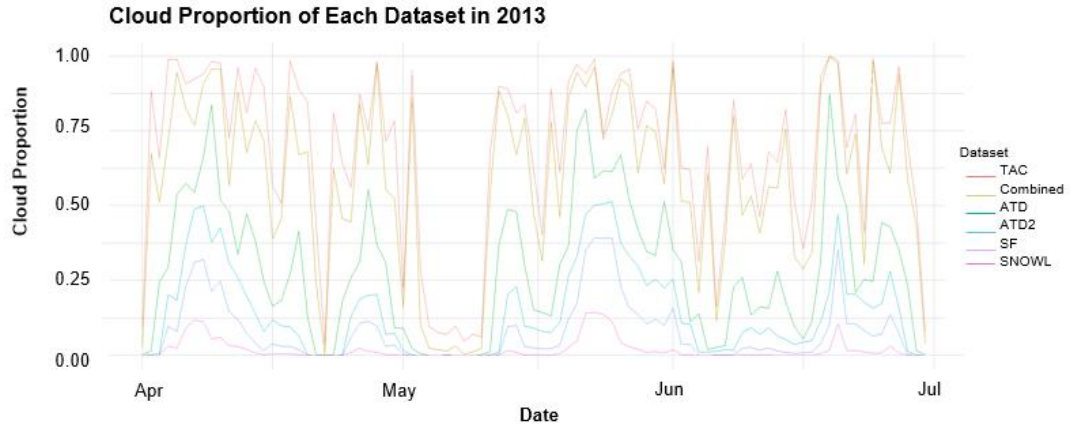
Cloud Proportion of Each Dataset in 2013
Cloud Proportion
1.00
0.75
0.50
0.25
0.00
Apr
May
Jun
Jul
Date
Dataset
TAC
Combined
ATD
ATD2
SF
SNOWL

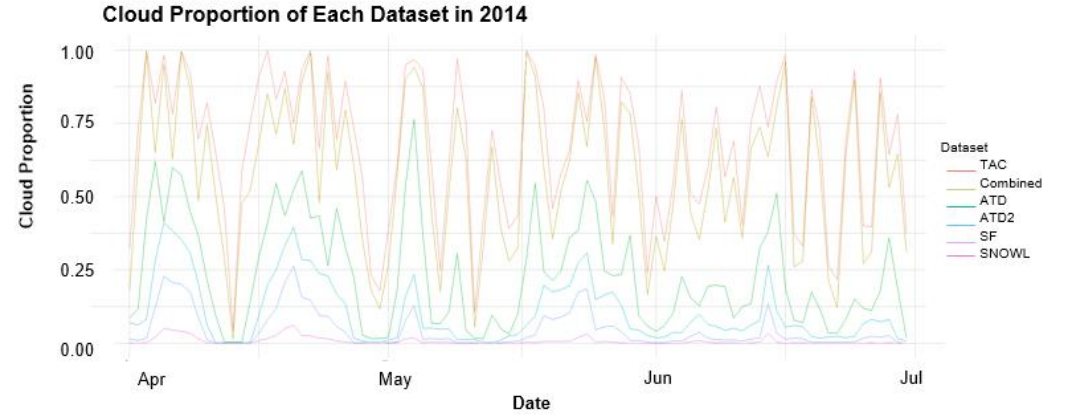
Cloud Proportion of Each Dataset in 2014
Cloud Proportion
1.00
0.75
0.50
0.25
0.00
Apr
May
Jun
Jul
Date
Dataset
TAC
Combined
ATD
ATD2
SF
SNOWL

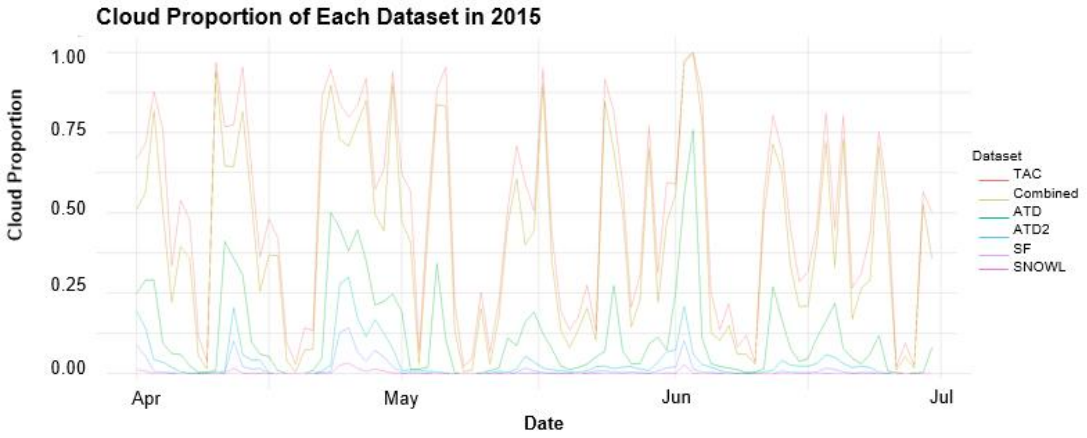
Cloud Proportion of Each Dataset in 2015
Cloud Proportion
1.00
0.75
0.50
0.25
0.00
Apr
May
Jun
Jul
Date
Dataset
TAC
Combined
ATD
ATD2
SF
SNOWL

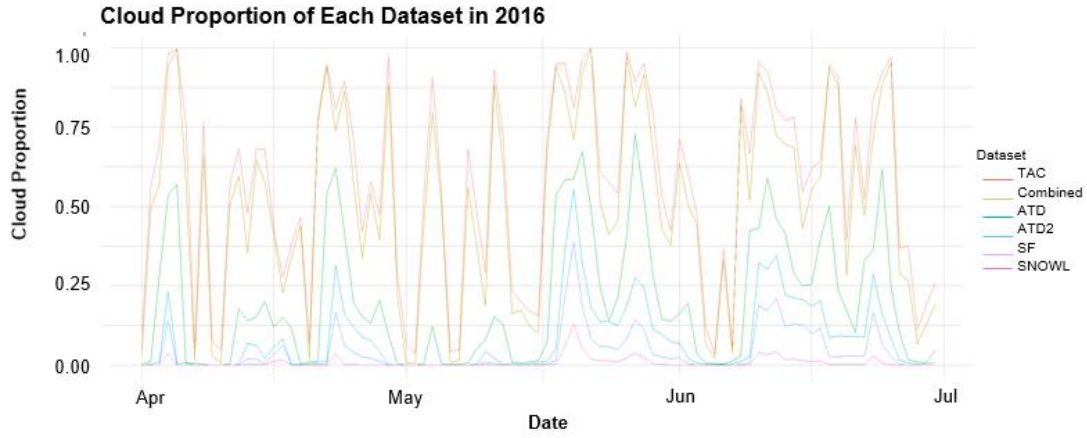
Cloud Proportion of Each Dataset in 2016
Cloud Proportion
1.00
0.75
0.50
0.25
0.00
Apr
May
Jun
Jul
Date
Dataset
TAC
Combined
ATD
ATD2
SF
SNOWL

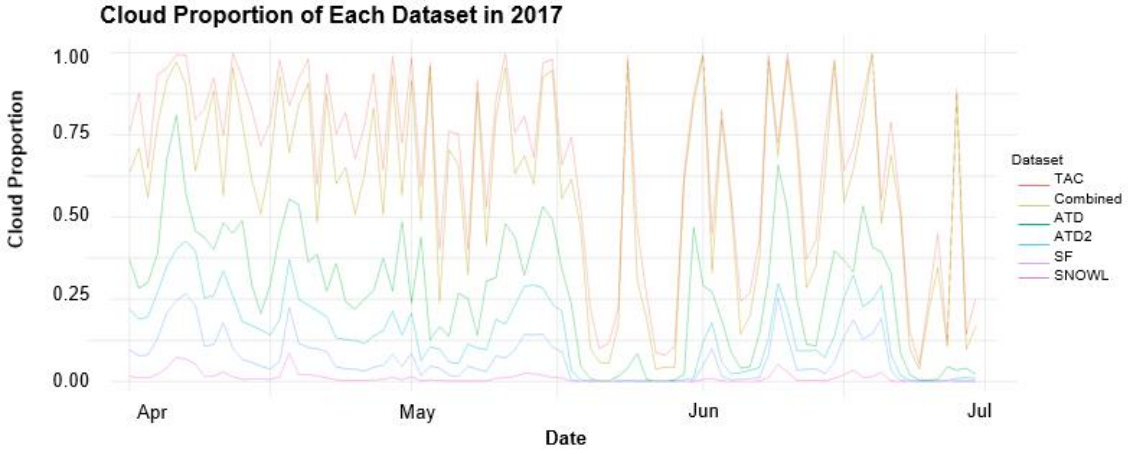
Cloud Proportion of Each Dataset in 2017
Cloud Proportion
1.00
0.75
0.50
0.25
0.00
Apr
May
Jun
Jul
Date
Dataset
TAC
Combined
ATD
ATD2
SF
SNOWL

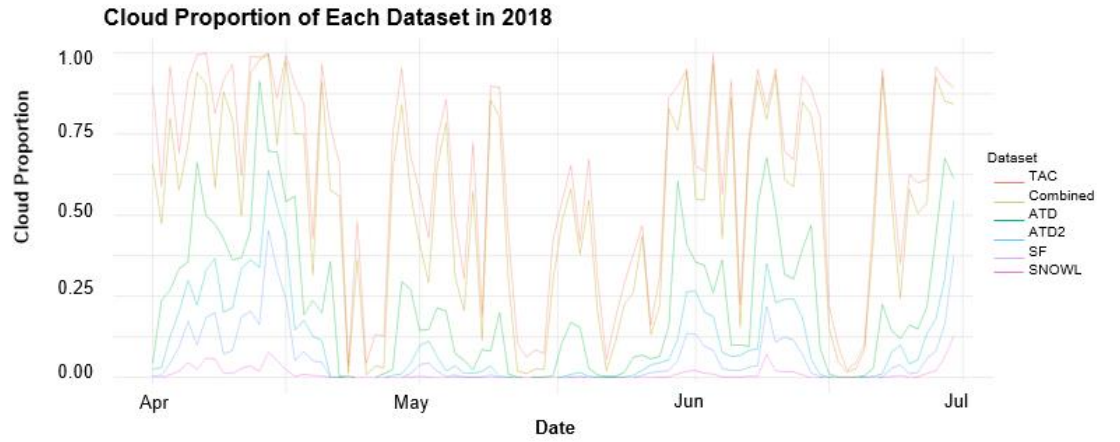
Cloud Proportion of Each Dataset in 2018
Cloud Proportion
1.00
0.75
0.50
0.25
0.00
Apr
May
Jun
Jul
Date
Dataset
TAC
Combined
ATD
ATD2
SF
SNOWL

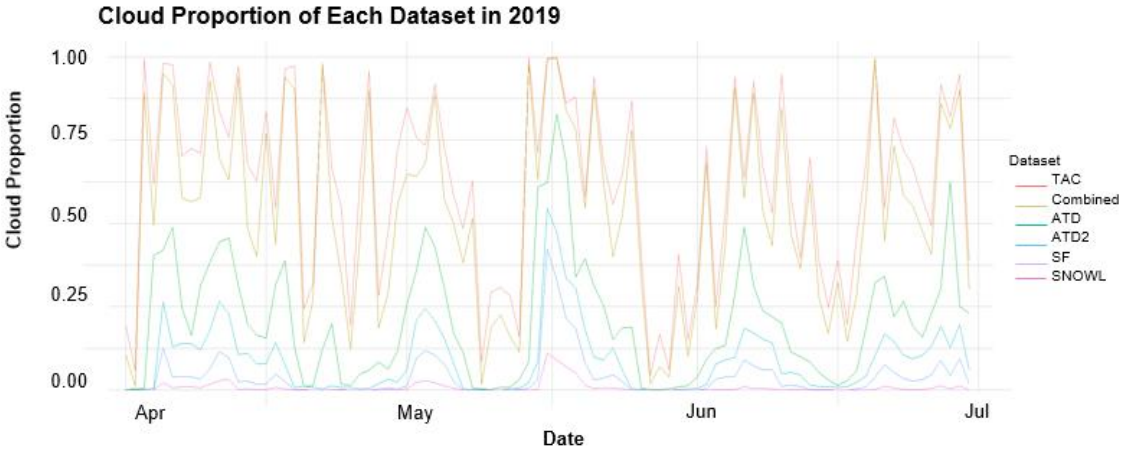
Cloud Proportion of Each Dataset in 2019
Cloud Proportion
1.00
0.75
0.50
0.25
0.00
Apr
May
Jun
Jul
Date
Dataset
TAC
Combined
ATD
ATD2
SF
SNOWL

Appendix E

Linearity Assumptions for Linear Regression Models

Multiple Linear Regression Residuals vs. Fitted Plots

a) <1000 m Elevation Median

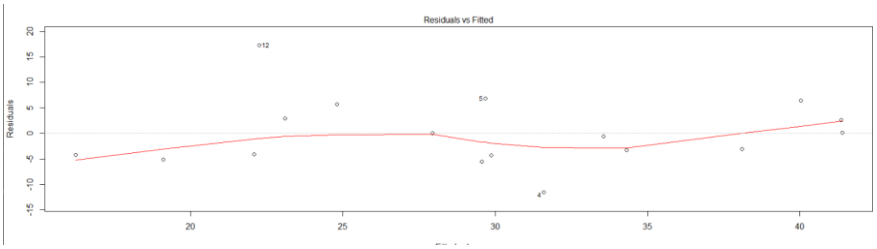

b) 1000-1200 m Elevation Median

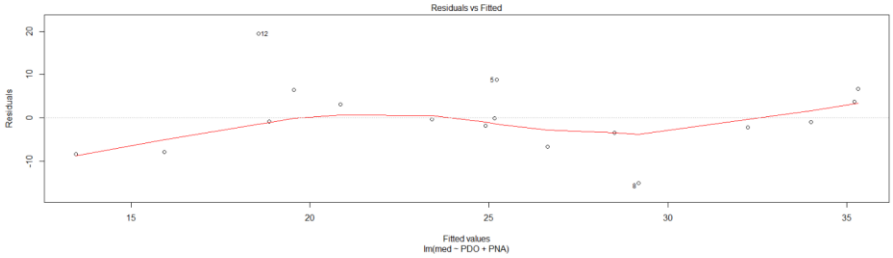

c) 1200-1400 m Elevation Median

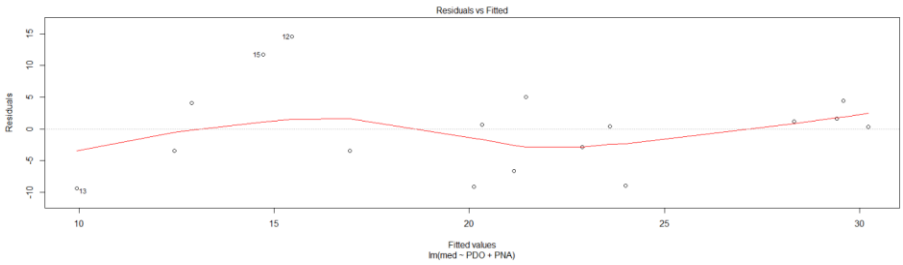

d) 1400-1600 m Elevation Median

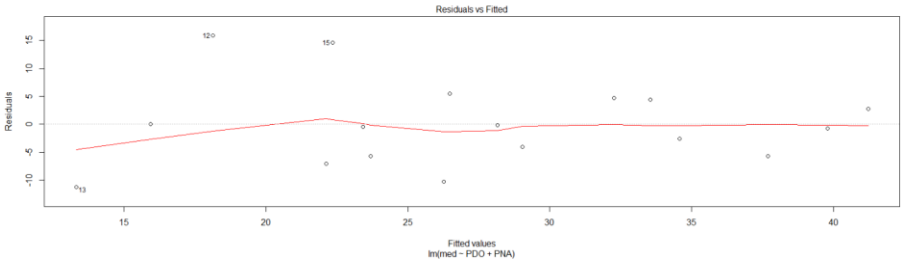

e) 1600-1800 m Elevation Median

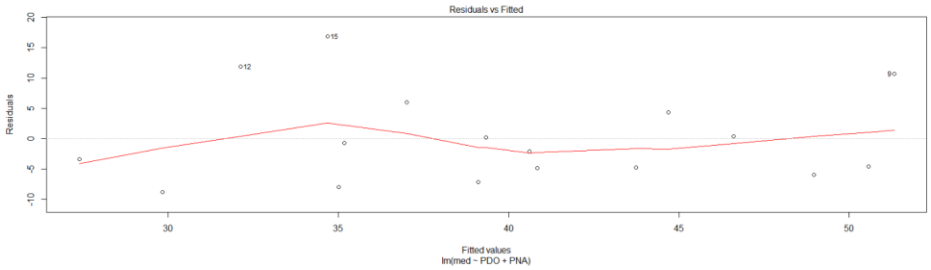

f) 1800-2000 m Elevation Median

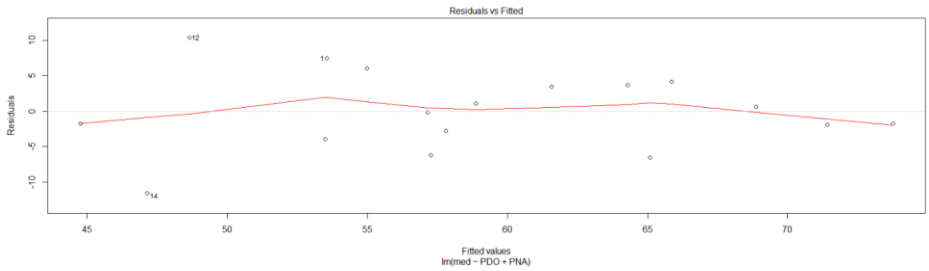

Simple Linear Regression Residuals vs. Fitted Plots

a) < 1000 m elevation medians for each 3-month interval

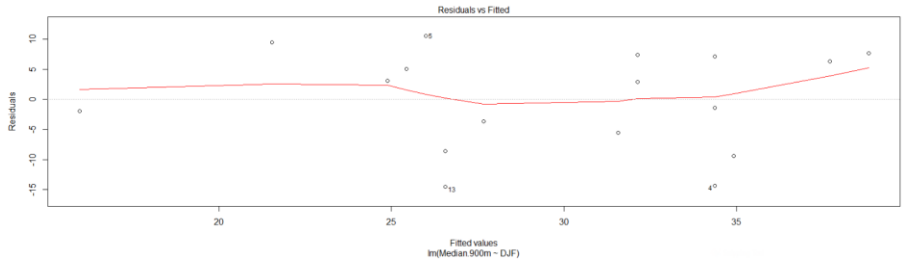

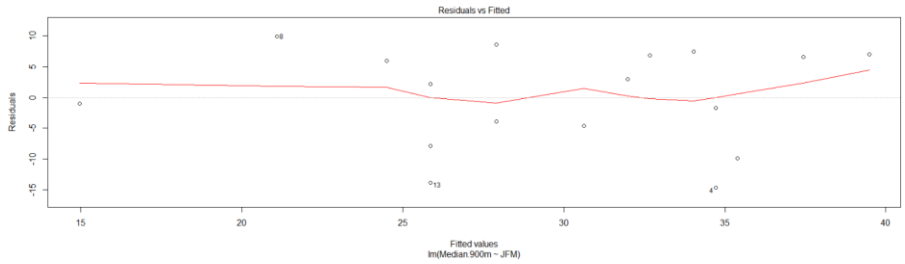

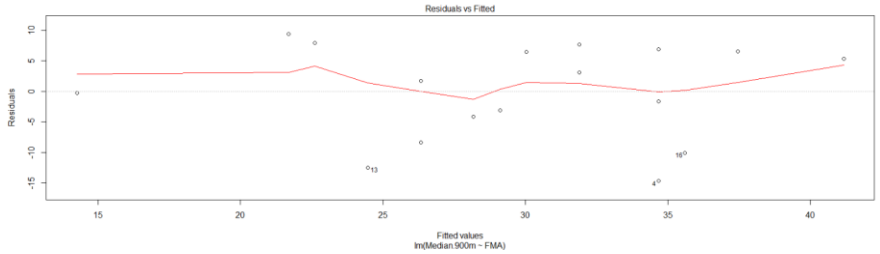

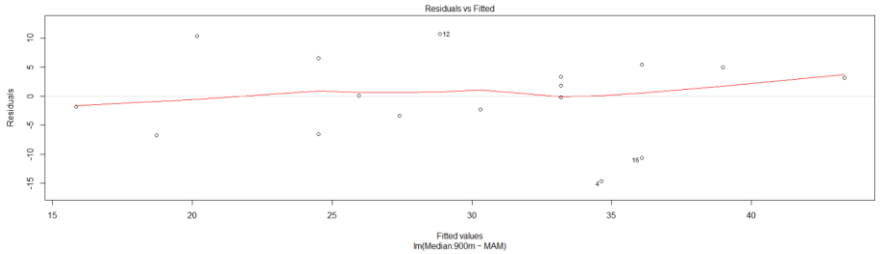

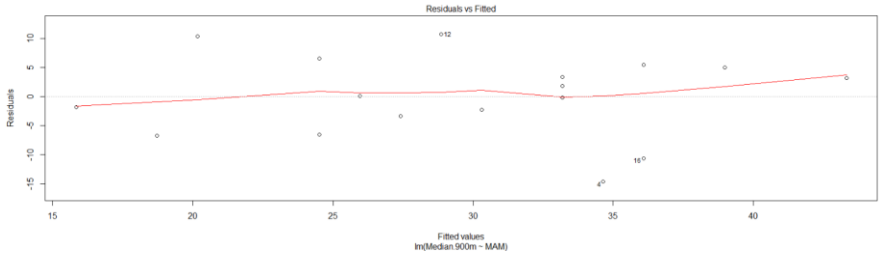

b) 1000-1200 m elevation medians for each 3-month interval

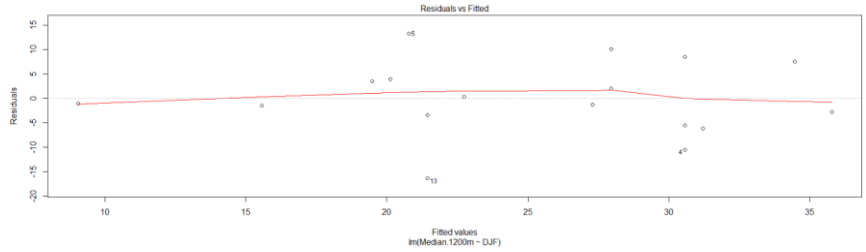

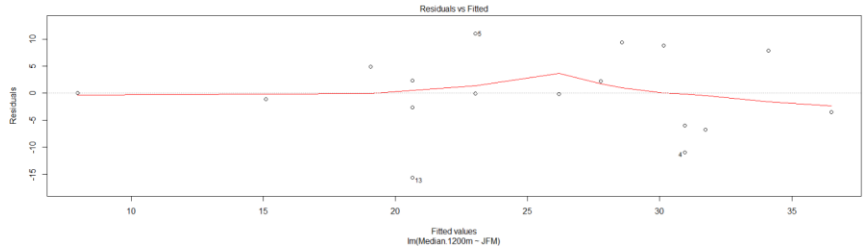

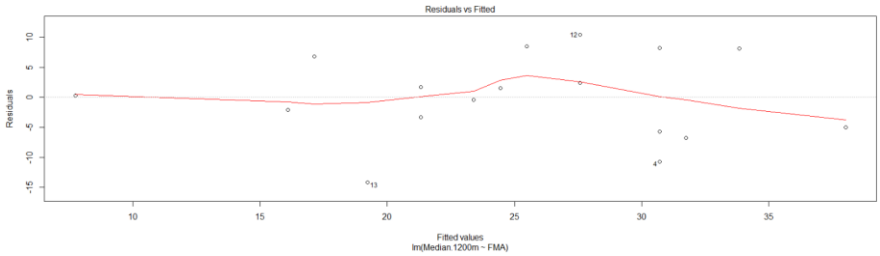

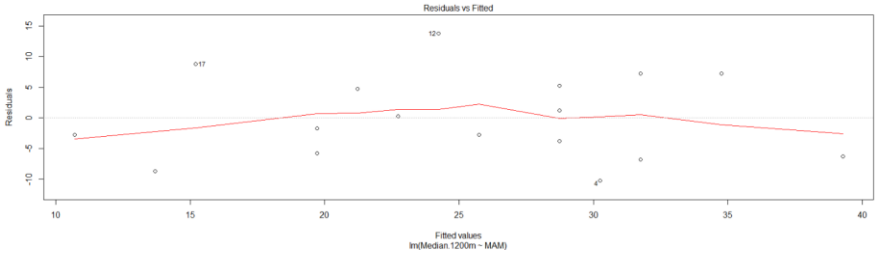

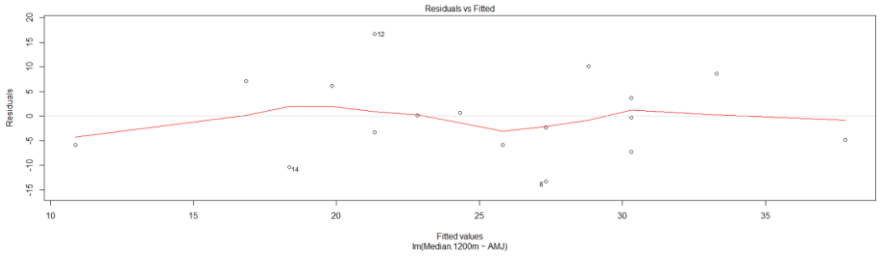

c) 1200-1400 m elevation medians for each 3-month interval

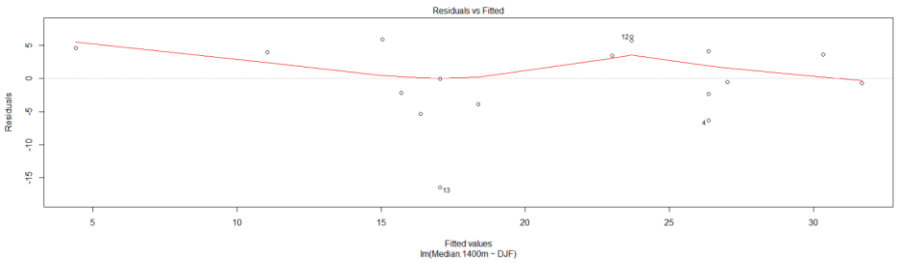

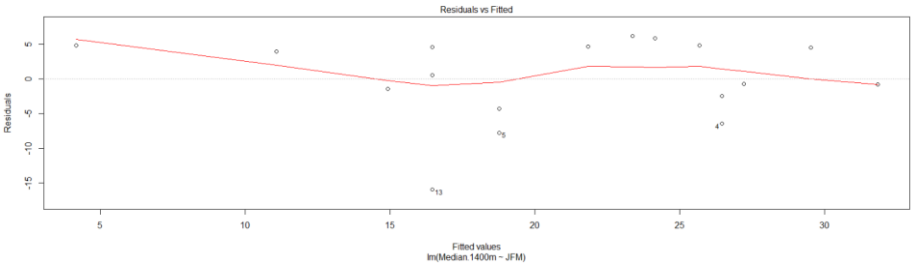

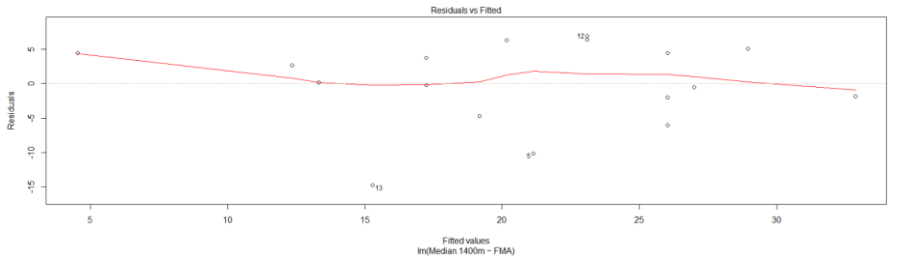

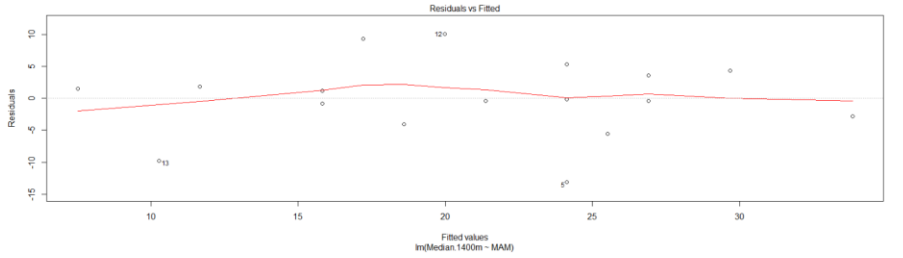

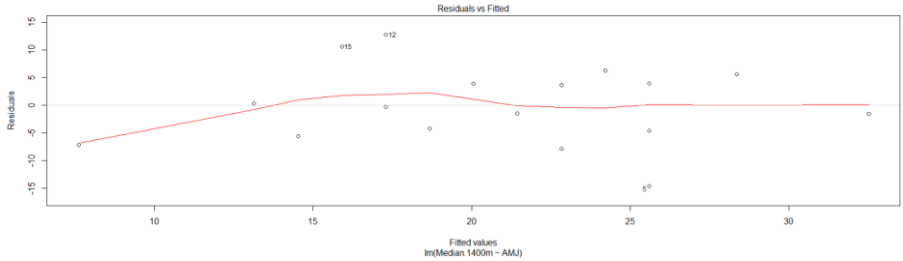

d) 1400-1600 m elevation medians for each 3-month interval

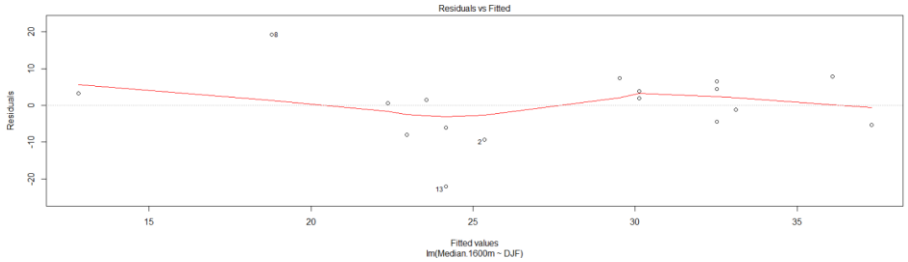

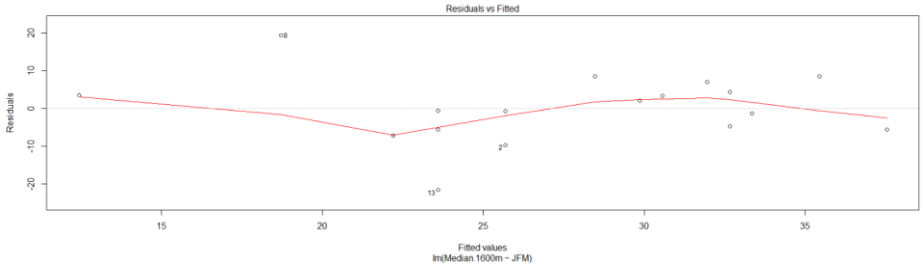

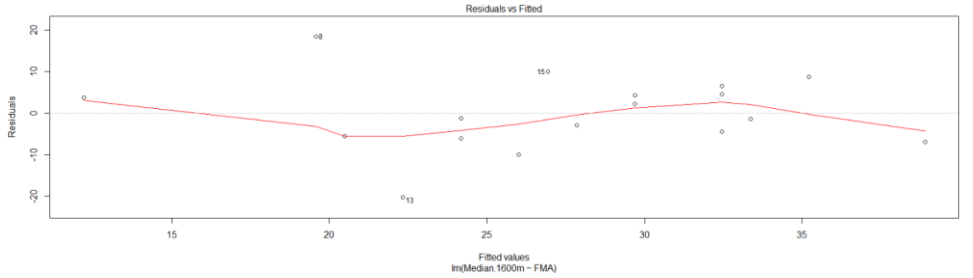

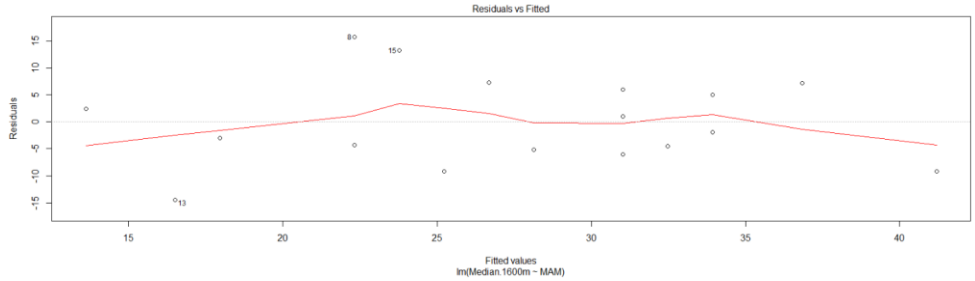

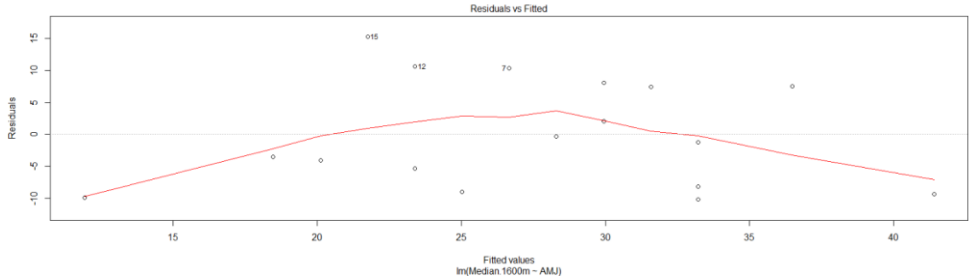

e) 1600-1800 m elevation medians for each 3-month interval

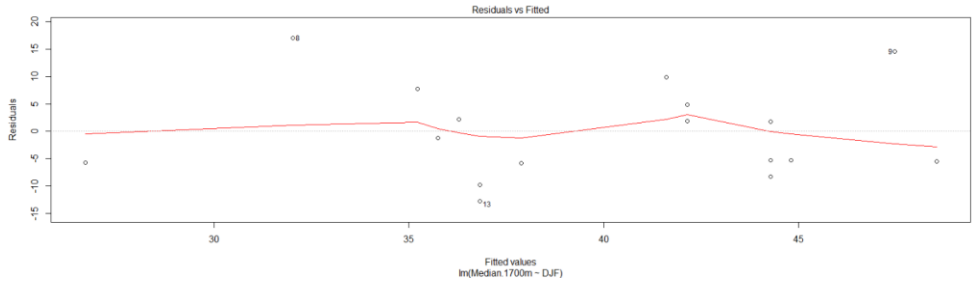

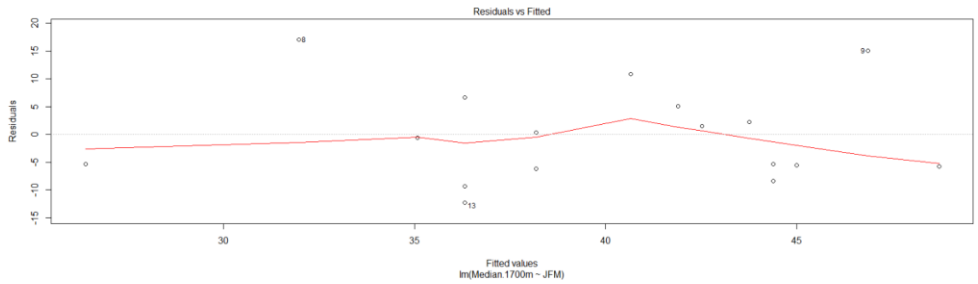

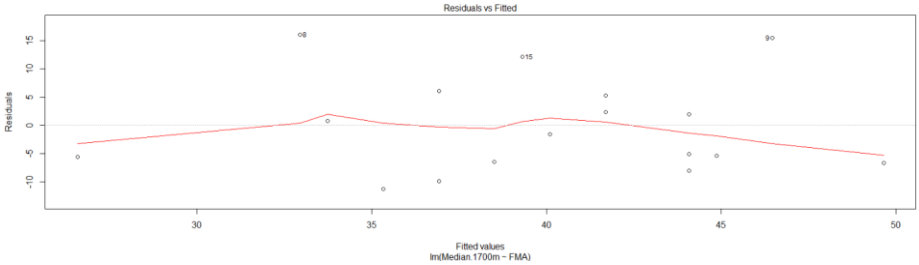

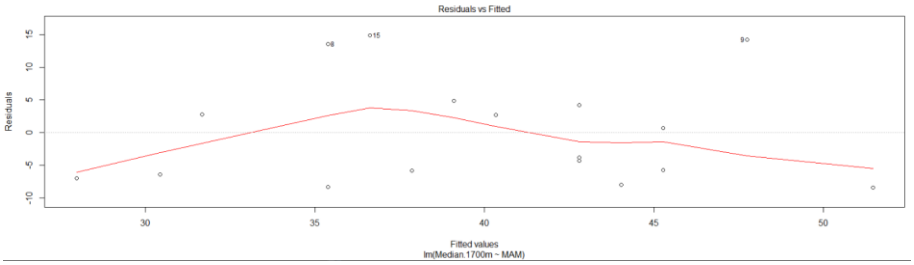

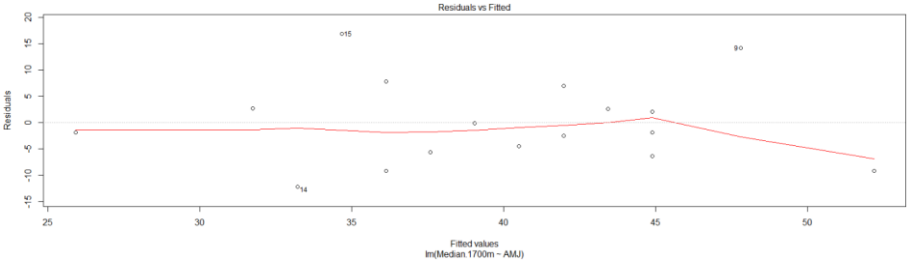

f) 1800-2000 m elevation medians for each 3-month interval

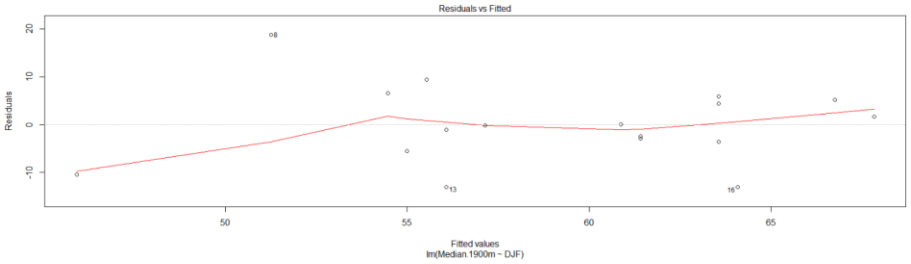

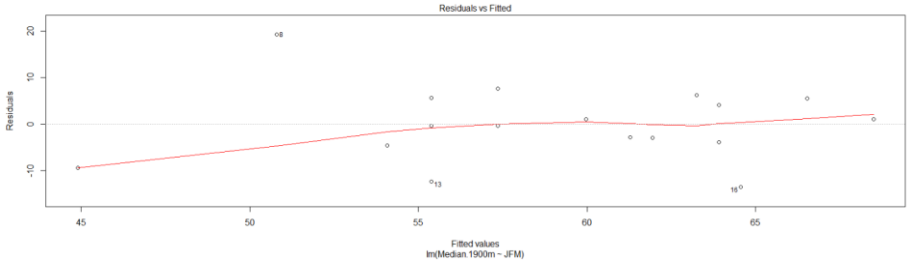

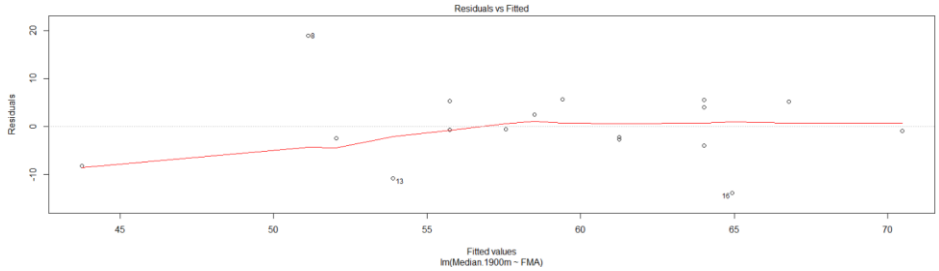
Residuals vs Fitted
Residuals
Fitted values
lm(Median.1900m ~ FMA)

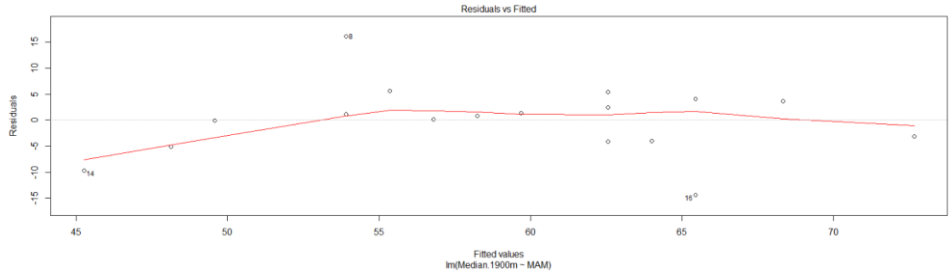
Residuals vs Fitted
Residuals
Fitted values
lm(Median.1900m ~ MAM)

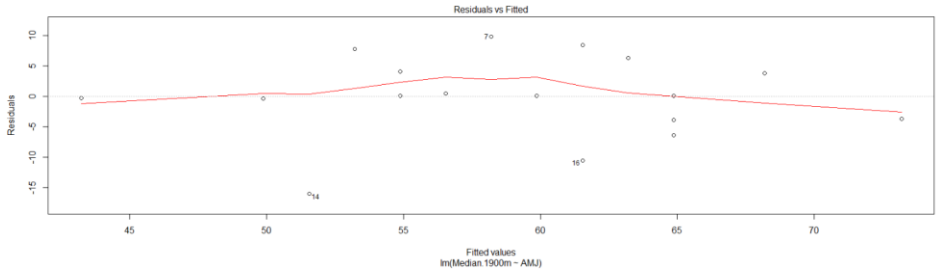
Residuals vs Fitted
Residuals
Fitted values
lm(Median.1900m ~ AMJ)